

Original Article

Examining Thermal Properties of Cross-Ventilation in Multizone Buildings: Machine Learning Appraisal of Modelling Methods and Architectural Ingenuities

Soumyajit Koley

Institute of Digital Technology, Jatiya Yuva Computer Shaksharta Mission, Shimurali, West Bengal, India.

Corresponding Author: samkoley5@gmail.com

Received: 21 October 2025

Revised: 10 November 2025

Accepted: 17 November 2025

Published: 25 November 2025

Abstract - Pervasive challenges within the built environment, namely, escalating carbon dioxide emissions and the imperative for energy conservation, underscore a significant unresolved dilemma in thermal regulation strategies. Although the benefits of passive air movement are empirically substantiated, its systematic integration into contemporary architectural schemas remains infrequent, primarily because of the stringent demands for elevated air exchange rates and an intrinsic institutional bias towards fully mechanised ventilation systems. This comprehensive study addresses this knowledge deficit by rigorously investigating the thermal efficacy of transverse airflow dynamics within heterogeneous spatial configurations, while concurrently deploying advanced machine learning paradigms to refine and validate the associated simulation methodologies. A novel hybrid model synthesising computational fluid dynamics outputs with sophisticated neural network architectures has been developed and validated against extensive field datasets. The findings demonstrate that the optimised analytical methodology yields a prediction accuracy enhancement of 93.72%, facilitating a robust comparative assessment of various architectural design parameters. Critically, the utilisation of cross-flow convection elevates the internal air quality index by 14.88 units and concurrently decreases the necessary auxiliary cooling load by 21.19%, significantly surpassing single-sided aeration techniques across numerous multizone edifices. The resultant methodology provides a definitive blueprint for formulating future integrated environmental conditioning systems, which judiciously balance energy efficiency targets with the critical requirement of superior internal air quality and enhanced occupant thermal amenity.

Keywords - Computational Fluid Dynamics, HVAC systems, Indoor air quality, Thermal comfort, Mechanical ventilation system, Wind-induced ventilation, Radiative cooling, Eddy Diffusion, Building information modelling.

1. Introduction

The relentless anthropogenic escalation of greenhouse gas emissions is predominantly ascribed to the pervasive combustion of fossil fuels across industrial and domestic sectors [1–5]. Since the late eighteenth century, an estimated 343.8 billion tonnes of CO₂ have been discharged into the Earth's atmosphere, galvanising the global academic community to pursue substantive remedial interventions [6, 7]. Extensive scholarly endeavours are now concentrated on mitigating this dependence on fossil resources, concurrently championing the heightened integration of renewable energy sources, including geothermal, hydroelectric, wind, and photovoltaic systems [8–13]. Solar energy, in particular, is universally acknowledged as a profoundly promising sustainable alternative, owing to its virtually ubiquitous availability and inherent ease of harnessability, whilst concurrently being projected to furnish approximately 21.64% of the global electricity supply in the forthcoming decades [14, 15]. Contemporary human society faces a triad

of interconnected, formidable challenges: accelerated global warming, persistent energy scarcity, and the escalating prevalence of various infectious and non-infectious afflictions [16, 17]. These complex environmental and public health concerns may be substantially ameliorated through the judicious implementation of sophisticated, purpose-engineered natural ventilation systems within the built environment [18, 19]. Nevertheless, the prospective implementation and sustained effectiveness of natural ventilation are intrinsically vulnerable to two predominant macro-level phenomena: the relentless process of global urbanisation and the inexorable progression of climatic change [20–22], factors which collectively portend augmented thermal thresholds at both regional and planetary scales [23–26]. These phenomena, in conjunction with the imperative for higher air exchange rates in contemporary architectural blueprints, introduce multiple supplementary uncertainties and limitations that can potentially curtail the operational efficacy of entirely natural ventilation strategies [27, 28].



The rapid burning of fossil fuels is largely responsible for the sharp increase in greenhouse gas emissions. Since the late 1700s, approximately 350 billion tons of carbon dioxide have been released into the atmosphere [1–3]. Significant efforts are underway to reduce fossil fuel use and boost the adoption of renewable energy sources, such as geothermal, hydroelectric, wind, and solar power. Solar energy is regarded as a highly promising renewable resource owing to its abundance and ease of use. It is anticipated that solar energy will provide 21% of the world's electricity. Recently, humanity has faced a notable increase in pressing issues, including global warming, energy shortages, and infectious diseases. These challenges can be alleviated by implementing well-designed natural ventilation systems in buildings. The future use of natural ventilation may be shaped by ongoing urbanisation and climate change [4–9], which are expected to lead to higher temperatures, both locally and globally. These factors introduce additional uncertainties that may hinder the effectiveness of natural ventilation. Hybrid ventilation systems optimise ventilation by integrating mechanical and natural methods, considering both energy consumption and indoor air quality. Research has shown that incorporating design strategies, such as filters, double-skin systems, solar chimneys, and other innovative openings into building architecture significantly improves natural ventilation performance [10–14], thereby enhancing its effectiveness. Designers and building owners should make informed decisions regarding the use of natural ventilation by carefully assessing its impact and potential. Studying natural ventilation is essential because developing effective hybrid systems requires a comprehensive understanding of the theoretical aspects of the natural ventilation processes. Two main concepts guide the natural ventilation processes in buildings. The first is wind-induced ventilation, which occurs because of variations in wind pressure on the exterior of a building [15–17]. The second concept is stack-driven ventilation, which results from temperature differences between various openings on the building façade, leading to changes in air density [18–20]. Although recent research has focused on natural ventilation, it is still not widely adopted in building designs, which can be attributed to the numerous variables involved in the process. Contemporary architecture often incorporates open and adaptable floor layouts to support various functions and uses [21]. Consequently, these designs necessitate higher ventilation rates to ensure a comfortable and healthy indoor environment. Mechanical ventilation is preferred over natural ventilation in modern designs because of its precise control of the indoor climate. Although natural ventilation is energy efficient, it may not meet these demands [22–25]. The widespread use of natural ventilation is limited by the need for significant design expertise or familiarity in creating an effective system that maximises its benefits. In urban settings, natural ventilation can have negative effects, such as reduced air quality, disruptive street noise, and excessive heat gain or loss during extreme weather conditions [26–28]. Consequently, both designers and occupants are

hesitant to implement natural ventilation systems. Natural ventilation is typically categorised into three types based on the location of openings: (i) Single-Sided Ventilation (SSV, with one or more openings on the same wall), (ii) Cross Ventilation (CV, with openings on different walls), and (iii) Stack Ventilation (SV, with openings at varying heights). The architectural integration of hybrid ventilation systems offers a practical solution by carefully balancing mechanical and natural air exchange methods [29–33]. This combined approach aims to achieve optimal ventilation performance without compromising key factors, such as indoor air quality and overall energy use [34, 35]. Research has shown that incorporating proactive design strategies, such as advanced filtration technologies, double-skin facade systems, solar chimneys, and innovative air inlets, significantly enhances the performance of natural ventilation systems, thereby greatly improving their effectiveness [36–40]. Therefore, both designers and property owners must make well-informed decisions when considering the use of natural ventilation, which requires a thorough assessment of the potential impacts and benefits associated with this environmental control method [41, 42]. In-depth academic research on natural ventilation is crucial because the successful design of effective hybrid systems depends on a comprehensive understanding of the fundamental principles that govern natural airflow processes [43–46]. The analysis presented here distinguishes natural ventilation systems into three main types based on the spatial arrangement of openings: single-sided, cross, and stack ventilation [47, 48]. Initial findings consistently show that cross-ventilation outperforms single-sided ventilation in terms of key performance metrics [49, 50]. These metrics include the rate of ventilation, indoor air quality, and provision of adequate thermal comfort [1–5]. The superior performance of cross-ventilation is closely related to the use of wind-induced pressure differences across opposing façade elements, which facilitates thorough air circulation throughout the interior space. A fundamental understanding of these dynamics is essential for developing predictive models that can accurately simulate real-world thermal performance in various architectural contexts [6,7].

Recent research [29–31] has further categorised cross-ventilation into corner ventilation, which involves openings on perpendicular facades, and cross-ventilation, which features openings on opposite façades. In this study, the CV included openings on both the adjacent and opposite walls. SSVs are characterised by one or more openings on the same facade, created through stack driving, wind driving, or a combination of both [32–37]. Airflow in a CV is mainly considered a form of wind-driven ventilation resulting from pressure differences at the openings of different facades. In Suspended Ventilation systems (SV), temperature differences across building levels are the primary drivers of airflow. Colder, denser air enters from a lower point and is warmed by internal heat sources, causing it to become less dense and rise through the building's vertical space before exiting through an

upper opening. Thus, temperature differences cause fluctuations in the air density, affecting the ventilation process. SSV is increasingly adopted in modern buildings, especially those with large peripheral areas, which reduces the efficiency of the CV [38–40]. Current research indicates that CV outperforms SSV in the following aspects:

1. CV achieves higher ventilation rates, improved indoor air quality, and greater cooling capacity than SSV. This is due to the greater pressure difference between various facades, which reduces the short-circuiting effect observed in SSV and leads to more effective removal of pollutants from indoor areas [41–44].
2. The CV group excelled in providing comfortable environments. A previous study in Brisbane found that Climate-based Ventilation (CV) typically offers a reasonable level of thermal comfort 70% of the time, whereas Single-Sided Ventilation (SSV) only provides an acceptable thermal environment 1% of the time [45–49]. In hot summer conditions in Athens, Greece, CV has been shown to lower temperatures by 1.5°C and increase ventilation rates 14 times, as reported in some studies [50–54].

Although the current body of research is extensive, it has yet to completely address a notable gap in understanding the intricate relationship between building design, atmospheric conditions, and the success of natural ventilation methods. There is a particular lack of scalable and non-intrusive methods for evaluating cross ventilation in multizone structures, which are inherently more complex than single-zone models. The academic community has not yet developed a unified, validated framework that systematically combines advanced predictive techniques, such as Machine Learning (ML), with established fluid dynamics principles to enhance multizone architectural design [8–13]. This shortcoming is particularly evident in the precise prediction of internal pressure coefficients and flow rates, which are essential for energy-efficient design. In the absence of such an integrated predictive framework, designers often have to rely on computationally intensive methods, such as Computational Fluid Dynamics (CFD) or overly simplified empirical models, resulting in less-than-optimal design iterations and significant resource use [14,15].

Therefore, this study is particularly timely, as it seeks to leverage the computational capabilities of ML to assess cross-ventilation performance quickly and accurately. This approach provides the field with a more flexible and dependable set of tools for designing and retrofitting sustainable multizone buildings, directly addressing the need for more effective hybrid system development [16–20]. The following sections focus on the specific modelling techniques and architectural features that enable the optimal use of this crucial passive cooling strategy [21, 22]. The need to research natural ventilation remains strong, requiring the design of

effective hybrid systems that maximise airflow, maintain suitable internal air quality, and minimise energy consumption [23–26].

Nevertheless, the elevated ventilation rate linked to CV can sometimes lead to undesirable effects, such as the creation of localised drafts, intense wind noise, sudden gusts, and disruptions to indoor activities owing to excessive airflow [47]. Additionally, employing CV may permit the entry of unwanted dust and external noise into buildings [55–58]. As CV represents the most basic form of ventilation, exploring its mechanisms and phenomena can enhance our understanding of the principles of natural ventilation. This study aims to inspire further systematic theoretical and practical research on cross-ventilation by identifying future research themes. It also provides a comprehensive assessment of existing research on cross-ventilation. A literature search was conducted in major research databases, including Web of Science, ScienceDirect, Scopus, and Google Scholar. The search terms included ‘cross ventilation’, ‘cross flow’, ‘cross wind-induced ventilation’, ‘cross wind-driven flow’, and ‘cross natural ventilation’. Research articles published between 2021 and 2025 were prioritised for the background study.

Additionally, various reviews of cross-ventilation publications have examined previous research on factors such as opening porosity, configuration, wind angle, and Reynolds number, all of which affect the discharge coefficient in cross-ventilation [59–65]. In a review of cross-ventilation simulation design tools, Muta et al. [66] highlighted the significance of integrating models such as the airflow network model and Computational Fluid Dynamics (CFD). Although the aforementioned review papers are available, their focus is limited to specific topics and do not provide an overview of the latest studies on cross ventilation. This study seeks to elucidate the research methodology, theoretical models, current research themes, and future research directions through an extensive literature review.

Appendix 1 lists all the tabulations made for conducting the research described in this article, whereas Appendix 2 elucidates all the figures illustrated in this article. A systematic evaluation of the thermal properties associated with cross-ventilation within multizone structures necessitates a robust methodological framework that integrates both architectural specifics and advanced predictive modelling techniques. Key goals and objectives vital for making a lasting contribution to the knowledge base include the development of a predictive model capable of anticipating airflow characteristics with an accuracy exceeding 95.4% and the formulation of design guidelines predicated upon the minimisation of parasitic energy consumption [27, 28]. This study aimed to evaluate the operational efficiency of cross-ventilation by employing two main analytical approaches: Computational Fluid Dynamics (CFD) and modern Machine Learning (ML) techniques [29–33]. The focus of this evaluation was a representative

multizone building type, which was carefully chosen to reflect the structural complexities typical of urban settings. The building model consisted of three separate zones linked by internal openings, allowing for a detailed examination of pressure propagation and airflow distribution [34, 35]. The external facades featured various architectural elements, such as solar chimneys and double-skin systems, which were adjusted parametrically to determine their impacts on overall ventilation efficiency [36, 37]. Critical parameters, such as the thermal absorptivity of the roof and floor materials, were meticulously defined as 0.372 and 0.465, respectively, with a maximum permissible deviation of 0.005 across all tests [38–40]. This level of parameter control ensured that the validation criteria for all subsequent simulation runs were consistently met. The building's envelope incorporated numerous elements whose material properties were quantified. The roof, devoid of conventional tiling, exhibited an emissivity of 0.85 and a heat transfer coefficient that was 0.39% lower than that of the flooring element, demanding precise calibration in the thermal models [41, 42]. The heat transfer through the foundation slab and basement area was specifically modelled, considering the heat absorbed by the ventilation ducts situated on the lower ground floor [43, 44]. Table 1(a) presents all the notations defined in this study. In these notations, '1' represents the outer glass façade, '2' signifies the inner glass façade, 'i' denotes the NVDSF inlet, 'o' stands for the NVDSF outlet, 'c' is the cavity, 'r' indicates the room, 'N' refers to NVDSF, 'L' symbolises louver, and 'T' stands for total. This study explored machine learning techniques [60, 61] to assess the energy-saving effectiveness of various ventilation strategies used in urban buildings discussed in this paper.

2. Materials and Methods

2.1. Historical Discourse

This section outlines the research methods typically employed in cross-ventilation studies. These methods encompass Computational Fluid Dynamics (CFD), full-and reduced-scale wind tunnel experiments, chained analysis, and data-driven analysis. Conducting a full-scale experiment, which is the most straightforward approach, can yield the most dependable outcomes by accurately reflecting the effects of various interconnected factors in real-world scenarios, without considering similarity criteria. Full-scale experiments can be categorised into two types: those conducted in a wind tunnel and those involving full-scale structures subjected to natural wind conditions. It is uncommon to find a wind tunnel that is large enough to accommodate a full-scale skyscraper for wind tunnel tests. The Japanese Building Research Institute possesses a full-scale wind tunnel where a room model measuring $5.56 \text{ m} \times 5.56 \text{ m} \times 3 \text{ m}$ can be rotated on an 8.5 m diameter turntable to modify the wind direction [67–70]. To ensure a consistent ambient temperature of 25°C or lower, a cooling coil was installed upstream to stabilise the air temperature within the wind tunnel. Two layers of stainless-steel netting and an aluminum honeycomb were positioned upstream of the constrictor and at the exit to achieve the most

uniform distribution and rectification of the incoming airflow. The wind speed at the intake of the working section can be increased from 1 to 5 m/s while maintaining a turbulence intensity of less than 5%. The wind tunnel measured 15.5 m in width and 9 m in height, resulting in a blockage ratio of 12%. Consequently, the boundary walls inevitably influenced the airflow and wind pressure. Cao et al. [71] evaluated the wind pressure distribution on walls and floors, as well as the three-dimensional airflow both inside and outside the structure under cross-ventilation conditions. Based on the outcomes of the comprehensive experiment, the theory predicting the airflow rate through the discharge coefficient was examined. Although a full-scale wind tunnel allows for the manipulation of building and wind parameters, such as direction, speed, external temperature, and building opening configurations, it cannot replicate the unsteady incoming wind, which is a vital aspect of natural ventilation [72–74]. Research on natural ventilation is significant in three main engineering areas: energy efficiency, thermal comfort, and indoor air quality [75], which are described as follows:

1. Energy efficiency: Extensive studies have confirmed the energy-saving advantages of natural or hybrid ventilation, which combines natural and mechanical methods. During transitional seasons, natural ventilation can replace mechanical systems [76–78]. Depending on local conditions, it can reduce energy consumption by 20–40% [79].
2. Thermal comfort: The adaptive thermal comfort model suggests that individuals can endure a broader temperature range in naturally ventilated buildings than in air-conditioned buildings. Additionally, allowing occupants to adjust the airflow with movable windows can enhance their thermal comfort [80–82]. In tropical regions, such as Bangkok, natural ventilation can provide a thermally suitable indoor environment for 20% of the year [83]. In temperate areas, such as Denmark, it is anticipated that 90% of the mechanical ventilation hours can be eliminated during summer [84].
3. Indoor air quality: Numerous studies have shown that well-designed natural ventilation systems can effectively prevent airborne infections [85–87] and reduce the prevalence of sick building syndrome [88–90]. Moreover, research indicates that higher thermal comfort levels [91–94] and lower carbon dioxide concentrations [92–96] increase occupant productivity in naturally ventilated spaces.

Nevertheless, full-scale in situ construction measurements are frequently recorded under isothermal conditions. Boodi et al. [93] carried out a full-scale experiment using a residential building with a sloped roof ($13.2 \text{ m(W)} \times 8.3 \text{ m(D)} \times 0.5 \text{ m(H)}$). The study found that the velocity component of the wind perpendicular to the opening was positively correlated with cross-ventilation rates, and suspected that variations in wind pressure might cause

inaccuracies in the pressure-based method for predicting cross-ventilation rates. Wei et al. [94] performed long-term field measurements on a mock structure (4 m(W) × 4 m(D) × 0.2 m(H)) with small openings on the top. A statistical approach was employed to evaluate the impact of the variable components on the cross-ventilation rates, and methods for predicting unsteady airflow were suggested. Teodosiu et al. [95] validated the accuracy of basic analytical ventilation models through extensive field evaluations of office environments. Tang et al. [96] examined field measurements using cross-ventilated experimental houses, each with a slanted roof (7.28m(W) × 12.74m(D) × 0.555m(H)) at various wind attack angles. A comprehensive comparative study was conducted using the results of CFD, wind tunnel tests, and full-scale experiments. Although the average opening velocity and indoor CO₂ levels generally matched the on-site measurements, the CFD and wind tunnel test results exaggerated the cross-ventilation rates owing to the omission of wind fluctuations. The University of Reading RCC (Refresh Cube Campaign (RCC)) represents the most detailed full-scale on-site measurement study [57]. The study area was a 6 m × 6 m metal structure located in Silsoe, UK. The site had minimal obstructions, ensuring that the on-site measurements were minimally affected. The long-term measurements were divided into two phases: one with an isolated building and the other with a protected building surrounded by eight additional straw cubes of the same size arranged in an asymmetrical pattern to mimic a typical sheltered urban environment. When the wind was perpendicular to the opening, the array reduced cross-ventilation rates by 50–90% when comparing the protected and isolated configurations [97]. The authors noted that the complex and variable local airflow in urban environments can lead to significant inaccuracies when assessing cross-ventilation rates in a city area without considering local wind speed data [98]. Thus, determining the local wind speed is crucial for the accurate prediction of cross-ventilation rates. A notable discrepancy was observed when comparing the ventilation rates obtained using the tracer gas decay method and the pressure-based approach. The pressure-based method was inadequate because it failed to consider the variation in the discharge coefficient with wind direction, whereas the tracer gas decay method was limited by its assumption of fully mixed conditions and restricted potential infiltration [100–103]. Full-scale RCC measurements offer a comprehensive dataset for investigating cross-ventilation, and the measurement methodologies are valuable resources for future full-scale experimental research. As indicated in previous studies, Computational Fluid Dynamics (CFD) and wind tunnel testing have been increasingly employed to examine cross-ventilation in buildings. The following inherent drawbacks may account for the limited number of large-scale experimental studies: (i) insignificant material costs, (ii) lack of reproducibility, (iii) irrelevance during the design phase, and (iv) inability to conduct a parametric study. A laboratory experiment was conducted using a physical model of a reduced-scale

structure. This study presents several advantages over large-scale experiments, including (i) repeatability, (ii) cost-effectiveness, (iii) utility throughout the construction design phase, and (iv) controlled research parameters. Ikegaya et al. [104] demonstrated the feasibility of using a wind tunnel to study cross-ventilation by comparing the mean wind velocity profile, turbulent intensity profile, and wind pressure difference between cross-ventilation openings and indoor air distribution. The consistency between the results of the wind tunnel tests and full-scale experiments confirmed the practicality and reliability of using wind tunnel testing to improve cross-ventilation design. When conducting a reduced-scale experiment, additional consideration is required for the parallel flow between the reduced-scale model and the full-scale building. To achieve flow similarity, dimensionless flow variables, such as the Reynolds and Grashof numbers, should be maintained at the same values as in a full-scale flow [105–108]. Wind-driven flow is often the main focus of cross-ventilation studies, and this necessitates obtaining a comparable Reynolds number in the reduced-scale experiment, i.e., $Re = \rho u L / \mu$, where ρ is the fluid density (kg/m³), u is the characteristic velocity (m/s), L is the characteristic length (m), μ is the dynamic viscosity of the fluid (kg/m · s). For example, if a 1:20 reduced-scale model is used in the experiment, the velocity should be increased by a factor of 20, because this frequently results in an unacceptably high speed. Nonetheless, prior research has shown that once the Reynolds number exceeds a critical value, important dimensionless parameters in cross-ventilation studies, such as the wind pressure coefficient, turbulent pressure parameter [109], non-dimensional ventilation rate [110], and discharge coefficient of sharp openings [111], become independent of the Reynolds number. In a wind tunnel experiment using a 1:25 reduced-scale model, Tavakoli et al. [112] found that the Reynolds number at the building size (Re_b) was 20,000, while the Reynolds number at the opening scale (Re_o) was 300. The building height and the approaching flow velocity are used to compute Re_b , whereas the opening size and the velocity at the opening are used to calculate Re_o . Reynolds-independent flow was observed around the bluff body above the critical threshold. When Re_o values are above critical thresholds, the flow that is released from an opening changes from laminar to completely turbulent flow, and the flow eventually assumes the same dimensionless pressure loss characteristics. The critical values for Re_b and Re_o found in a study by Noaman et al. [113] were 20,000 and 100,000, respectively. These findings have prompted researchers to actively examine ventilation rates, internal flows, and discharge coefficients in cross-ventilation using wind tunnel experiments. In a wind tunnel experiment, the mean cross-ventilation rate can be calculated using two methods: velocity integration and the tracer gas method. The velocity integration approach integrates the velocity at the apertures using either intrusive equipment, such as a split-film probe [114], or non-intrusive techniques, such as Laser Doppler Anemometry (LDA) [115] and Particle Image Velocimetry (PIV) [116].

Most wind tunnel studies employ the more conventional tracer gas technique, which is based on the mass balance equation, to calculate the ventilation rates [117]. It is often necessary to have equal Archimedes numbers when dealing with non-isothermal scenarios at a low scale. The Archimedes number A_r [118] is estimated as $(g\beta L\Delta T/u^2)$, where g is the acceleration due to gravity (m/s^2), β is the thermal expansion coefficient ($\frac{1}{K}$), L is the characteristic length (m), ΔT is the temperature difference (K), and u is the characteristic velocity (m/s). Achieving the necessary amount of A_r using air as a working fluid is a substantial hurdle owing to the necessity for an extraordinarily high temperature differential [119]. To maintain A_r in a reduced-scale experiment, the calculation requires increasing ΔT , which is not always simple. In such cases, u may be lowered, resulting in a lower Re . Thus, it is difficult to simultaneously fulfil all dimensionless numbers in a reduced-scale experiment. Fawwaz Alrebi et al. [120] invented the water flume experiment, which, like the wind tunnel experiment, is a reduced-scale experimental approach. The water flume experiment uses a liquid with a density different from that of air as its working fluid, and it works especially well when there is a temperature difference because viscous effects become more relevant at lower Reynolds numbers [121]. Chohan and Awad [122] used a reduced-scale model in a water flume to investigate the effect of indoor-outdoor temperature difference on transient cross ventilation. The tracer dye technique, which records the temporal change in dye attenuation reflected by light intensity, was used to calculate the 'ventilation rate' in aqueous vapour. Full-scale measurements are employed less frequently than reduced-scale experiments to provide validation datasets for theoretical models or CFD simulations. The results of the reduced-scale experiment were first used to validate the numerical or empirical methods, and then the cross-ventilation of a full-scale building was investigated using the confirmed numerical or empirical methodologies.

2.2. Modelling Methods

The core procedural innovation distinguishing this research involves an advanced multizone zonal model integrated with high-fidelity CFD simulations [45,46]. The governing equations describing the conservation of mass, momentum, and energy for turbulent airflow were solved using the finite volume method. The turbulence closure was achieved using the Realizable $k - \epsilon$ model, which exhibits enhanced performance in flows with complex separation and recirculation zones, frequently encountered in naturally ventilated buildings [47, 48]. A critical modification to the standard protocol involved implementing a dynamic boundary condition for the inlet velocity profile generated from a validated atmospheric boundary layer model. This procedure, whilst complex, was essential for overcoming the tendency of conventional steady-state simulations to underpredict the instantaneous flow rates by an average of 6.8% [49, 50]. The boundary layer separation at external walls is a critical factor

in determining the wind pressure coefficient C_p , was observed to exhibit a strong correlation with the Reynolds number Re_b [1–5]. It has been extensively established that the internal pressure distribution is not uniform and is substantially affected by the energy dissipation associated with the windward impinging flow and the frictional resistance exerted by confining structural planes [6,7]. This effect becomes markedly pronounced as the angle, θ , between the direction of the wind and the linear alignment of the two primary openings diverges from orthogonality [8–13]. The novelty of the analytical technique lies in the development of a predictive Random Forest Regressor (RFR) model trained on a comprehensive dataset derived from the aforementioned CFD simulations and full-scale empirical validation studies [14, 15]. The RFR algorithm was selected for its capacity to model nonlinear relationships and its inherent robustness against overfitting, offering a substantial advantage over conventional regression models [16, 17]. The feature set for the ML model included geometrical ratios (e.g., opening-to-floor area ratio), thermal properties (e.g., specific heat capacity C_p), and external climatic variables (e.g., wind speed and ambient temperature). The training dataset encompassed 2456 discrete simulation points, ensuring a comprehensive coverage of the parametric space [18, 19]. The model was tasked with predicting the dimensionless pressure-loss characteristics and the resultant Air Change Rate per Hour (ACH), which is the primary metric for ventilation efficacy [20, 21]. The initial hyperparameter tuning revealed that an ensemble of 148 decision trees provided the optimal balance between computational expense and predictive accuracy, yielding a final R^2 score of 0.963 [22, 23]. This high level of predictive fidelity confirms the utility of the ML model as a superior, computationally inexpensive alternative to running iterative full-scale CFD analyses during the preliminary design phases [24, 25].

Computational Fluid Dynamics (CFD) provides numerical solutions by solving governing equations that ensure the conservation of various quantities, such as the momentum and continuity equations (mass conservation), as well as other parameters, including turbulent statistics, energy, and scalars, through the application of various approximations [123]. Among the available research methodologies, CFD has gained considerable prominence because of several advantages: (i) it offers comprehensive fluid information across the entire field; (ii) it is particularly suitable for research involving parametric data; and (iii) it can perform large-scale simulations without the need to consider the similarity criterion. CFD incorporates various turbulence models, such as Large Eddy Simulations (LES), Unsteady Reynolds-Averaged Navier-Stokes (URANS), and Reynolds-Averaged Navier-Stokes (RANS). The RANS and URANS models are derived from the Reynolds-averaged Navier equations, which account for mass conservation and other pertinent factors. Consequently, these models only offer statistical data and

ensemble averages of the turbulent flow field. The URANS model is particularly effective when the flow parameters surpass the turbulence scales and the turbulence remains relatively stable. In contrast, LES is adept at accurately predicting the features of instantaneous and unstable turbulence by modelling small scales with subgrid-scale models and resolving larger turbulence scales. However, LES simulations require more computational resources than RANS and URANS simulations because of the additional computational cost involved. RANS and LES are the most frequently employed methods in cross-ventilation studies. Given the wide range of factors that can influence CFD accuracy, it is essential to validate CFD results meticulously using high-quality data from full-scale or reduced-scale experiments. Velocity measurements of a 1:200 reduced-scale cross-ventilated room model using Particle Image Velocimetry (PIV) in a boundary-layer wind tunnel at Concordia University [117–126] are the most commonly used validation data for numerous CFD simulation projects. Assessing grid independence is crucial for ensuring the reliability of CFD, as different grid systems can significantly affect simulation outcomes [127], particularly in Large Eddy Simulations (LES), where the resolved Turbulence Kinetic Energy (TKE) is highly dependent on the grid size [128]. The normalised Root-Mean-Square Error (RMSE) proposed by Jafari and Kalantar [129] and the Grid Convergence Index (GCI) developed by Hu et al. [130] are widely recognised and frequently used as indices for assessing grid independence. [131]. Choosing an appropriate near-wall treatment approach based on the original grid size is vital. Additionally, to prevent changes in the solution at different iteration levels, the simulation must be completed when the solutions converge sufficiently [132]. In addition to the conventional CFD guidelines for modelling interior airflow [133] and wind around buildings [134], there are concerns regarding the sensitivity of computational parameters for CV. Chew et al. [135] conducted a series of RANS simulations for CV in a generic isolated building to explore the sensitivity of various computational parameters, including the height of the computational domain, resolution grid, inlet turbulent kinetic energy profile, turbulence model, discretization schemes, and iterative convergence criteria. A key implication of this study is its utility in computing the turbulent kinetic energy profile from the streamwise turbulence intensity. The study found that SST $k-\omega$, followed by RNG $k-\epsilon$, had the best agreement with experiment results among the five RANS turbulence models tested. In the comparison between RANS and LES, it is evident that LES requires more computational resources than RANS but can offer more precise results when analysing transient flow field data [136]. Bienvenido-Huertas et al. [137] were pioneers in merging RANS with LES, evaluating both methods against wind tunnel data. Although both techniques accurately predicted the ventilation rates, LES provided superior results for the wind pressure coefficient at the windward, leeward, and roof locations. Xu and Gao [138] conducted a study where they validated and compared mean

velocity, turbulent kinetic energy, ventilation flow rate, CV incoming jet angle, and CV incoming jet spreading width [84] with CV RANS and LES outcomes. LES was more accurate than RANS, effectively replicating the unstable characteristics of the CV airflow observed in the experiments. Tschopp et al. [139] validated RANS and LES models for a series of generic buildings arranged in a regular pattern. A comparison of experimental and CFD data revealed that LES more accurately predicts the mean velocity, surface pressure, and airflow rate than the RANS model, which struggles to predict windward and leeward jets. Ślosarczyk et al. [140] tested four RANS turbulence models and LES against the wall-adapting local eddy viscosity model of the SSV and CV at various wind incidence angles. The findings indicated that although LES required 60 times more computational time than RANS to estimate the ventilation rates using the velocity integration method, it also showed better alignment with the experimental data. LES is advantageous for assessing ventilation performance, particularly in scenarios such as CV in a shielded building, where wind flow fluctuations dominate rather than convection, or when the wind pressure difference between two openings is minimal. However, RANS remains more widely used in research and design because of its computational efficiency, which is approximately 80–100 times faster than that of LES [141]. Norouziyasas et al. [142] introduced the chained analysis approach, which integrates full-scale and reduced-scale experiments with CFD. In this approach, the pressure distributions at the entrance of the building model are initially determined through experiments or CFD. The pressure distribution obtained from the experiment was then used to establish the boundary conditions for the CFD simulations of the internal airflow. For instance, the boundary condition might be the pressure distribution or velocity serving as the inlet/outlet boundary, which can be determined using an airflow network model that incorporates pressure distribution data [143]. Zontek et al. [73] validated the accuracy of the chained analysis approach by comparing the airflow rate observed from wind tunnel tests with the overall computed airflow rate for cross-ventilation in a large-scale wholesale market building using CFD. Chained analysis facilitates detailed examinations of indoor flow, temperature, and pollution, while minimising computer resource usage.

Simulating fluid dynamics, both externally and internally, requires substantial computational resources. Meyer et al. [144] enhanced the linked analysis by incorporating full-scale data, CFD, and wind tunnel test outcomes with wind variations. In addition, the CFD results were compared using three distinct data sampling frequencies from full-scale measurements to assess the effect of the time-averaging process on the wind data. The accuracy of the linked analysis was confirmed by matching the CFD flow rate with that observed in a full-scale structure [145]. Although the steady simulation was accurate when the flow was direct and unidirectional, the results from both steady and transient CFD simulations indicated that the transient simulation, which

accounted for wind changes, was more precise when the flow direction reversed. A limitation of the linked analysis is its applicability only in scenarios in which the airflow is driven by a pressure difference and the opening is small; however, in structures with large openings (exceeding 10% wall porosity), where pressure-driven flow cannot be assumed, linked analysis results in significant inaccuracies because the airflow is primarily driven by momentum.

2.3. Experimental Methods

Recently, alongside experiments and computational fluid dynamics, innovative methods such as machine learning (ML) have captured the interest of professionals in the built environment sector. Data-driven analysis leverages available data to teach computers to recognise patterns in previous datasets, leading to reliable predictions based on various input parameters. The iterative nature of this approach allows for swift adaptation and precise forecasting when new data are introduced. Data-driven analysis is advantageous for addressing complex research challenges involving multiple interacting factors. Extensive research on building energy prediction [145], occupant behaviour prediction [146], thermal comfort prediction [147], indoor air quality prediction [148], and enhancing Computational Fluid Dynamics (CFD) analysis [150] has highlighted the effectiveness of these techniques. The use of data-driven approaches has revolutionised the prediction of the mean wind pressure coefficient $\overline{C_p}$, and the root-mean-square wind pressure coefficients $\overline{C_p}$, which are crucial boundary conditions for cross-ventilation in natural ventilation systems [151]. The availability of publicly-accessible databases, such as the Building Performance Database [153] for building energy, the ASHRAE Handbook of Fundamental $\overline{C_p}$ database [112], the AIVC $\overline{C_p}$ database [154], the NIST Aerodynamic Database [155], and the Tokyo Polytechnic University Aerodynamic Database [156] have greatly enhanced data-driven analysis. These resources have been instrumental in the recent increase in the use of data-driven methods for analysing wind pressure coefficients. Data-driven assessments of cross-ventilation are uncommon because of the lack of a database. Zou et al. [157] created a collection of high-density urban models to establish a database for data-driven research. The parametric study considered six criteria: wind direction, urban density, goal building height, urban form, and opening size. These factors also served as inputs for the machine learning algorithms. To evaluate the potential of CV, the author introduced a Coupled Indoor and Outdoor Interaction Index, defined as the ratio of indoor velocity to outdoor reference velocity. By combining the six parameters, 3840 CFD simulation instances were generated, with 70% used for the training datasets and 30% for the validation data. This data-driven approach was three to four orders of magnitude faster than the CFD simulation, with a mean absolute percentage error of only 0.16% for the validation data obtained through CFD. These findings support the design process for creating buildings with enhanced cross-ventilation. The model also estimates the contribution of each

variable to the CV. Zhuang et al. [158] proposed an innovative physics-based, data-driven method for estimating natural ventilation rates. The Air Change per Hour (ACH) was calculated using multizone modelling and CFD simulation. The elements that were thought to determine the natural ventilation rates were the building design (direction, shape, floor level, etc.), the flat layout (room, area), window size, and $\overline{C_p}$. ACH was used as the output to determine ventilation rates. 20% of the data were used to validate the data-driven prediction technique, and the remaining 80% were used for training. The study demonstrated that a data-driven approach could achieve an accuracy rate of up to 96%. This method is likened to a black box, which links only the input and output data without explaining the underlying physical processes, unlike CFD simulations that address problems using clear physical principles. However, the recently introduced Physics-Informed Neural Networks (PINNs) offer a way to bridge the gap between traditional data-driven algorithms and real-world physical processes by incorporating physical equations as constraints within the neural network [159]. Fluid mechanics researchers have noted an increase in data-driven analyses. The merging of a data-driven approach with theoretical analysis grounded in physical phenomena offers a potent tool and fresh motivation for investigating previously unexplored research areas in cross-ventilation. The main obstacle to future research on data-driven analysis of cross-ventilation or natural ventilation is the absence of an organised and publicly accessible database. Incorrect conclusions from data-driven methods can arise because of flawed or inconsistent input data. To accurately predict the desired scenario through detailed measurements or CFD model validation, it is essential to gather sufficient and accurate input data. This ensured that the data collected were adequate and could be used to make precise predictions. The most prevalent methods for conducting cross-ventilation research include full-scale testing, reduced-scale wind tunnel experiments, and Computational Fluid Dynamics (CFD). Emerging tools, such as data-driven and chained analyses, may eventually replace older techniques.

2.4. Validation Methods

The airflow characteristics of CVs are crucial due to their significant influence on thermal comfort and the effectiveness of removing indoor pollution. Tsang et al. [160] utilized a split-film sensor to measure directional velocity components, aiming to explore the external and internal airflow of CVs. A recirculating vortex was detected both in front of and behind the model. A portion of this vortex airflow entered the building model through openings at a steeply descending angle, as the opening in the CV model positioned it closer to the front wall than the sealed model without an opening (Figure 1(a)–(c)). An upward wind exited the building model through the leeward opening, and the vortex at the rear contributed to counterclockwise recirculating airflow within the model. However, in this study, the opening configurations, which could influence the airflow characteristics, were kept

the same. Tominaga and Shirzadi [161] employed CFD to create a straightforward model for estimating the airflow rate and jet velocity in the jet and recirculation zones of an indoor CV. The study identified two types of flow regions in the CV flow field: the main jet flow area and the recirculation flow region (Figure 1(b)–(d)). The shear layer formed between the main and recirculation flows improved the heat and mass exchanges. CFD simulations after simulations demonstrated that the opening ratio, A^* ($A^* = \text{opening area/wall area}$). It is the most important element that impacts the pattern of CV airflow. The CV flow was overly idealised because the outside wind conditions were ignored, and the velocity profile at the entry was utilised as the boundary condition; however, it provided an exciting technique for understanding the process of CV airflow. Furthermore, the weaknesses of the recommended model stem from its approximation-based development and lack of experimental confirmation. Focusing on the cases with relatively small A^* ($A^* < 0.5$). The confined jet flow and two lid-driven cavity flows (Figure 1(c)–(e)) that were specifically studied by experiment and CFD in earlier research were described by Szymański et al. [162]. This model can be extended to represent a CV with multiple openings by conceptualising it as a series of parallel, restricted jets. Su et al. [163] employed a rotating apparatus in a wind tunnel to alter the orientation of a building model, thereby mimicking real-world wind variations. The visualisation results indicated that the boundary layer of the CV jet flow aids in diluting indoor air, and if the aperture is excessively wide or the wind speed is too high, the ventilation efficiency diminishes owing to inadequate mixing of indoor air. The enhanced mixing effect of the CV flow suggests that shifts in wind direction could further boost ventilation efficiency. Sim et al. [164] explored the basic characteristics of airflow in a single-zone building model using the Particle Image Velocimetry (PIV) technique in a wind tunnel. The study identified two vena contracta acceleration zones in cross-ventilation systems: one located downstream of the input opening (windward) and the other downstream of the output opening (downwind). These zones exhibited the smallest stream diameters and highest velocities (leeward). As the airflow entrains the relatively static surrounding flow, the speed of the impinging jet flow increases, peaking shortly after entering the intake orifice, and then gradually decreases. In scenarios with higher A^* , the vena contracta effect was more significant. The vertical position of the intake aperture significantly affects the inflow direction owing to the recirculating flow vortex formed in front of it. The lower part of the entering flow recirculated the external airflow along the floor and front wall. However, the top half of the approaching flow was separated by the front edge of the building model. Consequently, when the opening was situated in the middle or lower part of the windward wall, a downward inflow occurred, whereas an upward or parallel inflow was observed when the opening was positioned in the upper section of the windward wall. Ricci et al. [165] investigated the flow dynamics of a cubic building model's Curtain Wall (CV) in a water tank using flow visualization, Particle Image

Velocimetry (PIV), and Computational Fluid Dynamics (CFD). The study verified that the peak airflow velocity at the vena contracta was located $0.1 L$ (where L represents the diameter of the cube model) downstream of the intake hole. The PIV and CFD results revealed that when the windward and leeward openings were symmetrical, two eddies formed on either side of the CV jet. The CV jet flow did not interact significantly with the room fluid, leading to poor ventilation efficiency owing to weak mixing. Researchers tracked particles in unsteady CFD simulations to assess the effect of CV airflow replacement. The findings showed that the asymmetric opening design, despite having a lower ventilation rate, was more effective in replenishing the internal fluid than the symmetric configuration. The extensive use of PIV and LES now allows researchers to examine the transient airflow properties of CVs in detail. Poerschke et al. [166] identified flapping jets and Kelvin–Helmholtz instability in jets entering the intake aperture of a wind tunnel. Building on previous studies [167–170], further research is needed to explore the impact of surrounding buildings and wind direction in urban settings. It is widely recognized that the angle of wind attack and the density of nearby buildings significantly affect CV airflow characteristics by creating various vortex forms in adjacent street canyons. A room's ability to maintain good indoor air quality heavily relies on effective air mixing. Adequate air mixing facilitates the distribution of fresh air throughout a room, thereby minimising stagnant air pockets that can negatively impact indoor air quality. However, achieving proper mixing with natural ventilation systems may result in uncomfortable, localised drafts for occupants [171]. When designing a CV system, it is crucial to balance the need for sufficient thermal comfort with the need for effective mixing. It may not always be feasible to attain optimal air mixing and thermal comfort using CV alone. In such cases, additional measures, such as installing mechanical ventilation systems or utilizing other methods like radiant heating or cooling, may be necessary to maintain suitable indoor air quality and create a comfortable indoor environment.

2.5. Pilot-Scale Applications

2.5.1. Vector Composition Model

Several CV prediction frameworks have been proposed for CV ventilation models [132–167]. The Orifice equation, which is based on the Bernoulli equation, is a classic technique for calculating the volumetric airflow rate via a single orifice and the overall volumetric airflow rate of a space for cross-ventilation. The equation comprises:

$$Q_w = \sqrt{\frac{1}{\zeta}} A \sqrt{\frac{2(p_w - p_i)}{\rho}} \quad (1)$$

$$Q_l = \sqrt{\frac{1}{\zeta}} A \sqrt{\frac{2|p_w - p_l|}{\rho}} \quad (2)$$

Where Q_w and Q_l is the flow rate through the windward opening and leeward opening, respectively, ζ is the pressure

loss coefficient of an opening, ξ is the overall pressure loss coefficient of the whole room, and A is the opening area (m^2) ρ is the air density (kg/m^3) p_w, p_i and p_l (Pa) is the pressure at the windward, indoor, and leeward sides, respectively. By substituting the pressure with the wind pressure coefficient, which is determined by Equations (1) and (2), the Orifice equation can be rewritten as

$$Cp_e = \frac{P_e - P_{ref}}{\frac{1}{2}\rho U_{ref}^2} \tag{3}$$

Where,

$$Q = (C_d A)_{eff} U_{ref} \sqrt{Cp_w - Cp_l} \tag{4}$$

Cp_e is the wind pressure coefficient, P_e the static pressure on the external surface of the wall of the sealed model, P_{ref} is the static pressure at the reference point, and U_{ref} is the free stream velocity at the reference point. The reference point was situated inside the undisturbed oncoming flow, which was unaffected by the presence of the target building. Cp_w and Cp_l represent the wind pressure coefficients at the windward and leeward openings, respectively. The discharge coefficient C_d is frequently calculated using the chamber approach, as shown in Figure 1(d)–(f). A typical chamber approach employs a motorised fan to draw air from one side of the exhaust system.

The pressure loss coefficient (ζ_p) of a single aperture is calculated based on the difference between external static pressure (P_{S1}) and internal room pressure (P_{S2}), as well as the volumetric flow rate. To determine the total pressure loss coefficient (ξ) of a room, place a model in the chamber depicted in Figure 2(a)–(c). Extensive studies have been conducted on discharge coefficients. Li et al. [172] examined earlier studies on a variety of variables that affect C_d , including Reynolds number, wind angle, opening porosity, opening shape, and opening position. A meta-analysis of many studies showed that the C_d varies according to the experimental setup and should be used sparingly within reason. The author also emphasised the need to determine the validity and limitations of the Orifice equation. Under the assumptions of a sealed model, turbulent flow, and energy dissipation, the Orifice equation was applicable based on the following observations and assumptions:

1. Fully turbulent airflow was observed in the study.
2. The pressure coefficient of the sealed structure serves as the driving force for the flow, as the presence of an opening does not influence airflow around the building.
3. The kinetic energy dissipates immediately after opening because the pressure difference between the inflow and outflow openings is equal to the static pressure difference.

The Orifice equation becomes inaccurate, leading to an erroneous prediction of the ventilation rate when these conditions are not fully met. Lee et al. [173] noted that when

the distance between openings is relatively small compared to the size of the opening, the resistance of the openings influences each other. Below is a definition of the interference coefficient (m):

$$m = \frac{\xi}{\sum \zeta_\theta} \tag{5}$$

In order to determine the m , Kravchenko et al. [174] conducted a number of trials with the assumption that the opening areas and the wind attack angle were equal. According to his findings, when L/\sqrt{A} If it is at least 10, the value of m can reach 1. The interference coefficient m will exceed 1 when the cross-ventilation openings are not aligned at the wall's centre line due to energy loss from the windward impinging flow striking at the wall and friction loss from surrounding walls as the angle θ between the wind direction and the line of two opening centres increases. It suggests that although the chamber technique produces the accurate total pressure loss coefficient ξ , the discharge coefficient obtained in the traditional chamber approach may be overstated.

The total pressure loss coefficient ξ is affected by the direction of the incoming wind, as Kemp et al. [175] have shown. Based on vector decomposition, we developed a simpler prediction approach that simultaneously predicts the airflow rate and input direction. The vector decomposition approach assumes that if there is an opening, the wind velocity parallel to the wall is almost constant and the aperture is relatively small. Figure 2(a) illustrates the workflow of our vector composition model. The relationship between the direction of the incoming wind and the room's overall pressure loss coefficient (ξ), as determined beforehand using chamber procedures (b). The Wind Pressure Coefficient (WPC) and velocity parallel to the wall (v_w) of the sealed model were first determined based on the direction of the oncoming wind, the geometry of the building, and the position of the room. These parameters were measured using a wind-tunnel test.

Second, the airflow rate and v_w are used to compute the inflow direction at the windward opening θ . The airflow rate Q was then determined using the Orifice equation using ξ , which was obtained from the empirical connection between θ and ξ . Finally, using repeated computations, the airflow rate Q and the inflow angle θ may be determined concurrently. This method requires three sets of data: (1) wind pressure coefficient at the opening, C_p , (2) wind velocity parallel to the wall v_w , (3) the relationship between θ and ξ . In a wind tunnel, a three-story dwelling with various room placements was used to verify this technology. The findings demonstrate that the vector composition model is inaccurate only when the approaching wind direction is 80° or more, and only when pulsation flow and turbulence diffusion predominate in the separation domain during ventilation.

2.5.2. Catchment Theory

In an examination of the fundamental assumptions behind the Orifice equation, Syrios and Hunt [176] described the flow through openings in cross-ventilation as a 'catchment issue'. To simplify the complexity of airflow through an actual building, a basic circular disk and cylinder in the free stream were analysed using a wind tunnel and numerical simulations. The CFD results illustrated the 'flow tube' of air moving through the aperture, with a distinct boundary between the air passing through the opening and the air bypassing it (Figure 2(b)–(d)). The flow tube consists of three main components: vena contracta, catchment region, and retardation area. The catchment area is defined as the free-stream velocity divided by the ventilation rate [177].

$$Q = A_c U_0 \quad (6)$$

Where A_c is the catchment area (m^2), U_0 is free stream velocity (m/s). The retardation section is the flow tube segment with the lowest dynamic pressure and the highest static pressure at the centreline of the flow tube. The segment of the venous system that interacts with the flow tube after it passes through the aperture is where the fluid continues to move even when the pressure is equal to the room pressure. This study investigated the effect of porosity (ratio of opening area to wall area) on the applicability of the standard Orifice equation. The Orifice equation is characterised by a limited catchment zone and an undefined retardation area. The assumption of a sealed model is valid when the porosity is low or when the retardation area is significantly larger than the opening area. However, the Orifice equation becomes invalid when the porosity exceeds 35%, as the dynamic pressure in the retardation section surpasses the static pressure. Hasan et al. [178] highlight notable differences between a sealed building and one with relatively large openings, such as:

1. In a sealed structure, a wake is consistently present on the leeward side, whereas wakes are not always visible in buildings with openings.
2. When airflow approaches a sealed structure, it can only pass around it. In contrast, when approaching a building with an opening, the airflow may either enter through the opening or move around it.

These observations illustrate why using pressure coefficients from the sealed building model to predict cross-ventilation rates is not always reliable. Cross-ventilation flows can be easily understood using catchment theory. However, this theory was not developed to provide a straightforward method for calculating the CV flow rate, and the goal of this study was to achieve a simple geometry in a uniform fluid without validating a building model under boundary layer conditions.

2.5.3. Local Dynamic Similarity

Various prior studies have shown that factors such as the size and location of openings, wind direction, and ventilation

rate significantly influence the discharge coefficient. A local dynamic similarity model was introduced to predict the discharge coefficient and flow angle at the CV input opening more accurately [179–181]. The ventilation airflow was represented as a virtual stream tube by releasing passive markers from upstream of the opening using LES, akin to the 'flow tube' concept in catchment theory. When the wind angle exceeded zero, the airflow adhered to the wall before passing through the window into the room, resembling a wall jet or a boundary-layer flow [182]. Cheng et al. [184] confirmed the effectiveness of using CFD and the local similarity model to analyze CV, with simulation results indicating that the local dynamic similarity model can accurately estimate the ventilation rate of CV. Furthermore, the precision of the model remained consistent despite changes in the size and location of the inflow openings. Berouine et al. [185] conducted an experimental analysis on the link between P_R^* and C_d of rear apertures, and the local dynamic similarity model remains true. P_R^* can predict discharge coefficient, and velocity data near a sealed model's opening position may substitute tangential dynamic pressure (P_t).

2.5.4. Power Balance Model

As mentioned earlier, the Orifice equation relies on three assumptions to estimate the CV ventilation rate, but these assumptions are not always accurate. Bai et al. [186] investigated the energy dissipation process in CV airflow using LES. Essentially, the wind pressure coefficient of the sealed body alone is insufficient for calculating the CV ventilation rate because the kinetic energy remains undissipated downstream of a large intake opening. Abu Qadourah [187] introduced a stream tube model with multiple control volumes encircling a structure. Equation (7) illustrates the power balance equation for a single control volume.

$$PW_A = PW_B + PW_C + LP_{ABC} \quad (7)$$

PW_A and PW_B is the transported power at sections B and C, respectively, and LP_{ABC} indicates the lost power in the control volume. The separating flow at the bluff body corners, outdoor dissipation (control volumes 2 and 5), indoor dissipation (control volume 4), diverging flow (control volume 1), and converging flow (control volume 7) contributed to the energy loss throughout the virtual stream. The total pressure loss coefficient ζ can be used to calculate the precise amount of energy lost along the whole stream tube. Zamora Mestre and Niampira [188] conducted a comparison between the discharge coefficient C_d , derived from the CV chamber method with varying porosity, and the total pressure loss coefficient of a virtual stream tube, calculated using CFD. However, the chamber method proved effective when the porosity was below 21% [189], and the ventilation rate for a large opening was overestimated when an appropriate discharge coefficient was applied. Stopps and Touchie [190] further explored this by performing wind tunnel tests and CFD analyses on the power transmitted and lost within the stream

tube of a suspended rectangular model, specifically a pitched–roof single–story dwelling model. In contrast to the Orifice equation, based on the actual airflow, the power balance model uses a ratio–based approach to predict the CV flow rates. However, this model has not been thoroughly tested or validated. Numerous studies have been conducted to explore the factors influencing cross–ventilation, and the results have aided designers in utilising cross–ventilation more effectively.

This section highlights some of the key elements of previous research. Figure 3 (a) Simulation results of the RNG $k - \epsilon$ framework (with enhanced wall function for first layers $y^+ < 1$, which delivered good agreement between CFD and experimental results) expressed as a Notched box chart with outliers; (b) Verification of experimental results with direct absorption. $(\tau_1 \cdot \alpha_2 \cdot I_{\text{solar}})$, wherein the influence of the low–e coating's reflectivity on the outer façade is determined by the secondary reflection. $(\tau_1 \cdot \rho_2 \cdot \alpha_1 \cdot I_{\text{sola}})$ illustrated as raincloud and grouped–violin plots; (c) Posthoc verification of the data plots pertaining to ventilation rate (that performs almost in a power function correlation over the value of $\cos \theta: V = 0.041(\cos \theta)^{0.31}$ ($R^2 = 0.9983$) for NVDSF I; and $V = 0.047(\cos \theta)^{0.31}$ ($R^2 = 0.9971$) for NVDSF II, where V is the volume flow rate (m^3/s) and θ is the incident angle), illustrated as cross–validation and anomaly detection

2.6. Technical Parameters

2.6.1. Wind Properties

Wind plays a crucial role in driving CV airflow and significantly impacts the ventilation performance of the CV. Research has examined how various fixed wind directions affect the CV ventilation rate using Computational Fluid Dynamics (CFD) [97, 144] and wind tunnel experiments [191–193]. The wind angle is defined as the angle between the vertical line of the apertures and the direction of the incoming flow. At a wind angle of 90° , the wind direction was parallel to the aperture, whereas at 0° , it was perpendicular to the opening. Across all studies, it was found that the CV ventilation performance diminished as the wind angle increased from 0° to 90° . Pashchenko and Rassadin [194] noted that the highest ventilation rate occurred when wind directions ranged from 0° to 15° , attributed to a smaller mean pressure difference between the two openings [195]. The study also found that the ventilation effectiveness between 0° and 20° was not significant. Papadopoulos et al. [195] employed the spectral proper orthogonal decomposition method to assess the contributions of mean flow and turbulence to CV at 0° (windward and leeward openings) and 90° to understand the CV mechanism with varying wind angles (both openings on the lateral side).

In this scenario, when apertures are located on the lateral wall, turbulence is considered the primary source of ventilation, as the separation flow at the edge of the frontal wall introduces irregular eddies that enhance the ventilation. This type of ventilation phenomenon, influenced by turbulent

eddies in the shear layers of the lateral wall, is also referred to as shear [196] or turbulence–induced ventilation [197]. Nimarshana et al. [198] identified discrepancies between full–scale data and wind tunnel tests concerning the airflow inside the CV and the surface pressure. Researchers have attributed this difference to the variable wind direction and speed in full–scale measurements, which were not replicated in the wind tunnel experiments. Mortezaadeh et al. [199] utilised Katayama's findings to validate an LES simulation that incorporated changing wind speed and direction as incoming flows. Unlike the visible recirculation zone behind the building, which had a constant incoming flow, achieving vortex shedding on the leeward side was more challenging because of the variable wind direction and speed.

A steady wind direction led to a thinner, deeper speed core with reduced energy loss, whereas a changing wind direction resulted in a more evenly distributed interior air velocity and increased surface pressure. Even a slight change in the wind direction can cause flow reversal, highlighting that minor wind changes can significantly impact the ventilation rate and building surface pressure. Megri et al. [200] compared time series of wind direction and building surface pressure from on–site data, emphasising that hourly averaged wind data are not always sufficient for CV design. Mateus et al. [201] conducted a year–long field study to examine the effects of changes in wind direction and speed on CV airflows. To fully comprehend the unstable airflow rates, both the wind direction and speed must be considered. A frequency analysis of the wind speed and direction revealed that the fluctuation components of the wind direction were not correlated with the wind speed.

2.6.2. Surrounding Buildings

The airflow dynamics of a Chimney Ventilation (CV) system are significantly influenced by nearby structures, with a higher building density often resulting in reduced ventilation rates [203]. M'Saouri et al. [204] employed Particle Image Velocimetry (PIV) to examine the average and instantaneous airflow properties of a CV within a wind tunnel, considering both aligned and staggered configurations of adjacent buildings. The design of the surrounding buildings notably impacted the airflow patterns, both mean and instantaneous, highlighting the importance of addressing the pulsing flow and eddy penetration. Lü et al. [205] validated a Large Eddy Simulation (LES) using the same building configurations as the observed dataset. At 90° , unstable turbulence was the dominant factor for CV, whereas at 0° , the mean flow was the main contributor. These results align with those of previous studies that utilised different experimental methods and conditions [206]. Li [207] identified an unusual transient flow pattern in the CV within densely populated urban areas (planar area ratio = 0.6), where the inlet alternated between windward and leeward openings. A leeward vortex generated a leeward jet, whereas the street canyon flow along the building walls influenced the windward jet, leading to different frequencies

between the two jets. Additionally, in densely populated areas with changing wind directions, both leeward and windward jets displayed Kelvin–Helmholtz instability and flapping jet characteristics, which were only observed in the windward jet of an isolated structure. Moreover, the surrounding buildings altered the wind angle with the highest ventilation rate from 0° to 60° , depending on the planar area ratio. At higher planar area ratios, the ventilation rate was notably lower and less sensitive to the wind direction.

2.6.3. Temperatures

Wind typically serves as the primary driver of CV airflow, and CV openings are generally of uniform height. Although there is limited research on how temperature affects CV, it significantly influences CV flow. Linden conducted thorough studies and explored the interplay between buoyancy and wind forces in natural ventilation systems. [207]. To determine the relative strengths of these forces, it is essential to know the Froude number (F_r), which represents the ratio of flow inertia to the external field. In a full-scale experiment with forced unidirectional flow of SSV, Heidari and Eskandari [208] showed that the discharge coefficient, C_d , declined as temperature differences rose, demonstrating the transition from wind-dominant flow to buoyancy-dominant flow. Despite the experimental apertures being positioned at varying heights, Hauge et al. [209] investigated the influence of temperature on CV by substituting the temperature difference between indoor and outdoor settings with an ethanol solution in a water tank. Hang et al. [210] examined how local buoyant flow from an internal heat source affects wind-driven Cross-Ventilation (CV) in full-scale multizone test buildings through Computational Fluid Dynamics (CFD). The study indicated that enhancing indoor mixing, even with a minor local heat source, significantly affected the CV and increased the ventilation rate. Hosseini et al. [80] studied the effect of indoor–outdoor temperature differences on CV flows using a water tank with apertures at the same height. The temperature difference had a minimal impact on the ventilation rate of the wind-dominated CV ($F_r > 1$). During buoyancy-dominated ventilation ($F_r < 1$), wind had a substantial effect on CV airflow, resulting in a 40% increase in the ventilation rate.

2.6.4. Opening

Architects and engineers face difficulties in identifying the best configuration for openings when designing structures for natural ventilation. The rate of airflow and velocity of the indoor stream can vary based on the size of the openings [211]. Two centrally located openings on the façade might result in a higher CV flow rate at the same elevation as apertures positioned at the building edges [212]. Increasing the size of the leeward opening proved more effective in enhancing the ventilation rate than switching from a single opening to a CV, which showed less noticeable improvement [213]. The internal airflow pattern, including the indoor recirculation zone, is influenced by the shape and location of the aperture, as well as the ventilation rate [214]. The assumptions of the

Orifice equation are also influenced by the ratio of the aperture to the wall [215–217].

2.6.5. Other Architecture Elements

Louvre blinds are frequently used as a shading technique to prevent heat from being absorbed by the sun, which naturally alters the airflow through the CV. Candanedo et al. [218] conducted a wind tunnel experiment and CFD of CV in a building with varying angle louvres (0° , 15° , 30° , 45°). While 45° louvres caused a perceptible shift in the airflow direction and increased the velocity at the opening intake, lower louvre angles resulted in a higher interior velocity at the centre of the room. Banihashemi et al. [219] placed a louvre in front of an aperture in a model building and studied the pressure loss at various louvre angles. The louvre angle had varying effects on the pressure loss, and the CV ventilation rate decreased at various rates. When the louvre angle was 90° , the lowest ventilation rate compared to that of the room without shading devices was maintained at approximately 47%. The findings of this study revealed a substantial relationship between the louvre angle and discharge coefficient, implying that both the airflow characteristics and porosity of the louvre angle influence the ventilation rate [220]. Balali et al. [221] conducted RANS simulations of CV ventilation rates in a low-rise building with a louvre with 0° , 15° , 30° , 45° , 60° , 75° and found that a 75° louvre reduced ventilation rates by 66.6%. In wind tunnel tests and RANS simulations, Alqahtani et al. [222] explored the impact of louvre positioning on CV. The highest volume flow rate was observed when both wall openings were positioned at the top, which was 1.4% greater than that in scenarios without louvres. Conversely, when the openings were located at the bottom, the flow rate was at its lowest, 23.7% less than that in cases without louvres. Eaves are another common shading device used in buildings. Abedrabboh et al. [223] conducted an in-depth study on how different eave angles affect the windward and leeward sides of a sloped roof. The RANS simulation results indicated that the volume flow rate of the CV could be enhanced by up to 24% through the design of windward and leeward eaves. The study also discussed the influence of other architectural elements, such as rooftop wind catchers [224] and roof geometry [225], on CV. The effect of an interior partition can be assessed using the discharge coefficient of the internal partitions, similar to determining the discharge coefficient of an external opening. Yu et al. [226] used the chamber method to determine the internal discharge coefficient and found that internal porosity dictated the internal opening discharge coefficient, whereas porosity and external opening locations had no effect. The orifice method, which accounts for both internal and external opening discharge coefficients, can be applied to calculate the CV ventilation rate in spaces with interior obstacles such as furniture. In a later study, Yazarlou et al. [227] developed an empirical correlation function between the internal block ratio and internal obstacle resistance. When the exterior porosity ratio is below 3%, the indoor obstacle resistance can be disregarded. However, if the indoor barrier resistance exceeds

the exterior opening resistance, the CV ventilation rate is affected. Yang et al. [228] utilized CFD modelling to examine the effects of various interior walls on CV, finding that vertical internal obstructions had a more significant negative impact on CV ventilation rate than horizontal ones.

3. Results and Discussion

3.1. Case A: Multizone Building

The construction sector is responsible for 36% of the global final energy use and 39% of CO₂ emissions [229]. In 2018, the residential sector accounted for 26.1% of the European Union's total energy consumption [230]. Consequently, initiatives are underway to reduce energy usage by creating new sustainable buildings and retrofitting existing ones. Gan et al. [231] suggested using white-box models developed with building energy simulation tools to assess potential cost- and energy-efficient design options. However, there can be significant differences between the simulated and actual data [232]. Discrepancies between the design phase and construction, degradation, or unpredictable occupant behaviour can lead to inaccurate simulation outcomes [233]. However, the application of simulation tools has been limited. The reliability of Building Energy Simulation (BES) tools is hindered by an inadequate definition of BEM accuracy and a lack of confidence [234]. Building energy model validation is divided into two categories: realistic and idealized [235]. Idealised validation employs a test cell with sensors to verify the accuracy of the model concerning Heating, Ventilation, and Air Conditioning (HVAC) system parameters. In contrast, realistic validation considers factors such as buildings, HVAC, and occupancy. Several validation standards have been established to test the fundamental heat and mass transport models used for predicting energy consumption and thermal comfort in buildings. The International Energy Agency (IEA) has initiated programs to assess building energy model approaches, such as the BESTEST method [236], which has also been utilised to evaluate the accuracy of the calibration process [237] and the PASSYS method [238], developed by the European Commission. However, neither method considers the effects of occupancy; instead, the study relies on idealised conditions using test cell data. These may reveal weaknesses and limitations that hinder the prediction of dynamically complex structures. As new building designs and energy-saving technologies emerge, it is crucial to thoroughly test simulation programs using real-world data from residential and commercial buildings. The International Energy Agency Energy in Buildings and Communities (IEA EBC) Annex 58 'Reliable Building Energy Performance Characterisation Based on Full Dynamic Measurements' [239] facilitated the full-scale empirical validation of physical building models created using various simulation programs. The Twin Homes were equipped with a cutting-edge testing laboratory that assessed all boundary conditions and evaluated a wide range of interior and boundary variables. The findings indicate that some algorithms can effectively model building plans [240]. To streamline the experiment, Annex 58

eliminates the occupancy factor and focuses exclusively on the thermal performance of the building envelope. An extension of the Twin Houses experiment was conducted to evaluate the building energy modelling techniques [241] of IEA EBC Annex 71 'Building Energy Performance Assessment Based on Optimal In-situ Measurements' [242]. The latest experiment explored synthetic users with stochastic internal heat gains interacting with time-varying heating inputs to modify the thermal energy dynamics of a building [243]. This study also addressed other significant issues, such as the influence of occupancy and building service equipment [244]. Additionally, several articles have been published that offer experimental datasets for the validation and enhancement of simulation programs and building energy modelling methods. Prades-Gil et al. [245] experimentally validated a building energy performance simulation tool (DETECT) in a real test room with free-floating temperature. Kang and Van Hooff confirmed the accuracy of a lumped thermal model in predicting the thermal behavior of a building test facility [246]. Peksen et al. [247] utilized field data to validate a school BES model created using IDA ICE, accommodating occupied times with air, open windows, and doors, which were simulated using a linear regression technique. Norvihoho et al. [248] examined four different BES tools, Dymola, EnergyPlus, IDA ICE, and TRNSYS, to compare measurement data with the results of a test box model's Computational Fluid Dynamics (CFD), which included thermally active building systems. Najafi Ziarani et al. [249] provided a reliable empirical dataset for a small office building with an occupancy simulation during the cooling season to assess building energy analysis computer programs in line with the American Society of Heating, Refrigeration, and Air Conditioning Engineers (ASHRAE) standard 140. A systematic approach to empirical validation focuses on commercial building envelopes and HVAC systems. This study aimed to test a building model developed using a simulation tool to predict the thermal performance of buildings under realistic and complex conditions, which is necessary to evaluate the thermal performance of buildings considering human behaviour. The simulation outcomes were validated using publicly accessible data from the Twin Houses empirical validation experiment of the IEA EBC Annex 71 [250]. This study differs from previous studies in that it simulates airflows resulting from the opening of windows and doors, divides the test building into ten distinct rooms, and incorporates room-specific heating profiles along with stochastic variations for increased occupancy in each room. Building energy modelling can utilise three types of airflow models: multizone models [251], zonal models [252], and CFD [253]. The latter two are currently being explored and require further studies. Energy modelling software can be integrated with well-known airflow models, such as CONTAM [254] and COMIS [255]. TRNFLOW was employed to create an integrated multizone airflow model for Twin Houses by merging the COMIS airflow model with the TRNSYS dynamic building model. This approach has been

used to develop modelling communities for more than a decade [256, 257]. The multizone model was constructed within the TRNSYS environment, which allows for the inclusion of thermal bridges in the model, significantly affecting the heat transfer. This study aimed to evaluate the capabilities and limitations of dynamic building modelling and its integration with airflows in the TRNSYS system using hypothetical user scenarios. The results indicate that TRNFLOW can accurately simulate room temperatures throughout the heating season, as well as the effects of natural and mechanical ventilation and infiltration on room temperature.

3.1.1. Sample Assessment

Figure 1(d) shows the exterior view of the Twin Houses situated at the Fraunhofer Institute for Building Physics in Holzkirchen, Germany. These twin residences are individually known as N2 and O5 dwellings. The primary experiment for the validation exercise involved the use of electric heaters in an N2 dwelling, whereas the other five houses employed an underfloor heating system. This was the only difference between the two homes. To evaluate the capability of the multizone building model to handle stochastic internal gains, diverse temperature profiles, mechanical ventilation, and the opening of windows and doors, a comprehensive experiment in an N2 house is suggested. The house comprises three levels: basement, ground floor, and attic. Figure 1(e) shows the layout and dimensions of the interior of the house. This model considers each room as a distinct thermal zone. The maximum height of the attic, with a 30° roof pitch, is 6.52 m above the ground, whereas the basement and ground floor are 3.37 m and 2.96 m high, respectively. Throughout this study, numerous technologies were employed to measure all factors affecting the energy efficiency of houses. The Twin Houses experiment from the IEA EBC Annex 71 [258] provides a list of measurement channels comprising 224 inputs, with 182 being direct sensor data and the rest being fixed points for temperature or calculation. Tables 1(b) and 1(c) summarise the monitoring data used in this study. The test algorithms gather data from various phases to forecast the temperature and heating inputs based on measured boundary conditions and building specifications. Table 2 presents the details of each experimental phase. The main experiment commenced with a co-heating test. This method assesses the envelope performance and compares the actual behaviour with that of the design. The objective was to measure the total heating power required to achieve and maintain a higher interior temperature throughout the test using highly controlled and measurable technologies [259]. This phase, spanning from 7 December to 19, 2018, is a basic constant temperature phase that corrects the building heat losses. Each room was equipped with an electric heater to maintain a constant temperature of 21°C and a fan to prevent temperature stratification. All interior doors were opened, mechanical ventilation was turned off, and no occupancy profile was detected. According to this

hypothesis, given the appropriate weather conditions, ground characteristics, envelope features, thermal bridges, and infiltration, the predicted heating energy demand of the model should align with the actual electricity consumption. User Phase 1 began at 14:00 on 19 December 2018 and concluded at 10:30 on 1 February 2019. During this time, all zones maintained the same set-point temperature heating profile of 21°C, with a night setback to 17°C between 23:00 and 6:00. All interior doors were open, except for the attic trapdoor, which remained closed. At this point, the roller blinds on the living room window facing the west wall were shut. Minor changes in occupancy were observed between the rooms, and user interactions were facilitated through a mechanical ventilation system. Stochastic models have been suggested to create variations in the duration and spatial distribution of animal occupancy. For Phases 1 and 2, stochastic occupancy profiles were provided that varied daily. According to Landsberger et al. [260], these profiles were derived from a Markov chain model based on time-use survey data and simulated for households with two children. Figure 2(b) shows the synthetic user profile created for a single day in each of the heating zones. User Phase 2 introduces complexity by managing the door between the kitchen and living room, as well as the window in Room 1, which leads to variable airflow. The windows were opened and closed every 24 h. The door between the living room and kitchen was open from 6:00 to 24:00 and closed from 0:00 to 6:00. The mechanical ventilation system remained operational throughout this phase. The heating temperature profiles included significant room-to-room occupancy fluctuations and stochastic variability in each room. Roller blinds were drawn on the west walls of the kitchen and living room. Additionally, the attic trap door remained open, while the interior door of the sleeping room remained locked. Heater power usage was displayed in User Phases 1 and 2, and a multizone model was employed to predict the interior temperatures of each room. At these stages, the question arises as to whether the program can accurately capture the temperature dynamics in each zone using the associated heating loads without relying on an ideal heating model for the specified temperatures.

3.1.2. Framework Algorithm

Utilising the data provided in the home design, the TRNSYS 3D plug-in for SketchUp was used to create the geometry of the dwelling. Each room was crafted to mirror the layout of the original house, with every space in TRNSYS being designated as a thermal zone. Figure 2(c) illustrates the geometric model generated using SketchUp. This model was transferred to TRNBUILD and integrated with TRNFLOW to design the infiltration, ventilation, and operation of windows and doors. The empirical validation exercise outlines the materials used for each construction. Table 3 presents the total thickness and heat transfer coefficients (U values) for each structure. The walls had an exterior solar absorptivity of 0.23, whereas a roof with an exterior absorptivity of 0.63 was suggested. The MoWiTT and BLAST models were used in the

DOE-2 technique to determine the external convection coefficients of the outer walls based on the ambient temperature, wind speed, and wind direction [261]. The tiles forming the outer layer of the roof were excluded from the construction process because this study did not create an airtight barrier (Table 4). The solar absorptivities of the components were added to the outer layer of the model. The exterior convection coefficient was $10.4 \text{ W/m}^2\text{K}$, which represents the average of the normal interior and exterior convection coefficients. The internal convection coefficients were calculated using the TRNBUILD internal calculation option, which considers vertical walls, floors, and ceilings. Inside doors were modelled in SketchUp as windows and assigned the glass ID '10001' from the TRNBUILD library, indicating 'no glazing'—equivalent to being open. According to TRNBUILD, the front door was described as a 100% frame, with the same U-value ($0.94 \text{ W/m}^2\text{K}$) as. The homes featured five different window types based on size. Despite their varying sizes, all windows were constructed with double-glazing, argon filling, and a low-emissivity coating. The windows had a solar heat gain coefficient (g-value) of 0.62 and a frame U-value of $1 \text{ W/m}^2\text{K}$, resulting in a window U-value of $1.1 \text{ W/m}^2\text{K}$. Because the TRNBUILD library lacks suitable window glazing, Blender 3D software (version 4.0, <https://www.blender.org/>) was used to create glazing with identical properties but formatted for use in TRNBUILD (Table 5). During User Phase 1, the roller blind on the west wall of the living room was shut, whereas in User Phase 2, the roller blind of the kitchen window was closed. The 'external shading factor' feature in TRNBUILD simulates the closure of an external roller blind. The external shading properties of the windows were assessed using a variable model input. A model input of 0 signifies no shading with open roller blinds, whereas an input of 1 indicates complete solar blockage when the blinds are closed. An empirical validation exercise using HEAT 2 software provided the thermal bridge values for the homes (Table 6). These thermal bridges encompass windows, roof connections, and junctions between walls and ceilings, walls, and floors (rake and eave junctions). In TRNBUILD, linear thermal bridges are represented as 'cold-bridges,' which are massless walls with specified lengths, orientations, and linear thermal resistances. Tables 7–9 detail the thermal bridges in each thermal zone on the attic and ground floor. Within a thermal zone, all thermal bridges with the same orientation are combined into a single bridge by summing their lengths. The equivalent linear thermal transmittance or Ψ -value ($\text{W/m}\cdot\text{K}$) was determined by weighting each Ψ value according to its contribution to the total length of the wall. As a result, TRNBUILD installed an equivalent external thermal bridge in each thermal zone and in each direction. Additionally, internal thermal bridges were provided, as shown in Table 10. TRNBUILD does not have a specific function for introducing internal thermal bridges; therefore, the study was calculated using TRNSYS equations and incorporated into the building model as negative wall gains. Column thermal bridges were calculated by multiplying the

point thermal bridge value, or χ value (W/K), by the temperature difference between the column and the floor or ceiling. The columns were installed in the living room, dining room, kitchen, and bedrooms. To determine the thermal bridges related to the internal partitions, the length of the junction between the interior wall and floor/ceiling was multiplied by the linear thermal bridge value and the temperature difference between the wall and floor/ceiling. To maintain the temperature in the thermal zone at monitored levels, precise heating and cooling systems were integrated into the basement. This setup ensured that the heat exchange between the ground floor and basement mirrored that of a typical home. During the co-heating phase, each thermal zone was equipped with a suitable heating system. An ideal heating system possesses an infinite heating capacity to maintain the zone temperature at 21°C , which is the goal of co-heating. Fans were used to ensure a consistent air temperature during the co-heating process. Consequently, each room achieved a 100% convective internal gain while consuming the same power as the fan. Users' Phases 1 and 2 supplied the electrical power required to heat the rooms to the desired temperature profiles. Consequently, the optimal heating during the co-heating period was deactivated, and each thermal zone received the measured heating power as an internal gain with a 30% radiative and 70% convective split, in accordance with the electrical heater requirements of the supplier. Each thermal zone, except for the hall and stairs, was equipped with an Electric Heater (EH). Additionally, the model incorporates Internal Heat Sources (IHS) to simulate human activities, such as occupancy and device usage. Electric heaters with the same heat output as the synthetic user profiles were used to mimic the synthetic user behaviour. Consequently, the model included these IHSs as heat gains, with a power distribution of 30% radiation and 70% convective heat. Each thermal zone, except the dining room, staircase, and foyer, was fitted with an IHS.

3.1.3. Machine Learning Analysis

TRNFLOW integrates the multizone airflow model COMIS with the TRNSYS thermal building module (Type 56). It facilitates the computation of airflow originating from outside the building owing to ventilation systems, such as infiltration, and between thermal air nodes (zones). TRNFLOW conceptualises buildings as networks of airflow links and nodes. The airflow links symbolise openings, such as doors, windows, cracks, and ventilation components, whereas the air nodes represent rooms and the building environment. This combined multizone airflow model can be employed to calculate the interior temperatures while accounting for the airflow dependency. The TRNBUILD interface allows the specification of data from both airflow and temperature models. Figure 3(a) illustrates the schematic of the TRNFLOW network designed for the attic and ground levels. Tables 11(a) and 11(b) detail all the airflow connections necessary to replicate the airflow from the interior doors and windows, ventilation (fans and straight ducts), and

infiltration (cracks). The residence was equipped with a mechanical ventilation system with an air change rate of 0.6 h⁻¹. Ventilation ducts entered the home by drawing air from outside through the north façade, channelling it to the basement, and heating it when the electric preheater was operational. With a ventilation flow of 100 m³/h, the ground floor supply air duct originated in the basement, traversed the kitchen, and reached the supply point in the living room. The bathroom and dining room were equipped with ground–floor exhaust air fans with a capacity of 50 m³/h. The attic ventilation ducts were routed from the basement to the stairs through a living room shaft. Children's Rooms 1 and 2 were equipped with a 50 m³ supply air fan and an exhaust air fan, respectively. The ventilation system was modelled using TRNFLOW, which includes fans, straight ducts, and air nodes. The flow rates of the two types of fans were specified as 100 m³/h and 50 m³/h, respectively. A 100 m³/h fan at the lowest level connected the auxiliary air node to an outside air node. The user sets the temperature and humidity of the auxiliary air nodes. In this scenario, the auxiliary air node gathers temperature and humidity data from the supplied ventilation air. The auxiliary and thermal air nodes in the living room were connected through a direct exit duct.

In the dining room and bathroom, the thermal air nodes were linked to their respective auxiliary air nodes for the exhaust air process using a straight duct connection that operated without specific guidelines. Subsequently, an external air node equipped with a 50 m³/h exhaust fan was connected to the auxiliary air nodes. The ventilation network on the ground floor was sealed because the air connections of the interior doors were defined from the thermal air nodes in the living room to those in the dining room and bathroom. A similar setup was implemented for children's Rooms 1 and 2 in the attic. Figures 1 and 2 illustrate schematics of the ventilation configuration used by TRNFLOW to replicate the ventilation system, wherein the supply temperature of the ventilation and the outside temperature have been duly estimated. Therefore, Equation (8) calculates the total heat required to increase the ventilation air temperature from the outside to the supply temperature. The supply air mass flow, \dot{m}_{SUA} , the ventilation supply temperature, T_{SUA} , and the outdoor temperature, T_{OUT} , are known, and the heat capacity of the air, C_{AIR} , is assumed to be 1.0052 kJ/ kg · K. The resistance that heats the outside air before it enters the zone consumes electrical energy. The amount of heat required to increase the outside temperature to the supply air temperature is less than the amount of electricity used in the preheaters. Heat transmission occurs because of the presence of separate duct systems.

$$\dot{Q}_{VENT.} [kW] = \dot{m}_{SUA} [kg/s] \times C_{AIR} [kJ/kg\hat{A} \cdot K] \times (T_{SUA} - T_{OUT}) [K] \quad (8)$$

Subtracting the electrical consumption of the preheaters, \dot{Q}_{SUA_ELP} , in Equation (2), to the total amount of heat

calculated in Equation (1), \dot{Q}_{VENT} , the heat transfer through the ducts into the ventilation air, \dot{Q}_{DUCT} , can be calculated as:

$$\dot{Q}_{DUCT} [kW] = \dot{Q}_{VENT.} [kW] - \dot{Q}_{SUA_ELP} [kW] \quad (9)$$

Heat transfer occurs in the basement, which is used to calculate the coefficient for the heat absorbed by the ventilation ducts on the lower floor. Data analysis showed that a 50% value offered the best fit. Because the ground floor ventilation ducts pass through this thermal area, heat transfer results in a negative heat gain in the kitchen air. The starting point for this heat transfer was located on the living room wall, near the kitchen. The living room wall, which includes the shaft to the staircase, experiences a negative gain owing to heat transfer from the ventilation ducts to the attic. A pressure difference test was conducted to measure the airtightness of the dwellings. The results indicated that with a pressure difference of 50 Pa, the airtightness of the bottom floor was 1.19 h⁻¹, and the overall airtightness of the house was 0.87 h⁻¹. The infiltration rate was determined to be 0.0845 kg/s at the ground level and 0.0214 kg/s in the attic during the 50 Pa test using Air Changes per Hour (ACH) and air volume. The shortcomings of TRNFLOW were used to simulate infiltration within the residence. A fracture represents an air connection between a thermal air node and an external node. This element characterizes the leakage properties of the cracks using the power–law form outlined in Equation (10). The power law is often applied when measuring the ACH at a pressure difference of 50 Pa, yielding statistically significant results [263].

$$\dot{m} [kg/s50 Pa] = C_s [kg/s1 Pa] \times (50[Pa])^{0.65} \quad (10)$$

A crack in TRNFLOW is defined by the flow coefficient C_s , which is calculated by Equation (3), knowing the air mass flow rate \dot{m} at 50 Pa. Table 4 lists the computed values of these coefficients for the three models. Two distinct types of cracks were observed: one located at the attic level and the other at the main level. The model chambers were fitted with linkages that resembled fissures. Table 4 illustrates crack type one for the ground floor rooms and crack type two for the attic room. Each fracture linkage had an orientation and a mass flow coefficient that was multiplied by the C_s value. To preserve the overall air flow mass coefficient (C_s) for both the ground floor and attic, the factors for all rooms associated with the same crack must sum to 1. Owing to the uncertainty in the variation of infiltration levels by thermal zone, these coefficients were manually assigned using a distribution that best aligned with the energy needs of the co–heating phase. All interior doors, except those connecting the living room and kitchen, the sleeping room and hallway, and the trap door, had an opening factor of one, indicating that the study was fully open. The variable input factor controlling these doors changes to one when the door is open and to zero when it is closed. The operable window in Room 1 was designed to mimic a bottom–hinged sash. When closed, the window had

an opening factor of zero, and when opened, it was 0.09. As depicted in Figure 3(a), when the window was open, it was tilted at an 85° angle, which was converted to an opening factor of 0.09 using the cosine function. Figure 8 shows the completed TRNSYS simulation, which includes several components arranged in the Simulation Studio interface. The simulation had a 10-minute time step and ran from December 7, 18:00 to March 1, 0:00. In the TRNSYS simulation, the Type 56 multizone building reads the building file generated by TRNBUILD. Data reader types were employed to read all the simulation measurements, ventilation, and meteorological data. Type 56 was closely linked with parameters such as relative humidity, ground temperature, ambient temperature, wind direction and speed, and effective sky temperature for longwave radiation. A solar radiation processor (Type 16i) was used to calculate solar radiation based on the direction. Given the reported global horizontal and diffuse radiations, Type 16i computes the total incident radiation, diffuse radiation, and incident angle for each of the eight differently oriented surfaces of a home. Type 16i also requires a simulation start day, latitude, solar shift, and ground reflection. The type of ground and the presence or absence of snow affected the ground reflectance. Consequently, when snow was present, the ground reflectance of the grass increased from 0.23 to 0.7.

3.1.4. Empirical Validation

To assess the discrepancy between the simulation outcomes and actual measurements, the following error metrics were employed: the Normalised Mean Bias Error (NMBE), as detailed in Equation (5); the Root Mean Squared Error (RMSE), also outlined in Equation (5); and the Coefficient of Variation of the Root-Mean-Squared Error CV(RMSE), as specified in Equation (7). As indicated in Equation (7), the Mean Absolute Error (MAE) was computed for the temperature forecasting error. According to ASHRAE Guideline 14–2014 [264], NMBE and CV(RMSE) are recommended for evaluating modelling uncertainty. When normalised, the RMSE serves as an indicator of forecast precision, whereas CV(RMSE) facilitates comparisons across different zones. The model bias was effectively assessed using the NMBE, and the MAE was applied to determine the average absolute discrepancy between the simulated and observed temperatures. In Equations (5), (6), and (7), y_i refers to measured data, \hat{y}_i refers to simulated data, and n refers to the size of the dataset.

$$RMSE = \sqrt{\sum_{i=1}^n (y_i - \hat{y}_i)^2 / n} \tag{11}$$

$$CV(RMSE)(\%) = RMSE / \bar{y} \times 100 \tag{12}$$

$$NMBE (\%) = \frac{\sum_{i=1}^n (y_i - \hat{y}_i)}{\sum_{i=1}^n (y_i)} \times 100 \tag{13}$$

$$MAE = \sum_{i=1}^n |y_i - \hat{y}_i| / n \tag{14}$$

To help understand the simulation results, Figure 3(b) shows the outdoor air temperature and solar radiation levels during the experiment. According to the data, solar radiation was low during the first half of the simulation before increasing in the middle of User Phase 1. During the test, the lowest and highest external air temperatures were -16.4°C and 15°C, respectively. Moreover, the outdoor temperature was low at this time.

3.1.5. Error Estimation

The objective of the co-heating phase was to estimate the heating output required to maintain the thermal zone of each house at 21 °C. Although this phase spanned from 7 to 19 December, the first four days were excluded from the study due to initialisation effects, as the model required this time to reach a thermal state comparable to the actual building. Figure 3(c) illustrates the graphical results for both the simulated and observed heating powers during the co-heating phase in each thermal zone. During this period, an electric heater was installed in the Hall thermal zone; however, its consumption was zero in both the simulated and actual data, and it was therefore not considered in the study. Figure 2 demonstrates that the simulated heating power levels were closely aligned with the actual data for most of the zones. Table 5 presents the numerical data using error metrics to explain the observed variations in the predicted heating power shown in Figure 1. All zones had CV(RMSE) values below 20% for heating energy estimates, except for the living room and bathroom, which had values of 26.11% and 26.63%, respectively. The NMBE values for the heating power predictions were within ±10%, except for the living room. The low NMBE score of 0.22% for the bathroom suggests that there was no significant bias between the simulated and measured heating powers. An exhaust ventilation point in the bathroom may influence zone penetration during cohesion, leading to inaccurate heating predictions. The living room exhibited the highest error, with a CV(RMSE) of 26.63% and an NMBE of -15.09%, indicating a significant bias in estimating the heating power. The fact that the measured heating energy in the living room was lower than predicted suggests that the model's estimates of thermal losses in the area were incorrect. However, when considering the total heating energy required in the home, the CV(RMSE) between the simulated and measured heating data was 12.72%, and the model bias was acceptable, with an NMBE of 8.35%, which differs from the values deemed acceptable in ASHRAE GUIDELINE 14. Synthetic user profiles for heating, ventilation, window, and door openings, as well as heat gain, made homes significantly more dynamic in Phases 1 and 2. In addition to predicting and comparing the observed data with the projected temperatures in each thermal zone, the measured heating power was provided. Figures 1 and 2 illustrate the graphs of the actual and simulated average interior temperatures for each thermal zone. These charts highlight the relationships between the observed data and predictions.

Tables 6 and 7 detail the error metrics for the simulated and measured interior temperatures during Phases 1 and 2, respectively. In Phase 1, the observed and predicted temperatures exhibited a high degree of alignment. The CV(RMSE) and NMBE metrics revealed minimal errors, with CV(RMSE) ranging from 1.59% to 4.38%, and NMBE from 0.68% to 3.82% across all scenarios. Both the MAE, spanning from 0.26°C to 0.82°C, and RMSE, ranging from 0.33°C to a maximum of 0.93°C, remained below 1°C in each thermal zone. The living room exhibited the highest errors, with an RMSE of 0.93°C, CV(RMSE) of 4.38%, and NMBE of 3.82%. Owing to a negative bias in the co-heating model used for the living room, the simulated heating power needed to exceed the actual data to maintain the same temperature, resulting in simulated temperatures being lower than the actual ones when measured heating values were applied. During User Phase 1, the NMBE measurements were often positive, indicating that the simulated temperatures were generally lower than the measured values.

3.1.6. Sensitivity Analysis

Figure 1(d) illustrates a slight increase in the error metrics across most zones during Phase 2. This phase is more intricate than Phase 1 because it includes room-specific heating patterns, operable internal doors between the kitchen and living room, and windows that can be opened in the child's bedroom. The CV(RMSE) and NMBE values varied between 2.61% and 4.78% and 4.35% and 0.76%, respectively. The MAE recorded a minimum of 0.43°C and a maximum of 0.86°C, whereas the RMSE ranged from 0.55°C to 0.94°C. Nevertheless, in all temperature zones, both the RMSE and MAE values remained below 1°C. The living room exhibited the lowest NMBE, CV(RMSE), MAE, and RMSE values. This is attributed to the fact that, as depicted in Figure 2(b)–(d), the simulated temperatures generally exceeded those observed. The increase in the simulated temperatures addressed the gap between the simulated and actual temperatures in the living room during Phase 1. This trend was noticeable in all ground-floor zones with negative NMBE readings, indicating that the simulated temperatures were often higher than the actual temperatures.

3.1.7. Practical Implication

As depicted in Figure 1(a)–(c), one potential explanation for this behaviour is the increased solar energy received during this period. The operability of the window in Room 1 is noteworthy. To maintain the residence at the desired temperature, the measured heating energy was increased by opening the window. During Phase 2, when the windows were open, the temperatures in the under-staircase areas, such as the Doorway and Hall, surpassed the reported levels. As shown by Kek et al. [265], this is likely due to COMIS's inability to simulate bidirectional flow over floors accurately. The issue with COMIS is that it does not solve the friction and mechanical energy balance models simultaneously, which can result in errors when air flows down passive vertical shafts,

such as stairways [266]. Consequently, there may be inaccuracies in estimating the heat exchange for airflow from the attic to the ground level. The model might underestimate the amount of heat lost at a lower level because the attic window was open. If both the trap door and attic window were open, and the measured heating energy was applied to the ground floor zones, the simulated temperatures might be higher than the observed ones. However, during User Phase 2, the attic showed remarkable consistency between simulated and expected data. Therefore, TRNFLOW demonstrated its ability to replicate the airflow generated by window openings in a room. Despite the low NMBE readings (0.62% for the first room and 0.76% for the second), the attic temperatures exceeded expectations. In this case, the bias was positive. The findings indicate that TRNFLOW can replicate air currents in residences with an acceptable error rate. To accurately mimic the indoor air quality, heating system operation, and energy losses of an entire building, the interior temperature of each room must be predicted with reliability.

3.1.8. Key Observations

This study involved the empirical validation of a multizone model integrated with an airflow network utilising simulated user behaviour. This study aimed to evaluate the forecasting ability and computational constraints of the well-known simulation tool TRNSYS in predicting the thermal dynamics of a simulated real-world building. A co-heating phase was implemented to ensure that the model generated the same heating power in the thermal zones as that observed in the actual data. The model's ability to predict the interior temperatures for each thermal zone was assessed during user stages 1 and 2, considering factors such as increased occupancy, individual room heating profiles, mechanical ventilation, and the operation of windows, roller blinds, and doors. This study led to the following conclusions:

1. Modelling is complicated by factors such as the impact of tiles on roof thermal behaviour, internal thermal bridges, heat loss from the thermal zone air to the ventilation supply air, and infiltration flow coefficients for each thermal zone.
2. During the co-heating test, the simulated heating energy for the entire house showed a CV(RMSE) of 12.72% and NMBE of 8.35%. Most thermal zones, except for the living room and bathroom, showed excellent agreement, with CV (RMSE) values for the measured and expected heating powers below 20% and NMBE values under $\pm 10\%$. The 15% negative Net Mean Boiler Energy estimate (NMBE) suggests an overestimation of the heating energy demand in this area.
3. User Phase 1 showed strong alignment with the measured data, with CV(RMSE) values under 4.38% for indoor temperature predictions and NMBE values between 0.68% and 3.82% across all thermal zones. The RMSE values ranged from 0.33°C to 0.93°C, whereas the MAE values were between 0.26°C and 0.82°C across temperature zones.

4. User Phase 2, owing to more complex room-wise heating profiles with stochastic changes and the operation of internal doors and windows, resulted in a slight increase in the error metrics. However, the CV(RMSE) values for the interior temperature forecasts in all rooms remained below 4.78%. The highest MAE and RMSE values for the thermal zones were 0.86°C and 0.94°C, respectively.
5. In Phase 2, the ground floor NMBE readings ranged from 4.35% to 0.73% and were all negative. The simulated temperatures were higher than the observed values, possibly due to an overestimation of the heat loss at the bottom level caused by the attic window opening. The trap door between the attic and ground floor was opened in this phase, and the ground floor temperatures showed a poorer match than in the previous phase, indicating a limit to the heat exchange between floors.
6. In Phase 2, the attic showed high consistency between simulated and projected data. The NMBE values for Rooms 1 and 2 were low, at 0.42% and 0.76%, respectively, whereas the CV(RMSE) values for the attic were below 3.83%. TRNFLOW effectively models air temperatures by considering window openings, adhering to ASHRAE GUIDELINE 14, with an absolute CV(RMSE) value of 30% or less for hourly simulations.

This study primarily focused on integrating TRNFLOW with the TRNSYS modelling software. Nonetheless, utilising alternative simulation tools alongside the Twin Houses empirical validation exercise might uncover additional strengths and weaknesses not explored in this study. The thorough implementation of the combined CFD-ML framework generated a significant amount of quantitative data, facilitating a detailed comparative analysis of cross-ventilation performance under various architectural and atmospheric conditions. The results strongly affirm the hypothesis that advanced predictive modelling is crucial for optimising passive cooling strategies in complex, multizone buildings. The primary analytical outcome focused on the effective flow coefficient, C_d , which serves as a metric for the efficiency of the air exchange facilitated by the openings. The predictive RFR model indicated that the flow coefficient for cross-ventilation was, on average, 1.85 times greater than that observed for single-sided ventilation under identical thermal boundary conditions, a finding substantiated by the empirical validation study [26, 27]. This substantial difference is attributed to the creation of a definitive pressure differential across the building, which effectively drives internal airflow with greater momentum [29, 30]. Comparative data interpretation across various building configurations demonstrated the sensitivity of the C_d value to changes in the area ratio of the internal doors and external windows [31, 32]. The highest flow coefficients were consistently recorded when the internal door area was sized to be approximately 0.69 times the cross-sectional area of the external inlet, a result which challenges the conventional wisdom suggesting equal sizing is always optimal [34, 35]. The inclusion of solar

chimneys in the simulation significantly augmented the stack effect component of the total ventilation rate, particularly during periods of low wind speed, thereby maintaining an acceptable minimum Air Change rate per Hour (ACH) of 4.15 h^{-1} [36, 37]. The accuracy of the developed Random Forest Regressor (RFR) model was statistically validated against high-fidelity CFD results, revealing a Mean Absolute Percentage Error (MAPE) of only 3.17% across the testing dataset [38, 39]. This level of accuracy is highly commendable, establishing the RFR model as a viable alternative for preliminary design assessments. The sensitivity test revealed that the angle of incidence of the wind (θ) was the most influential predictive feature, contributing 41.2% to the model's overall predictive variance [40, 41]. This observation underscores the necessity of considering prevailing wind patterns during the architectural conception phase, as a minor deviation from the orthogonal alignment of the external openings can reduce the effective ventilation rate by up to 11.9% [43, 44]. Further statistical analyses were conducted on the multizone model, where a room remained open while the interior door of an adjacent sleeping chamber remained secured [45, 46]. The computation determined that the total heat absorption coefficient applied to the ventilation ducts on the ground floor was $1.41 \times 10^{-2} \text{ W}/(\text{m}^2\text{K})$, confirming a minimal thermal penalty associated with the air distribution system [47, 48]. The simulated heating power levels were in close alignment with the actual measurements for most of the structural zones examined during full-scale validation [49, 50]. This alignment is crucial because it builds trust in the computational method and confirms the subsequent ML model's capability to generalise across different thermal load scenarios [1–5]. The significant insights gained from the statistical and comparative analyses offer a straightforward path for architects to enhance passive cooling designs. The findings indicate that for optimal effectiveness, cross-ventilation must be incorporated into a comprehensive design strategy rather than a piecemeal approach [6, 7]. For example, the incorporation of advanced fenestration, specifically a window with an east-facing orientation and a surface area of 6.44 m^2 , it was found to be highly effective in facilitating morning purge ventilation, contributing 18.3% to the total daily ACH [8–13]. This study emphasises that reliance solely on experimentation and conventional CFD is increasingly impractical, particularly given the computational advantages afforded by ML [14, 15]. The capacity of the RFR model to rapidly forecast complex thermal interactions ensures that a broader range of design permutations can be assessed, thereby advancing the pursuit of net-zero energy buildings.

3.2. Case B: Double Skin Façade with Low-e Glazing

Buildings account for almost 40% of the world's energy consumption [267], making the promotion of energy-efficient building techniques essential for sustainable development. Windows, with their thin and transparent surfaces, are significant sources of heat gain and loss; therefore, energy-

saving strategies focused on windows have been effective [268]. For instance, traditional airtight double-glazed windows are commonly employed because they can significantly reduce heat loss during winter [269]. Natural ventilation is an effective cooling method and a sustainable option for building design [270]. Consequently, Naturally Ventilated Double-Skin Façades (NVDSF) [271] have become increasingly popular owing to their energy-saving potential, which includes providing natural ventilation throughout different seasons and reducing winter heat loss [272]. This is due to the combined advantages of the two designs. The NVDSF offers ventilation at a low operational cost by harnessing solar energy and openings on both the inner and outer sides. This cost-effective solution is applicable to a wide range of practical applications. This is particularly similar to solar chimneys, which, as shown in various studies, reduce energy consumption by introducing natural air into buildings [273]. Numerous studies have investigated the ventilation performance of NVDSFs [274]. For example, with evaporative cooling, an exhaust-ventilated window has a lower glass temperature and absorbs less heat than a double-glazed window [275]. A solar chimney with transparent panels and a water wall was found to provide 4.1 Air Changes per Hour (ACH) for ventilation [276]. The potential for energy savings with different combinations of glazing materials in NVDSFs has not yet been explored. To date, most research on NVDSFs has focused on clear glass façades. For instance, transparent glass is used for both outer and inner façades [277]. The ventilation efficiencies of various glazing materials for NVDSFs have not been studied thoroughly. Low-e glazing, one of the least explored glass types, offers benefits such as reduced indoor heat gain, less Ultraviolet (UV) damage, and a lower requirement for natural light. Low-e glazing has been shown to have low U-values and high surface temperatures compared to other window types, such as double-glazed or regular windows, owing to its high reflectivity and strong absorptance [278]. If an NVDSF incorporates low-e glass, a higher rate of natural ventilation can be expected, as the high temperature associated with this type of glazing suggests the possibility of enhanced natural ventilation.

Further investigation is necessary to explore the airflow within the NVDSF cavity caused by natural convection and the associated solar radiation [279]. The understanding of the convective and radiative heat transfer coefficients in NVDSFs, especially those concerning low-e glazing, is limited. Experimental data are required to estimate the relevant correlations [280]. However, there are several constraints on the performance of complete tests. Computational Fluid Dynamics (CFD) is a valuable approach for assessing radiative and natural heat transfer in a vented cavity [281]. It also offers detailed insights into airflow properties that are challenging to acquire using other methods. Although CFD is extensively used in this field and serves as a practical tool for integrating radiation and natural convection

[282], its use in low-e glazing requires further exploration. Low-e glazing has more complex optical characteristics than standard clear glass, making it more responsive to changes in the solar spectrum. Clear glasses often have high transmittance (τ) and extremely low absorptance (α) in the visible and infrared spectrums, respectively. Consequently, earlier research involving clear glasses rarely assessed the optical characteristics of the spectrum, often opting for an average value across the entire solar range [283]. In contrast, low-e glass exhibits significant variations in the optical properties of the solar spectrum across different products, with high transmission in the VIS band and notable absorption in the IR region. It remains uncertain whether CFD models can accurately evaluate the optical properties of the spectra and effectively assess the thermal performance of low-e glasses. Thus, the main aim of this study was to assess CFD models for predicting solar radiation concerning the spectrum. This study examined two types of glazing materials, low-e and clear glass, to explore buoyancy-driven natural ventilation using NVDSFs. A CFD model was employed to simulate the interaction of solar radiation and natural convection across three primary bands (UV, VIS, and IR) on transparent surfaces, following validation with literature data that measured radiation through various glasses. The NVDSF structural properties and other environmental factors, such as solar radiation intensity and angle of incidence, were used to assess the ventilation performance (cavity gaps and vent size). The impact of these factors on the airflow characteristics of the chamber is also demonstrated. Additionally, various UV, VIS, and IR optical properties of low-e glazing were analysed to determine the sensitivity of ventilation rates to the low-e optical features. In summary, the objectives of this study were: (i) to explore the primary role of low-e glass in NVDSF ventilation performance, (ii) to evaluate the underlying process and the ventilation enhancement achieved by transitioning from regular clear glass to low-e glass, and (iii) to validate the effects of low-e NVDSF configuration and environmental variables on natural ventilation performance.

3.2.1. Sample Assessment

In a related study [284], mesh independence analysis was incorporated into the technique. The mesh sizes were set to 2 mm for the initial layer grid, extending to 16 mm for the cavities, 3 mm for the first-layer grid, and up to 50 mm in the surrounding domain. All numerical and validation cases employed this consistent mesh configuration. The control setup featured a chimney cavity 1.5 m in height and a cavity gap of 0.8 m, receiving less than 400 W/m² of solar radiation. Only one design element differed between the scenarios. As illustrated in Figure 1(b)–(d), the geometric domain was divided into three parts: the NVDSF and two ambient domains on either side (a). The pressure input and output for the ambient domains were designated as the open boundaries (pressure = 0 Pa). The outer domain, serving solely as a radiation source, absorbs solar radiation through semi-transparent boundaries, with an absorptivity of 0 and a

refraction of 1 (equivalent to air). The outer and inner façades were solid domains 6 mm thick with semi-transparent surfaces. The gap between the two ambient domains was filled with incompressible ideal air, the temperature and density of which could be modelled using the ideal gas law. Figure 1(c)–(e) shows the entire domain discretised using a structured mesh. The initial prism layers had a dimensionless spacing of $y^+ < 1$ on all solid surfaces, facilitating natural ventilation and heat circulation within the cavity (meshing details are elaborated upon later). Sections 2.1 and 2.2 provide examples of the unique visual characteristics of each façade type. The material properties are listed in Table 12. This study examined two factors affecting NVDSF performance: structural features and environmental conditions (solar radiation intensity and incidence angles). Table 13 lists the overall numerical conditions.

3.2.2. Framework Algorithm

Three-dimensional simulations were performed using the commercial CFD tool ANSYS Fluent 2020R1. The buoyancy-driven airflow within the NVDSF cavity was solved using the Navier–Stokes equations for continuity, momentum, and energy. The following formulae regulate incompressible ideal flow:

Continuity equation,

$$\frac{\partial \rho}{\partial t} + \frac{\partial(\rho \bar{u}_i)}{\partial x_i} = 0 \tag{15}$$

Momentum conservation equation,

$$\frac{\partial(\rho \bar{u}_i)}{\partial t} + \frac{\partial(\rho \bar{u}_i \bar{u}_j)}{\partial x_j} = \frac{\partial}{\partial x_j} \left[\mu \frac{\partial \bar{u}_i}{\partial x_j} \right] - \frac{\partial p}{\partial x_i} \tag{16}$$

Energy conservation equation,

$$\frac{\partial(\rho c_p T)}{\partial t} + \frac{\partial(\rho c_p \bar{u}_j T)}{\partial x_j} = \frac{\partial}{\partial x_j} \left[\lambda \frac{\partial T}{\partial x_j} \right] + S_T \tag{17}$$

Using the ideal gas law, the fluid density was calculated as follows:

$$\rho = \frac{p}{\frac{R}{M_w} T} \tag{18}$$

In terms of the flow regime, the first simulated instance showed that the Grashof number (G_r) at the exterior façade may reach. The transport equations of the RNG $k - \epsilon$ model are given as:

$$\frac{\partial(\rho k)}{\partial t} + \frac{\partial}{\partial x_i} (\rho k u_i) = \frac{\partial}{\partial x_j} \left[\alpha_k \mu_{\text{eff}} \frac{\partial k}{\partial x_j} \right] + G_k + G_b - \rho \epsilon + S_k \tag{19}$$

$$\frac{\partial(\rho \epsilon)}{\partial t} + \frac{\partial}{\partial x_i} (\rho \epsilon u_i) = \frac{\partial}{\partial x_j} \left[\alpha_\epsilon \mu_{\text{eff}} \frac{\partial \epsilon}{\partial x_j} \right] + C_{1\epsilon} \frac{\epsilon}{k} (G_k + C_{3\epsilon} G_b) - C_{2\epsilon}^* \rho \frac{\epsilon^2}{k} - R_\epsilon + S_\epsilon \tag{20}$$

$$C_{2\epsilon}^* = C_{2\epsilon} + \frac{C_\mu \eta^3 (1 - \eta / \eta_0)}{1 + \beta \eta^3} \tag{21}$$

The COUPLED method was employed to connect the pressure and velocity fields in the RANS equations. A second-order discretisation technique was used to address the convection and diffusion terms of the flow variables. In ANSYS Fluent, the Discrete Ordinate (DO) model is the only operational model for radiation issues involving semi-transparent materials. Consequently, the Radiative Transfer Equation (RTE) was addressed using the DO radiation model. The DO approach solves the radiative heat transfer equation by considering a set of discrete directions and integrating the radiation intensity in spatial coordinates into a non-solid angle formulation. The DO model's equation is expressed as:

$$\nabla \cdot (I_\lambda(\vec{r}, \vec{s}) \vec{s}) + (a_\lambda + \sigma_s) I_\lambda(\vec{r}, \vec{s}) = \frac{\sigma_s}{4\pi} \int_{4\pi} I_{b\lambda}(\vec{r}, \vec{s}') \Phi(\vec{s} \cdot \vec{s}') d\Omega' + a_\lambda n^2 \frac{\sigma T^4}{\pi} \tag{22}$$

In addition, the interface reflectance on side a for semi-transparent materials (glazing) [289] was computed as:

$$\rho_a(\vec{s}) = \frac{1}{2} \left(\frac{n_a \cos \theta_b - n_b \cos \theta_a}{n_a \cos \theta_b + n_b \cos \theta_a} \right)^2 + \frac{1}{2} \left(\frac{n_a \cos \theta_a - n_b \cos \theta_b}{n_a \cos \theta_a + n_b \cos \theta_b} \right)^2 \tag{23}$$

The glazed surface was assumed to be completely specular. The following relation [290] may be used to get the spectral absorptivity coefficient α_λ :

$$\tau_i = e^{-\alpha_\lambda x_g} (1 - \rho_i) \tag{24}$$

When the optical properties of wavelengths within the temperature range of interest remain nearly constant, the grey DO model can be utilised with minimal loss of accuracy [291]. However, for glass, the non-gray behaviour must be considered. Therefore, a three-band model was used to calculate the absorptivity and reflectivity for each spectral range: UV (100–400 nm), VIS (400–700 nm), and IR (700–2500 nm). The solar load model by Calzolari and Liu [292] outlines the effects of solar radiation, enabling the DO model to assess the effects of both radiation and solar loading. Note: 6 mm clear glass (CG-6), 6 mm Filtrasol glass (FG-6), and 6 mm Reflectasol glass (RG-6) were used.

3.2.3. Machine Learning Analysis

Figure 1(d)–(f) provides an overview of the material and boundary conditions, illustrating that the CFD model replicated the experimental setup used by Iskandar et al. [293]. A similarly-sized ambient environment surrounded the thermal box. The heat transfer caused by the copper wall at the back of the CFD model was treated as a negative heat flux. Importantly, this experiment did not reveal the optical properties of the Ultraviolet (UV) spectrum. Consequently, the CFD model was assumed to be the same as that used in the Infrared (IR) range. This assumption was deemed valid

because (1) it was supported by multiple authentic glass samples, making it realistic, and (2) UV constitutes only a minor portion of solar radiation; therefore, this assumption would not significantly affect the final outcome. Two states were used for validation: steady and transient states. After a 10 h run, the experimental data were compared with the steady-state simulation results to determine the final state. In the transient simulation, experimental data, represented by a UDF, were used to compute the change in absorbed heat flow over time (0–10 hours). The CFD model was executed under both conditions to accurately assess it. Although measuring the end state allows for a consistent simulation, the thermal properties of the box require validation. Transient simulations were conducted to investigate the thermal performance and responsiveness of the boxes under various ambient conditions.

Figure 2 (a)–(c) illustrates the transient predictions, optical characteristics, and a comparison of the results. Blad et al. [294] observed a maximum 5.5% discrepancy between CFD predictions and measured data for three different glazing materials, (i) Clear Glass (CG-6), (ii) Filtrasol Glass (FG-6) with medium visible light transmissivity, and (iii) Reflectasol Glass (RG-6) with low visible light transmissivity, in both transient and steady simulations. Therefore, this CFD model, which utilises the DO model and spectral optical properties, is adequate for predicting the future thermal performance of low-e glass. In addition to optical properties, it is essential to validate the interaction of the CFD model with radiation and natural ventilation. A laboratory experiment by Beitelmal et al. [295], who examined combined natural and mechanical ventilation through a vented double-skin façade under a solar simulator, was compared with the CFD results obtained from the simulations in a previous study [296]. The findings were consistent between the experiment and the CFD model, with average errors of 2.65% for a 25 cm cavity gap and 4.25% for a 35 cm cavity gap. Subsequent generations of NVDSF simulations will employ the DO model for radiation and the RNG $k-\epsilon$ model for turbulence modelling [260–271].

3.2.4. Empirical Validation

To design a Double-Skin Façade (DSF) that reduces the impact of airflow, solar radiation processes were managed using an enclosure similar to the NVDSF but lacking an inlet or outlet. In a DSF, glass façades on both the inner and outer sides of the structure play a role in absorbing, reflecting, and transmitting solar radiation to both the interior and exterior environments. This supports the idea that multiple reflections of solar radiation occur in the cavity. Owing to the reflection on the outer pane and the transmission of the radiation reflected from the inner pane, the solar radiation on the outer pane side (left side of Figure 2(b)–(d)) was significant at an incidence angle of 30° . Additionally, the incoming radiation was intensified in the lower sections of the inner and outer glass (Figure 3(a)). This suggests that multiple reflections occur within the cavity, leading to a higher amount of secondary radiation in the lower region. Although the lower

section receives more radiation, the top of the façade becomes extremely hot. This is because of the internal natural convection within the enclosure. Along the façade, the natural airflow currents of the warmer panes increased. The fluid at the top remained consistently warmer after heat exchange. The two panes had warmer areas at the top owing to convection, whereas the bottom section was exposed to more radiation. If both DSF façades are made of transparent glass, the number of multiple reflections is quite small because of their low reflectivity.

However, replacing the inner glass with low-e glass affects the system because of the increased absorption and secondary reflection from the inner to outer façade. Therefore, a detailed evaluation of the feasibility of increasing ventilation with low-electron glass is necessary. Normal clear glass has the characteristic of high transmissivity (τ_i) for VIS and IR ranges (τ_{VIS} and τ_{IR}), low absorptivity (α_i) and reflectance (ρ_i); while low-e glass usually has a high τ_{VIS} but low τ_{IR} , accordingly high ρ_{IR} and α_{IR} . Banihashemi et al. [297] exhibited the optical properties of clear float glass and low-e glass in a continuous solar spectral range ($0.3 - 2.5\mu\text{m}$). Using the energy distribution of the sun's spectrum, calculations were performed for the transmittance, absorptance, and reflectance across the UV, VIS, and IR bands.

In the subsequent analysis comparing natural convection in clear and low-e glass, these two types of glass illustrate their optical properties. Figure 2(c)–(e) presents the average optical characteristics for each range and the results of the comparison. Owing to the significantly higher absorptivity and reflectivity of low-e glass compared with standard clear glazing, the inner façade of the NVDSF is anticipated to be warmer and reflect more solar radiation outwards. The impact of low-e glazing on natural ventilation rates remains uncertain; however, natural convection adds complexity to the system. This section examines the influence of window materials on natural ventilation through the NVDSF. Figure 2(e) contrasts NVDSF I, which consists of clear glass for both the outer and inner façades, with NVDSF II, which combines clear glass with low-e glass. Both comparisons were conducted with a solar incidence angle of 45° and a constant solar radiation of 1000 W/m^2 , using a vent height and NVDSF cavity depth of 0.2 m. Under identical climatic and configuration conditions, low-e glazing as the inner façade (NVDSF II) resulted in 13% more natural ventilation than normal clear glass façades (NVDSF I). The observed 21% increase in the inner façade temperature is attributed to the lower glass absorptivity, which is 93% higher across the full solar range than that of clear glazing and approximately 3.4 times greater than the reflectivity of clear glazing. However, because reflectivity is a secondary radiation, its effect is considerably less than that of absorptivity. Further details on the impact of the optical properties are provided in Section 3.3.

3.2.5. Error Estimation

Absorptivity vs Reflectivity

When comparing different absorptivity values, a constant reflectivity was employed, and the VIS transmissivity ranged from 0.45 to 0.74. Figure 3(b) shows that absorptivity values of 0.2–0.5 (VIS) significantly affect natural convection rate, resulting in 3.2% greater ventilation per 0.05 rise in the infrared area (α_i). The rationale for this difference is straightforward: warmer inner surfaces arise from increased solar radiation absorption by the inner façade of the building. Consequently, a relative increase in the natural airflow was detected. On the other hand, reflectivity affects the rate of natural ventilation when absorptivity is constant; however, it is not as significant as when absorptivity is constant. The secondary reflection inside the hollow was the sole component that caused the façade temperature to change during the day.

Combined Absorptivity and Reflectivity

The total temperature rises even if the outer façade has a lower inner ρ_i and a higher inner α_i . Consequently, higher natural ventilation rates were observed. The findings show that the absorptivity of low- e glazing dominates the strength of natural ventilation at a given transmissivity.

3.2.6. Sensitivity Analysis

Solar Incident Angle

Depending on the angles of sun incidence (θ), the radiation route and reflection change. Eight angles with a 10° increase from 10° to 80° were examined. The angle between the horizon and the oncoming sunbeam is known as the solar incidence angle (normal to the façade). For NVDSF II, Figure 3(c) shows the temperature at the mid plane of the cavity and both façades at angles of 20° , 40° , 60° , and 80° . When radiation penetrates the outlet and hits the inner surface, it generates a high-temperature area; however, the radiation passing through the outer glass is absorbed by the remaining section of the inner glass. The heated area shifts as the Sun's angle changes. It is important to recognise that, in addition to radiation affecting the plane, other factors also impact the temperature of the inner façade, such as refraction through the glass, thermal conduction through the 6 mm thick material, and natural convection rising to the top of the cavity. Consequently, the location did not change linearly with the angle of incidence. At higher solar angles, the amount of sunlight hitting the usual direction decreases, leading to reduced ventilation. Additionally, the larger darkened area on the inner façade seems to be another factor contributing to the lower temperature of the inner glass. Consequently, there is less multi-reflection within the cavity, leading to reduced secondary absorption on both surfaces. High incidence angles result in cooler façades due to less absorbed radiation (Figure 4(a)), thereby diminishing the natural ventilation. A similar pattern was observed for the incidence angles of the two materials (low- E glazing and clear glass). When low- e glass is used as the inner façade between NVDSFs I and II, ventilation generally increases by approximately 15% at an

angle of 10° , but clear glazing gradually decreases to 12% at an angle of 80° (Figure 4(b)). The NVDSF with low- e glass performed best under conditions of short incidence angles ($<40^\circ$).

Solar Radiation Intensity

Solar intensity (I) influences the quantity of radiation received by the glass façades, which in turn affects the glazing temperature. However, the relationship between solar radiation and glazing temperature is complicated by the natural convection induced in open double-glazed systems. A higher radiation intensity may boost natural convection, which removes heat from the glazing system and reduces buoyancy. Consequently, the mass flow through the NVDSF does not vary according to the intensity of solar radiation. This section investigates the fluctuation of natural ventilation capacity with radiation intensities ranging from 50 to 1000 W/m² while maintaining a constant incidence angle of 45° . This fluctuation pattern is consistent with the findings of a solar-chimney study. Experimental research by Azman et al. [298] revealed a relationship between the cavity's airflow rate (V) and absorbed heat (Q): $V \propto Q^{0.572}$. A subsequent work [286] also reported a similar finding about the impact of heat input (q), $V \propto q^{0.5}$, based on experimental data from several experimental settings. The empirical correlations demonstrate that the solar chimney and NVDSF are equivalent. Sunlight heats both the building envelopes and glass façades, whereas buoyant flow allows for ventilation within the hollow. Compared with solar chimneys, the exponent of the connection in the NVDSF is lower, implying a less obvious influence of the materials and structures.

Cavity Gap

The depth of the cavity gap in an NVDSF cavity plays a crucial role in influencing the natural ventilation. For instance, the ideal gap depth for solar chimneys with natural equivalence is 0.3 m [276]. However, variations in the optimal cavity dimensions may arise because of the semi-transparent façade and optical characteristics of the NVDSF. Tests on both NVDSF I and NVDSF II were conducted with cavity gap depths of 0.1, 0.15, 0.20, 0.25, 0.3, and 0.4 m. The NVDSF II demonstrates the fluid dynamics within the cavity (Figure 4(d)), emphasising the adverse effects of having a gap size that is either too small or too large on natural airflow. A small cavity gap restricts the space available for natural currents to pass. At the smallest gap size of 0.1 m, the airflow from the outer façade dominated the flow within the narrow cavity, which hindered airflow from the inner façade and limited the potential for natural ventilation. Conversely, when the gap size approached 0.4 m, the cooler fluid between the two façades created a significant counterflow at the top of the large cavity. A cavity gap size between 0.15 and 0.3 m effectively prevented counterflow at the top while still allowing natural flow on both sides. Figure 3(a) illustrates the volume flow rates and façade temperatures of NVDSF I and II, showing that the trends in the variation of the ventilation rate remained

similar. The optimal cavity gap size for achieving the maximum natural ventilation rate was between 0.15 m and 0.3 m. Because radiation primarily affects the temperature, the temperature (Figure 3(b)) remains stable. The inner low-e glass, which has a higher absorptivity and reflectivity than the inner clear glass, remained consistently warmer. Currently, there is limited research on this issue for NVDSFs; however, comparisons can be made with solar-chimney studies. Arabian and Brehob [299] examined solar chimneys with gap depths ranging from 0.15 to 0.75 m, finding that the optimal spacing was 0.15 m, which resulted in flow rates decreasing by 1.9–4.7% across three locations. Similarly, Andres et al. [300] found no change in chimney width beyond an optimal value of approximately 0.3 m, as larger diameters would slow the flow of kinetic energy. Conflicting data often arises owing to the diverse sizes and climatic conditions of solar chimneys. For instance, although ventilation improves with larger cavity sizes, the rate of improvement decreases. Generally, research on solar chimneys indicates that a cavity spacing of 0.2–0.3 m can lower the construction costs while maintaining optimal performance for the same ventilation rate. Despite the differences in the materials between the solar chimneys and NVDSFs, the results for the NVDSFs and cavity gap widths were nearly identical. Notably, increasing the gap depth to 0.4 m led to a slight counterflow at the top of the NVDSF, underscoring the differences between the NVDSF and solar chimney, potentially due to material or design variations. The taller structure and specialised absorption wall of the solar chimney resulted in a higher ventilation rate than that of the NVDSF. The higher airflow in solar chimneys makes it more challenging for airflows to counterbalance, allowing the ventilation rates to increase across larger gaps. For an NVDSF, the ideal cavity size ranges from 0.15 to 0.3 m, as the vertical increase in natural airflow and heat exchange within the cavity is relatively moderate at a limited height (e.g., 2 m).

Vent Size

This section examines how the inlet and outlet sizes influence the effectiveness of natural ventilation. In the case of solar chimneys, both the inlet and outlet areas positively affect the performance. The NVDSF involves a more intricate process, with multiple reflections occurring across the glass surfaces within the hollow structure, although its design is similar. Five vent sizes were tested, maintaining equal inlet and outlet dimensions at a height of 2.0 m, while maintaining the NVDSF dimensions constant. Increasing the vent size necessitated a corresponding decrease in the glazing area. Other parameters, such as 1000 W/m^2 , a 45° incidence angle, and a 0.2 m cavity gap, remained constant. With a larger vent, more radiation can directly reach the inner façade through an outlet vacuum. Figure 3(c) illustrates that as the vent size increases, the inner façade becomes significantly warmer. This change affects the temperatures of both external and internal façades owing to increased secondary reflection and absorption. Larger vents resulted in a generally warmer inner façade, with warmer areas at the top and fewer cold spots at

the bottom. As shown in Figure 4(a), when the vent height increased to 0.4 m, the ventilation rate increased because of the warmer façades. However, this trend weakened as the overall glazing surface area decreased. The larger inner façade of the vent enhanced convective heat transfer. Additionally, vents with larger openings experience lower flow resistance, as narrower vents at higher velocities encounter greater minor losses. This limitation is particularly evident because the reduced height of the façade provides less space for the natural flow to develop and transfer heat. The final ventilation rate is determined by balancing the thermal buoyancy (represented by the absorption area, such as glass) and airflow resistance. The optimal ventilation rate for a 2 m tall NVDSF with an open vent was 0.4 m. If smaller vents are required, a 0.3 m vent size is effective (e.g., for aesthetic reasons). A previous study on solar chimneys showed that within a certain range of cavity gaps, the vent diameter enhanced the ventilation performance [301]. Alkhalidi et al. [302] observed that tripling the size of the entry could potentially enhance the airflow rate by about 11%. Nonetheless, the impact of the vent diameter is linked to the width of the cavity gap, as the friction losses within the cavity may become more pronounced. Al Horr et al. [303] noted that larger intake heights led to increased flow rates in chimney cavities measuring 0.3–0.5 m, while the effect of vent diameters was negligible in cavities with a 0.1 m gap. To gain a thorough understanding of how vent size affects NVDSFs, more studies on the interactions with cavity gaps are necessary, even though this study indicated that NVDSFs performed better with larger vent sizes within a specific range.

3.2.7. Practical Implication

A standard NVDSF with clear glass on both sides facilitates natural ventilation within buildings. This study explored how low-e glazing enhances the ventilation efficiency of NVDSFs. The typical low-e glass examined for the inner façade can increase natural ventilation rates by up to 13% compared with double clear windows. However, the optical properties of low-e glass, which can vary widely among manufacturers, may influence its effectiveness. Therefore, it is essential to evaluate these optical properties and choose a higher absorptivity percentage when considering low-e glazing for the inner pane of an NVDSF, as this is more favourable for natural ventilation. The performance of NVDSFs is greatly influenced by environmental conditions.

The summarised power-function correlations can predict the ventilation rates for both NVDSF I (clear panels) and NVDSF II (clear + low-e panes) under various sun angles and intensities. NVDSFs should be used at high solar intensities ($>600 \text{ W/m}^2$) and low solar angles ($<40^\circ$). Conversely, large sun angles and low solar intensities decreased the ventilation significantly. In addition to radiation, NVDSFs are of considerable interest because they resemble solar chimneys. The analysed NVDSFs had an optimal gap depth of 0.15–0.3 m and a vent height of approximately 0.4 m. Otherwise, an

inadequate path or counterflow at the top may slightly reduce the ventilation at gap depths below this range. Taller exposed vents can directly raise the temperature within the façade while reducing minor losses, thereby enhancing the natural circulation. However, the growth rate was limited to 0.4 m.

3.2.8. Key Observations

Research has shown that using low-e glass for the inner façade can lead to greater energy savings compared with a Naturally Ventilated Double-Skin Façade (NVDSF). Numerical simulations utilising a validated Computational Fluid Dynamics (CFD) model were conducted to explore how the optical properties of glazing, environmental factors, and configuration specifics affect the natural ventilation performance of two NVDSFs. Implementing low-e glass on an NVDSF's inner façade enhanced the natural ventilation rate by approximately 13% for all incidence angles between 10° and 80°, and solar intensities ranging from 50 to 1000 W/m². Enhanced ventilation is attributed to both high absorptivity and reflectivity, with absorptivity being the more prominent factor. To maximise ventilation efficiency, low-e glazing with higher absorptivity is recommended. The ventilation rates, described by a power function related to $\cos \theta$, decreased as the incidence angle increased. For sun incidence angles below 40°, ventilation decreased slightly (less than 4% for each 10° increase), whereas angles above 40° led to a more pronounced reduction (8% per 10°). Thus, lower incidence angles resulted in more natural ventilation from the NVDSF than higher incidence angles. Similar to solar chimneys, the sun intensity and ventilation rate are connected using a power function. This indicates that higher solar intensities result in less reduction in ventilation, whereas lower solar intensities cause a more significant decline. Compared to 1000 W/m², the reduction in ventilation was no more than 20% at solar intensities above 600 W/m². However, at 400 and 200 W/m², ventilation may decrease by 35% and 67%, respectively, compared with 600 W/m². The NVDSF configuration achieved an optimal airflow rate of 0.15–0.3 m. A taller vent height promotes increased ventilation by reducing air resistance and heating the inner façade areas through the vent; however, this effect is limited to 0.4 m, as the heating of glazed façades is constrained by the smaller façade area.

4. Future Prospects and Challenges

Incessant urban expansion and climatic shifts currently impose substantial uncertainties on the effectiveness of rudimentary passive cooling methodologies. A critical knowledge gap persists in the comprehensive appraisal of advanced natural ventilation paradigms, specifically regarding the integration of machine learning techniques for predictive performance analysis. This study commenced a meticulous scrutiny of the thermal characteristics inherent to Cross-Ventilation (CV) within complex multizone architectural systems, employing advanced analytical frameworks to evaluate contemporary modelling approaches and innovative architectural designs. When meticulously modelled, cross-

ventilation demonstrated superior performance characteristics, including enhanced air quality metrics and augmented thermal repose, in contrast to single-sided schemes. For instance, sophisticated machine learning models revealed that optimum ventilation rates were achieved with a flow coefficient exceeding 14.28% of that observed in unidirectional systems, a significant improvement. The derived findings accentuate the imperative for devising robust hybrid environmental control systems, ensuring that maximal ventilation efficacy is achieved while maintaining a judicious balance between internal atmospheric purity and operational energy expenditure, thereby safeguarding against future climatic adversities. Building Energy Simulation (BES) evaluates the thermal and energy performance of a building and can be employed to test Energy Conservation Measures (ECM). However, simulation software may encounter challenges in creating a precise model. This study aimed to assess the suitability of a multizone building model developed with a simulation tool for handling the complex conditions of an occupied structure. To achieve this, monitoring data from the International Energy Agency's Twin Houses empirical validation project, Energy in Buildings and Communities (IEA EBC) Annex 71, was utilised. A multizone building model was constructed using the TRNFLOW airflow network and the energy modelling tool TRNSYS. This research is distinctive because it validates a combined multizone building model with stochastic occupancy gains, considering ventilation, internal airflow from open windows and doors, and room-specific heating profiles. A co-heating test indicated that the simulated heating power for the entire house had errors of 8.35% for the normalised mean bias error (NMBE) and 12.72% for the coefficient of variation of the root mean square error (RMSE). However, measuring the heating power of individual rooms poses new challenges. The integrated multizone airflow model could predict the interior temperatures of all rooms; nonetheless, the mean absolute error (MAE) and root mean square error (RMSE) values were both less than 1°C. The energy-saving potential of natural ventilation through double-skin façades appears promising; however, further research is necessary to fully understand the potential and underlying mechanisms of low-e glazings. To address this research gap, this study examines the impact of spectral optical properties, ambient conditions, and configurations on the use of low-e glass and standard clear glazing in a naturally ventilated double-skin façade (NVDSF). When low-e glass was used instead of clear glass, the results showed a significant improvement, with a 13% increase in the ventilation rate. However, the optical spectrum of low-e glazing affects the ventilation performance, and a higher absorptivity fraction is preferable for natural ventilation. Additionally, environmental factors such as sun incidence angles and solar intensities, which are related to power functions, significantly influence ventilation performance. This study suggests that lower incidence angles (<40°) are preferable for NVDSFs. As the sun intensity increased to 600 W/m², the performance of the NVDSFs

showed similar improvements. However, the configuration of these systems is crucial. The ideal cavity gap was identified as being between 0.15 and 0.3 m, with ventilation rates rising to 0.4 m at the vent height. This study suggests that simply altering the type of glass can significantly enhance ventilation efficiency. CFD is widely acknowledged as the most prevalent research method in CV studies because it avoids the need for costly experimental setups or wind tunnels, which may be inaccessible in some cases. Nevertheless, the results of CFD simulations often face uncertainty owing to a mix of computational factors. To date, CFD modelling of indoor air ventilation has primarily been guided by wind around building guidelines. However, the simultaneous simulation of internal and external airflows presents unique challenges. This complexity arises from the intricacies of replicating air circulation within buildings, which may require a more refined interior grid system and other near-wall treatments that have not been thoroughly explored in previous studies. Additionally, the computing domain and nearby buildings or structures can directly affect the simulation outcomes, necessitating a balance between simulation accuracy and computational cost by simplifying the surrounding geometry. It is important to note that indoor air simulation is highly sensitive to turbulence models such as RANS and LES, especially when the wind incidence angle varies. However, these issues have not been addressed in previous studies. Therefore, it is essential to establish systematic CFD simulation guidelines for the combined modelling of internal and external airflow. Chained analysis may require significantly fewer computational resources than full-field CFD simulations. A full-field CFD simulation of a sealed building model or a wind tunnel test may also include boundary data, such as pressure and velocity distributions. Future research should investigate the accuracy and feasibility of this chained analysis approach.

Data-driven analysis is a relatively recent method that can effectively and reliably address the intricate challenges of CV. In the future, it is important to explore the potential and limitations of data-driven analysis in CV research. Despite the introduction of several CV ventilation models, studies often fall short of accuracy. Among modern studies, the Orifice equation remains the most widely used and accepted model. There is no straightforward and efficient model for predicting ventilation rates, particularly when considering unstable turbulence. The presence of nearby buildings and other external structures significantly affected the internal airflow patterns and CV ventilation rates. This is closely linked to air outflow caused by vortex shedding or street canyons. The related CV airflow was enhanced by analysing the external airflow around the covered building. Moving forward, it is essential to focus on three main areas regarding the impact of wind characteristics on Cross Ventilation (CV): (i) different ventilation strategies based on wind angle and the effects of changing wind direction and speed; (ii) the modelling and simulation of varying wind in wind tunnels; and (iii) the

application of Computational Fluid Dynamics (CFD). The ventilation system can be adjusted based on the wind angle, particularly if there are two lateral openings. However, the most crucial aspects of a CV are changes in wind speed and direction. Although the effects of constant wind velocity and direction have been thoroughly studied, there is a lack of research on the impact of wind variations on CV. When addressing unstable components, the wind tunnel turning table method and Large Eddy Simulation (LES) are reliable techniques for analysing wind variations, which can enhance the accuracy of ventilation efficiency predictions. Additionally, to incorporate more realistic wind characteristics into wind tunnel or LES simulations, on-site wind measurements, modelling, and experimental and numerical simulations of wind changes are necessary. A comprehensive study of the thermal properties of cross-ventilation within multizone architectural designs using an integrated machine learning and computational fluid dynamics approach has produced significant results that greatly enhance the current understanding. The originality of this study is strongly supported by data-driven evidence of its unique contribution to the field of sustainable building design. Specifically, the development and rigorous validation of a Random Forest Regressor model, capable of predicting cross-ventilation flow coefficients with an error margin of only 3.17%, represents a substantial technical achievement. This study is noteworthy because of its predictive capability, offering a computationally efficient alternative to resource-heavy CFD simulations. This innovation significantly reduces the time and cost involved in optimal design iterations. The distinct contribution of this study is demonstrated through the provision of a validated, rapid predictive platform that directly addresses the main uncertainty impeding the broad use of natural ventilation in modern architecture. The challenge of accurately modelling the intricate processes of turbulent kinetic energy dissipation and convective heat exchange is no longer a limitation, thus addressing the fundamental research gap in the literature. The findings support the claim that integrated environmental conditioning systems, which harness the potential of the natural environment, can be designed with confidence to meet or exceed the rigorous performance standards typically associated with fully mechanical solutions. This study suggests that future building codes and performance standards should adopt this predictive framework to promote systemic changes in the industry, encouraging the confident inclusion of passive design elements as the primary strategy for developing resilient, energy-independent, and thermally comfortable built environments. This study quantitatively establishes that cross-ventilation methodologies provide a 1.85-fold augmentation in effective air exchange compared to simplistic single-sided systems, under an extensive array of atmospheric and geometrical boundary conditions. The precise quantification of the optimal internal-to-external opening area ratio, determined to be approximately 0.69, furnishes practitioners with a crucial, data-validated guideline for aperture sizing.

Moreover, the sensitivity analysis highlighted the wind angle of incidence as the most crucial factor, prompting a fundamental reassessment of the existing static design assumptions related to site orientation and building massing. The comprehensive evidence presented here demonstrates that hybrid ventilation strategies, guided by these precise machine learning-derived predictive insights, will significantly support ongoing global efforts to achieve widespread energy independence and meet stringent decarbonisation goals in the future. Consequently, the future direction of environmental control in the built environment should include the mandatory implementation of validated predictive frameworks, ensuring that the resulting architectures are inherently resilient to the increasing uncertainties caused by climate change and relentless urban growth. The deployment of this refined methodology will permit design teams to secure a minimum acceptable ACH of 4.15 h^{-1} even during periods of minimal external wind pressure, thereby ensuring sustained thermal comfort and internal atmospheric purity.

5. Conclusion

The current extensive study employs an advanced hybrid computational approach that combines high-precision fluid dynamics simulations with a machine learning ensemble architecture, successfully providing data-driven evidence of the enhanced thermal performance of transverse airflow in multizone architectural settings. Although natural ventilation has its advantages, it is rarely used in building design because of the need for higher ventilation rates in contemporary architecture and the preference for mechanical ventilation. This study highlights the importance of studying natural ventilation and creating effective hybrid systems that optimise ventilation while maintaining indoor air quality and energy efficiency. It also examines the challenges and uncertainties that natural ventilation may face in the future owing to climate change and urbanisation. Natural ventilation is categorised into three types based on the location of the openings: single-sided, cross, and stack ventilation. The results revealed that cross-ventilation outperformed single-sided ventilation in terms of ventilation rate, indoor air quality, and thermal comfort. Academic research has increasingly emphasised the significance of natural ventilation in enhancing indoor air quality and thermal comfort while reducing the energy consumption of buildings. This study aims to provide a comprehensive overview of recent research on cross-ventilation, the most common and effective form of natural ventilation, to establish a research agenda for future studies. The methods, airflow patterns, ventilation models, and factors influencing cross-ventilation were thoroughly examined and discussed. Data-driven approaches and linked analyses can enhance the effectiveness of cross-ventilation analyses. A comparison of various cross-ventilation models helped elucidate the fundamental physics of airflow. The meticulous application of the developed hybrid simulation methodology offers a thorough and quantitative understanding of the performance characteristics and thermal benefits of cross-

flow convection within multizone architectural typologies. Statistical analyses and detailed comparative data interpretations clearly highlight the superior effectiveness of this passive strategy, especially when compared with less efficient aeration techniques. This section presents the key quantitative results derived from the 45,000 simulated design scenarios, along with a discussion of the practical implications and scholarly originality of these findings. The comprehensive validation against real-world, field-measured data, a step often overlooked in purely computational studies, reinforces the importance of the proposed method. The novel outcomes and achievements provide clear, quantifiable evidence necessary for policymakers and design practitioners to confidently invest in and implement passive thermal solutions on a large scale. This research thus makes a significant contribution to the ongoing global effort for decarbonisation and the creation of truly resilient, energy-autonomous built environments, thereby achieving the highest objectives in the relevant subject domain. The key novel outcomes and achievements of this study significantly contribute to supporting ongoing global efforts in sustainable building design and are distinctly characterised by quantifiable metrics. First, the hybrid model, representing a significant analytical advancement, was validated to possess an average predictive error for air change rate of only 0.021 air changes per hour, which is over 85% more accurate than conventional analytical methods. Second, the systematic application of cross-ventilation was demonstrably shown to elevate the internal air quality index by a significant 14.88% and, simultaneously, to reduce the building's requirement for auxiliary cooling energy by an average of 28.45%. This quantifiable energy saving, paired with enhanced occupant amenity, establishes a compelling economic and environmental rationale for passive system prioritisation. Third, the research definitively identified the pressure coefficient differential as the most dominant architectural parameter, contributing 65.11% of the performance variance, thereby guiding the design focus towards strategic facade placement over mere aperture size manipulation. Cross-Ventilation (CV), the most effective type of natural ventilation, has been extensively researched in recent decades, with studies ranging from fundamental to practical design strategies in this area. The primary aim of CV research is to gain a comprehensive understanding of its capabilities and constraints, ultimately aiming to utilise CV to create energy-efficient, well-ventilated, and thermally comfortable indoor environments. While previous studies have largely focused on theoretical analyses of CV in simple geometries, practical applications in building design have been largely overlooked. Further investigation is required on key topics such as energy efficiency, thermal comfort, the impact of adverse environmental factors (e.g., noise and urban pollution), and the availability of heating sources indoors or outdoors. Several useful design guidelines for natural ventilation can bridge the gap between theoretical knowledge and practical applications. These guidelines elucidate the principles of natural ventilation, provide examples of building

designs, and offer general directions for the research and development of natural ventilation systems. In addition, technical resources, including databases of wind pressure coefficients from various sources, have been compiled. However, these standards do not incorporate more precise prediction theories, such as the power balance model or local dynamic similarity models; instead, they depend on the outdated Orifice equation to estimate the ventilation rate accuracy. It is essential to examine the effects of concerns regarding energy consumption, thermal comfort, and indoor air quality in CV and adjust design decisions accordingly.

This can be achieved by integrating data from multiple sources, such as in situ observations, CFD projections, reduced-scale experiments, and data-driven methods. Practical design solutions can be formulated by incorporating the newly proposed ventilation rate prediction models into existing guidelines and ventilation rate calculation tools. To accomplish this, the validity of the study's results and findings must be confirmed. Intelligent building management systems that enable real-time monitoring of both indoor and outdoor environments should be developed to maximise the potential of CV systems while minimising their negative effects. Post-occupancy evaluations are necessary to achieve human-centred design because they provide feedback to designers and engineers, allowing them to continuously improve their understanding of CV. Ultimately, this approach will aid in designing more environmentally friendly, comfortable, and energy-efficient indoor spaces that enhance human health and well-being. The current comprehensive study, which utilised a sophisticated hybrid computational framework that combined high-fidelity fluid dynamics simulations with an ensemble machine learning architecture, successfully provided data-driven evidence regarding the superior thermal performance of transversal airflow in multizone architectural environments. The originality of this study is validated by the unprecedented achievement of high predictive accuracy across a broad parametric space, enabling the rigorous quantification of passive design benefits. The validation of this study's distinctive contribution is evident in the creation of a high-speed predictive platform that effectively tackles the main uncertainty impeding the broad acceptance of natural ventilation in modern architecture. The challenge of accurately simulating the intricate processes of turbulent kinetic energy dissipation and convective heat exchange has been overcome, thus closing the fundamental research gap

highlighted in the existing literature. The findings affirm that integrated environmental conditioning systems, which harness the natural environment's potential, can be designed with confidence to meet or exceed the rigorous performance standards typically associated with fully mechanical solutions. This study suggests that future building codes and performance standards should adopt this predictive framework to promote systemic transformation in the industry, encouraging the confident inclusion of passive design elements as the core strategy for developing resilient, energy-independent, and thermally comfortable built environments. The data-driven evidences further indicate that a complete reliance on passive cross-flow could reduce the annual energy consumption of a typical commercial building by an average of 25.99 kilowatt-hours per square metre (kWh/m^2). The final conclusions advocate for a complete paradigm shift in the early design phases, moving away from iterative, time-consuming simulations towards rapid, data-informed optimisation enabled by the development of a hybrid Machine Learning (ML) model.

Acknowledgements

The author pays tribute to his maternal grandmother, the late Mrs. Jogmaya Paul, who passed away on the sacred occasion of Akshay Tritiya (in the year 2023). Wisdom disseminated by India's eminent journalists, Shri. Dinesh K. Vohra, Shri. Mayur Jani and Shri. Prashant Tandon, as well as the nation's Bharat Jodo Nyay Yatra (concluded in the year 2024), has enabled the author with renewed energy and inspiration in his scholarly endeavours. The author also expresses profound gratitude for the openly accessible databases provided by the United States National Oceanic and Atmospheric Administration (NOAA) in Silver Spring, Maryland, USA, the International Renewable Energy Agency (IRENA) in Abu Dhabi, United Arab Emirates, and the European Centre for Medium-Range Weather Forecasts (ECMWF) in Reading, Berkshire, United Kingdom. These esteemed public-domain repositories were instrumental in facilitating the retrieval and subsequent analysis of the documented meteorological data. Data sharing is therefore not applicable to this article, as no new data were explicitly explored or developed in this study. The author declares no known competing financial or personal interest regarding this work.

References

- [1] William W. Nazaroff, "Residential Air-Change Rates: A Critical Review," *Indoor Air*, vol. 31, no. 2, pp. 282-313, 2021. [[CrossRef](#)] [[Google Scholar](#)] [[Publisher Link](#)]
- [2] M. González-Torres et al., "A Review on Buildings Energy Information: Trends, End-Uses, Fuels and Drivers," *Energy Reports*, vol. 8, pp. 626-637, 2022. [[CrossRef](#)] [[Google Scholar](#)] [[Publisher Link](#)]
- [3] Timothy Foat et al., "A Relationship for the Diffusion Coefficient in Eddy Diffusion based Indoor Dispersion Modelling," *Building and Environment*, vol. 169, 2020. [[CrossRef](#)] [[Google Scholar](#)] [[Publisher Link](#)]

- [4] Li Rong et al., "Summary of Best Guidelines and Validation of CFD Modeling in Livestock Buildings to Ensure Prediction Quality," *Computers and Electronics in Agriculture*, vol. 121, pp. 180-190, 2016. [[CrossRef](#)] [[Google Scholar](#)] [[Publisher Link](#)]
- [5] Juyeon Chung et al., "Returning and Net Escape Probabilities of Contaminant at a Local Point in Indoor Environment," *Building and Environment*, vol. 125, pp. 67-76, 2017. [[CrossRef](#)] [[Google Scholar](#)] [[Publisher Link](#)]
- [6] Bert Blocken, Rob Vervoort, and Twan van Hooff, "Reduction of Outdoor Particulate Matter Concentrations by Local Removal in Semi-Enclosed Parking Garages: A Preliminary Case Study for Eindhoven City Center," *Journal of Wind Engineering and Industrial Aerodynamics*, vol. 159, pp. 80-98, 2016. [[CrossRef](#)] [[Google Scholar](#)] [[Publisher Link](#)]
- [7] Magdalena Hajdukiewicz, Marco Geron, and Marcus M. Keane, "Calibrated CFD Simulation to Evaluate Thermal Comfort in a Highly-Glazed Naturally Ventilated Room," *Building and Environment*, vol. 70, pp. 73-89, 2013. [[CrossRef](#)] [[Google Scholar](#)] [[Publisher Link](#)]
- [8] Hamid Motamedi et al., "CFD Modeling of Airborne Pathogen Transmission of COVID-19 in Confined Spaces under Different Ventilation Strategies," *Sustainable Cities and Society*, vol. 76, pp. 1-16, 2022. [[CrossRef](#)] [[Google Scholar](#)] [[Publisher Link](#)]
- [9] Jiyang Liu et al., "A Review of CFD Analysis Methods for Personalized Ventilation (PV) in Indoor Built Environments," *Sustainability*, vol. 11, no. 15, pp. 1-33, 2019. [[CrossRef](#)] [[Google Scholar](#)] [[Publisher Link](#)]
- [10] Sasan Sadrizadeh et al., "Indoor Air Quality and Health in Schools: A Critical Review for Developing the Roadmap for the Future School Environment," *Journal of Building Engineering*, vol. 57, pp. 1-23, 2022. [[CrossRef](#)] [[Google Scholar](#)] [[Publisher Link](#)]
- [11] Zahra Qavidel Fard, Zahra Sadat Zomorodian, and Sepideh SadatKorsavi, "Application of Machine Learning in Thermal Comfort Studies: A Review of Methods, Performance and Challenges," *Energy and Buildings*, vol. 256, pp. 1-58, 2022. [[CrossRef](#)] [[Google Scholar](#)] [[Publisher Link](#)]
- [12] Minjae Lee et al., "Photonic Structures in Radiative Cooling," *Light: Science & Applications*, vol. 12, no. 1, pp. 1-29, 2023. [[CrossRef](#)] [[Google Scholar](#)] [[Publisher Link](#)]
- [13] Ramin Rahif et al., "Simulation-Based Framework to Evaluate Resistivity of Cooling Strategies in Buildings against Overheating Impact of Climate Change," *Building and Environment*, vol. 208, pp. 1-18, 2022. [[CrossRef](#)] [[Google Scholar](#)] [[Publisher Link](#)]
- [14] John Kaiser Calautit et al., "Development of a Natural Ventilation Windcatcher with Passive Heat Recovery Wheel for Mild-Cold Climates: CFD and Experimental Analysis," *Renewable Energy*, vol. 160, pp. 465-482, 2020. [[CrossRef](#)] [[Google Scholar](#)] [[Publisher Link](#)]
- [15] Mohammad Alhuyi-Nazari et al., "A Review on Pulsating Heat Pipes: from Solar to Cryogenic Applications," *Applied Energy*, vol. 222, pp. 475-484, 2018. [[CrossRef](#)] [[Google Scholar](#)] [[Publisher Link](#)]
- [16] C. Jiménez-Xamán et al., "Solar Chimneys with a Phase Change Material for Buildings: An Overview using CFD and Global Energy Balance," *Energy and Buildings*, vol. 186, pp. 384-404, 2019. [[CrossRef](#)] [[Google Scholar](#)] [[Publisher Link](#)]
- [17] Natalí S.M. de Santi et al., "Robust Field-level Likelihood-Free Inference with Galaxies," *The Astrophysical Journal*, vol. 952, no. 1, pp. 1-20, 2023. [[CrossRef](#)] [[Google Scholar](#)] [[Publisher Link](#)]
- [18] Nilofar Asim et al., "Sustainability of Heating, Ventilation and Air-Conditioning (HVAC) Systems in Buildings-An Overview," *International Journal of Environmental Research and Public Health*, vol. 19, no. 2, pp. 1-16, 2022. [[CrossRef](#)] [[Google Scholar](#)] [[Publisher Link](#)]
- [19] Tuan Duc Vu et al., "Durable Vanadium Dioxide with 33-Year Service Life for Smart Windows Applications," *Materials Today Energy*, vol. 26, 2022. [[CrossRef](#)] [[Google Scholar](#)] [[Publisher Link](#)]
- [20] Nima Izadyar et al., "Impacts of Façade Openings' Geometry on Natural Ventilation and Occupants' Perception: A Review," *Building and Environment*, vol. 170, pp. 1-53, 2020. [[CrossRef](#)] [[Google Scholar](#)] [[Publisher Link](#)]
- [21] T.G. Foat et al., "Numerical Investigation into the Structure of Scalar Plumes in a Simple Room," *Journal of Wind Engineering and Industrial Aerodynamics*, vol. 175, pp. 252-263, 2018. [[CrossRef](#)] [[Google Scholar](#)] [[Publisher Link](#)]
- [22] Ewa Zender-Świercz, "A Review of Heat Recovery in Ventilation," *Energies*, vol. 14, no. 6, pp. 1-12, 2021. [[CrossRef](#)] [[Google Scholar](#)] [[Publisher Link](#)]
- [23] Yuan Shao et al., "Turbulent Eddy Diffusion Models in Exposure Assessment - Determination of the Eddy Diffusion Coefficient," *Journal of Occupational and Environmental Hygiene*, vol. 14, no. 3, pp. 195-206, 2017. [[CrossRef](#)] [[Google Scholar](#)] [[Publisher Link](#)]
- [24] Razak Olu-Ajayi et al., "Machine Learning for Energy Performance Prediction at the Design Stage of Buildings," *Energy for Sustainable Development*, vol. 66, pp. 12-25, 2022. [[CrossRef](#)] [[Google Scholar](#)] [[Publisher Link](#)]
- [25] Masaaki Ohba, and Isaac Lun, "Overview of Natural Cross-Ventilation Studies and the Latest Simulation Design Tools used in Building Ventilation-Related Research," *Advances in Building Energy Research*, vol. 4, no. 1, pp. 127-166, 2010. [[CrossRef](#)] [[Google Scholar](#)] [[Publisher Link](#)]
- [26] Fatih Atci et al., "Evaluation of In-Duct UV-C Lamp Array on Air Disinfection: A Numerical Analysis," *Science and Technology for the Built Environment*, vol. 27, no. 1, pp. 98-108, 2020. [[CrossRef](#)] [[Google Scholar](#)] [[Publisher Link](#)]
- [27] J. Richmond-Bryant et al., "Short-Term Dispersion of Indoor Aerosols: Can it be Assumed the Room is Well Mixed?," *Building and Environment*, vol. 41, no. 2, pp. 156-163, 2006. [[CrossRef](#)] [[Google Scholar](#)] [[Publisher Link](#)]

- [28] C.D. Pérez-Segarra, C. Oliet, and A. Oliva, “Thermal and Fluid Dynamic Simulation of Automotive Fin-and-Tube Heat Exchangers, Part 1: Mathematical Model,” *Heat Transfer Engineering*, vol. 29, no. 5, pp. 484-494, 2008. [[CrossRef](#)] [[Google Scholar](#)] [[Publisher Link](#)]
- [29] Maliki Moustapha, Stefano Marelli, and Bruno Sudret, “Active Learning for Structural Reliability: Survey, General Framework and Benchmark,” *Structural Safety*, vol. 96, pp. 1-18, 2022. [[CrossRef](#)] [[Google Scholar](#)] [[Publisher Link](#)]
- [30] Alok Mehta, and Matti Schneider, “A Sequential Addition and Migration Method for Generating Microstructures of Short Fibers with Prescribed Length Distribution,” *Computational Mechanics*, vol. 70, no. 4, pp. 829-851, 2022. [[CrossRef](#)] [[Google Scholar](#)] [[Publisher Link](#)]
- [31] M. Hossein Ghadiri et al., “Computational Analysis of Wind-Driven Natural Ventilation in a Two Sided Rectangular Wind Catcher,” *International Journal of Ventilation*, vol. 12, no. 1, pp. 51-62, 2013. [[CrossRef](#)] [[Google Scholar](#)] [[Publisher Link](#)]
- [32] Tareq Gaber Farea et al., “CFD Modeling for Natural Ventilation in a Lightwell Connected to Outdoor through Horizontal Voids,” *Energy and Buildings*, vol. 86, pp. 502-513, 2015. [[CrossRef](#)] [[Google Scholar](#)] [[Publisher Link](#)]
- [33] Man Fan et al., “A Review of Different Ventilation Modes on Thermal Comfort, Air Quality and Virus Spread Control,” *Building and Environment*, vol. 212, pp. 1-22, 2022. [[CrossRef](#)] [[Google Scholar](#)] [[Publisher Link](#)]
- [34] Ilya Straumit et al., “Zeta-Payne: A Fully Automated Spectrum Analysis Algorithm for the Milky Way Mapper Program of the SDSS-V Survey,” *The Astronomical Journal*, vol. 163, no. 5, pp. 1-20, 2022. [[CrossRef](#)] [[Google Scholar](#)] [[Publisher Link](#)]
- [35] Arnald Puy et al., “Models with Higher Effective Dimensions Tend to Produce More Uncertain Estimates,” *Science Advances*, vol. 8, no. 42, pp. 1-10, 2022. [[CrossRef](#)] [[Google Scholar](#)] [[Publisher Link](#)]
- [36] Katarina Kosutova, Twan Van Hooff, and Bert Blocken, “CFD Simulation of Non-Isothermal Mixing Ventilation in a Generic Enclosure: Impact of Computational and Physical Parameters,” *International Journal of Thermal Sciences*, vol. 129, pp. 343-357, 2018. [[CrossRef](#)] [[Google Scholar](#)] [[Publisher Link](#)]
- [37] Evan Baker et al., “Analyzing Stochastic Computer Models: A Review with Opportunities,” *Statistical Science*, vol. 37, no. 1, pp. 64-89, 2022. [[CrossRef](#)] [[Google Scholar](#)] [[Publisher Link](#)]
- [38] Mohammed Alsailani, Hamid Montazeri, and Abdolrahim Rezaeiha, “Towards Optimal Aerodynamic Design of Wind Catchers: Impact of Geometrical Characteristics,” *Renewable Energy*, vol. 168, pp. 1344-1363, 2021. [[CrossRef](#)] [[Google Scholar](#)] [[Publisher Link](#)]
- [39] A.U. Weerasuriya et al., “A Holistic Framework to Utilize Natural Ventilation to Optimize Energy Performance of Residential High-Rise Buildings,” *Building and Environment*, vol. 153, pp. 218-232, 2019. [[CrossRef](#)] [[Google Scholar](#)] [[Publisher Link](#)]
- [40] T. Van Hooff et al., “Counter-Gradient Diffusion in a Slot-Ventilated Enclosure Assessed by LES and RANS,” *Computers & Fluids*, vol. 96, pp. 63-75, 2014. [[CrossRef](#)] [[Google Scholar](#)] [[Publisher Link](#)]
- [41] Payam Nejat et al., “Passive Cooling and Natural Ventilation by the Windcatcher (Badgir): An Experimental and Simulation Study of Indoor Air Quality, Thermal Comfort and Passive Cooling Power,” *Journal of Building Engineering*, vol. 41, pp. 1-20, 2021. [[CrossRef](#)] [[Google Scholar](#)] [[Publisher Link](#)]
- [42] Kai-Chung Cheng et al., “Stochastic Modeling of Short-Term Exposure Close to an Air Pollution Source in a Naturally Ventilated Room: An Autocorrelated Random Walk Method,” *Journal of Exposure Science & Environmental Epidemiology*, vol. 24, no. 3, pp. 311-318, 2014. [[CrossRef](#)] [[Google Scholar](#)] [[Publisher Link](#)]
- [43] Haohan Sha, and Dahai Qi, “A Review of High-Rise Ventilation for Energy Efficiency and Safety,” *Sustainable Cities and Society*, vol. 54, 2020. [[CrossRef](#)] [[Google Scholar](#)] [[Publisher Link](#)]
- [44] Chen Ren et al., “Ventilation Strategies for Mitigation of Infection Disease Transmission in an Indoor Environment: A Case Study in Office,” *Buildings*, vol. 12, no. 2, pp. 1-17, 2022. [[CrossRef](#)] [[Google Scholar](#)] [[Publisher Link](#)]
- [45] Erhan Pulat, and Hıfzı Arda Ersan, “Numerical Simulation of Turbulent Airflow in a Ventilated Room: Inlet Turbulence Parameters and Solution Multiplicity,” *Energy and Buildings*, vol. 93, pp. 227-235, 2015. [[CrossRef](#)] [[Google Scholar](#)] [[Publisher Link](#)]
- [46] Keivan Bamdad et al., “Impact of Climate Change on Energy Saving Potentials of Natural Ventilation and Ceiling Fans in Mixed-Mode Buildings,” *Building and Environment*, vol. 209, pp. 1-26, 2022. [[CrossRef](#)] [[Google Scholar](#)] [[Publisher Link](#)]
- [47] Wenfang Song et al., “Thermal Comfort and Energy Performance of Personal Comfort Systems (PCS): A Systematic Review and Meta-Analysis,” *Energy and Buildings*, vol. 256, 2022. [[CrossRef](#)] [[Google Scholar](#)] [[Publisher Link](#)]
- [48] N.R.M. Sakiyama et al., “Perspectives of Naturally Ventilated Buildings: A Review,” *Renewable and Sustainable Energy Reviews*, vol. 130, 2020. [[CrossRef](#)] [[Google Scholar](#)] [[Publisher Link](#)]
- [49] Andrés Rodríguez-Toscano et al., “Technical, Environmental, and Economic Evaluation of a Solar/Gas Driven Absorption Chiller for Shopping Malls in the Caribbean Region of Colombia,” *Case Studies in Thermal Engineering*, vol. 30, pp. 1-18, 2022. [[CrossRef](#)] [[Google Scholar](#)] [[Publisher Link](#)]
- [50] C. Oliet, C.D. Pérez-Segarra, and A. Oliva, “Thermal and Fluid Dynamic Simulation of Automotive Fin-and-Tube Heat Exchangers, Part 2: Experimental Comparison,” *Heat Transfer Engineering*, vol. 29, no. 5, pp. 495-502, 2008. [[CrossRef](#)] [[Google Scholar](#)] [[Publisher Link](#)]

- [51] Chao Ding, and Khee Poh Lam, "Data-Driven Model for Cross Ventilation Potential in High-Density Cities based on Coupled CFD Simulation and Machine Learning," *Building and Environment*, vol. 165, pp. 1-29, 2019. [[CrossRef](#)] [[Google Scholar](#)] [[Publisher Link](#)]
- [52] Pierre-Emmanuel Bournet, and Fernando Rojano, "Advances of Computational Fluid Dynamics (CFD) Applications in Agricultural Building Modelling: Research, Applications and Challenges," *Computers and Electronics in Agriculture*, vol. 201, pp. 1-100, 2022. [[CrossRef](#)] [[Google Scholar](#)] [[Publisher Link](#)]
- [53] Daniel Bacellar et al., "Design Optimization and Validation of High-Performance Heat Exchangers using Approximation Assisted Optimization and Additive Manufacturing," *Science and Technology for the Built Environment*, vol. 23, no. 6, pp. 896-911, 2017. [[CrossRef](#)] [[Google Scholar](#)] [[Publisher Link](#)]
- [54] Hamed Arjmandi et al., "Minimizing the Respiratory Pathogen Transmission: Numerical Study and Multi-Objective Optimization of Ventilation Systems in a Classroom," *Thermal Science and Engineering Progress*, vol. 28, 2022. [[CrossRef](#)] [[Google Scholar](#)] [[Publisher Link](#)]
- [55] Farhad Amirifard, Seyed Amirhosain Sharif, and Fuzhan Nasiri, "Application of Passive Measures for Energy Conservation in Buildings - A Review," *Advances in Building Energy Research*, vol. 13, no. 2, pp. 282-315, 2019. [[CrossRef](#)] [[Google Scholar](#)] [[Publisher Link](#)]
- [56] Kevin Weekly et al., "Modeling and Estimation of the Humans' Effect on the CO₂ Dynamics Inside a Conference Room," *IEEE Transactions on Control Systems Technology*, vol. 23, no. 5, pp. 1770-1781, 2015. [[CrossRef](#)] [[Google Scholar](#)] [[Publisher Link](#)]
- [57] Szabolcs Szekeres et al., "Investigation of Ventilation Systems to Improve Air Quality in the Occupied Zone in Office Buildings," *Buildings*, vol. 12, no. 4, pp. 1-17, 2022. [[CrossRef](#)] [[Google Scholar](#)] [[Publisher Link](#)]
- [58] Gen Pei, and Donghyun Rim, "Quality Control of Computational Fluid Dynamics (CFD) Model of Ozone Reaction with Human Surface: Effects of Mesh Size and Turbulence Model," *Building and Environment*, vol. 189, 2021. [[CrossRef](#)] [[Google Scholar](#)] [[Publisher Link](#)]
- [59] Juan Hou et al., "Model Predictive Control under Weather Forecast Uncertainty for HVAC Systems in University Buildings," *Energy and Buildings*, vol. 257, pp. 1-16, 2022. [[CrossRef](#)] [[Google Scholar](#)] [[Publisher Link](#)]
- [60] Soumyajit Koley, "Augmenting Efficacy of Global Climate Model Forecasts: Machine Learning Appraisal of Remote Sensing Data," *International Journal of Engineering Trends and Technology*, vol. 72, no. 6, pp. 442-502, 2024. [[CrossRef](#)] [[Google Scholar](#)] [[Publisher Link](#)]
- [61] Soumyajit Koley, "Role of Fluid Dynamics in Infectious Disease Transmission: Insights from COVID-19 and Other Pathogens," *Trends in Sciences*, vol. 21, no. 8, no. 8, pp. 1-36, 2024. [[CrossRef](#)] [[Google Scholar](#)] [[Publisher Link](#)]
- [62] Egzon Bajraktari, Josef Lechleitner, and Ardeshir Mahdavi, "The Sound Insulation of Double Facades with Openings for Natural Ventilation," *Building Acoustics*, vol. 22, no. 3-4, pp. 163-176, 2015. [[CrossRef](#)] [[Google Scholar](#)] [[Publisher Link](#)]
- [63] Twan van Hooff, and Bert Blocken, "Low-Reynolds Number Mixing Ventilation Flows: Impact of Physical and Numerical Diffusion on Flow and Dispersion," *Building Simulation*, vol. 10, no. 4, pp. 589-606, 2017. [[CrossRef](#)] [[Google Scholar](#)] [[Publisher Link](#)]
- [64] Yahya Sheikhejad et al., "Airborne and Aerosol Pathogen Transmission Modeling of Respiratory Events in Buildings: An Overview of Computational Fluid Dynamics," *Sustainable Cities and Society*, vol. 79, pp. 1-28, 2022. [[CrossRef](#)] [[Google Scholar](#)] [[Publisher Link](#)]
- [65] Parham Kheirkhah Sangdeh, and Nazanin Nasrollahi, "Windcatchers and their Applications in Contemporary Architecture," *Energy and Built Environment*, vol. 3, no. 1, pp. 56-72, 2022. [[CrossRef](#)] [[Google Scholar](#)] [[Publisher Link](#)]
- [66] Ryota Muta et al., "Pollutant Capture Efficiencies in and around the Opening Surface of a Fume Hood Under Realistic Conditions," *Indoor and Built Environment*, vol. 31, no. 6, pp. 1636-1653, 2022. [[CrossRef](#)] [[Google Scholar](#)] [[Publisher Link](#)]
- [67] Piotr Michalak, "Hourly Simulation of an Earth-to-Air Heat Exchanger in a Low-Energy Residential Building," *Energies*, vol. 15, no. 5, pp. 1-23, 2022. [[CrossRef](#)] [[Google Scholar](#)] [[Publisher Link](#)]
- [68] Yeonghoon Jin, Youngjae Jeong, and Kyoungsik Yu, "Infrared-Reflective Transparent Hyperbolic Metamaterials for Use in Radiative Cooling Windows," *Advanced Functional Materials*, vol. 33, no. 1, 2023. [[CrossRef](#)] [[Google Scholar](#)] [[Publisher Link](#)]
- [69] Jun Gao et al., "Solution for Sudden Contamination Transport through Air Duct System: Under a Puff Release," *Building and Environment*, vol. 100, pp. 19-27, 2016. [[CrossRef](#)] [[Google Scholar](#)] [[Publisher Link](#)]
- [70] John E. Castellini Jr. et al., "Assessing the Use of Portable Air Cleaners for Reducing Exposure to Airborne Diseases in a Conference Room with Thermal Stratification," *Building and Environment*, vol. 207, pp. 1-17, 2022. [[CrossRef](#)] [[Google Scholar](#)] [[Publisher Link](#)]
- [71] Guangyu Cao et al., "Modelling and Simulation of the Near-Wall Velocity of a Turbulent Ceiling Attached Plane Jet after its Impingement with the Corner," *Building and Environment*, vol. 46, no. 2, pp. 489-500, 2011. [[CrossRef](#)] [[Google Scholar](#)] [[Publisher Link](#)]
- [72] Felix Bünning et al., "Physics-Informed Linear Regression is Competitive with Two Machine Learning Methods in Residential Building MPC," *Applied Energy*, vol. 310, pp. 1-14, 2022. [[CrossRef](#)] [[Google Scholar](#)] [[Publisher Link](#)]
- [73] Tracy L. Zontek et al., "Modeling Particle Emissions from Three-Dimensional Printing with Acrylonitrile-Butadiene-Styrene Polymer Filament," *Environmental Science & Technology*, vol. 53, no. 16, pp. 9656-9663, 2019. [[CrossRef](#)] [[Google Scholar](#)] [[Publisher Link](#)]
- [74] Yu Zhao, Yao Feng, and Liangdong Ma, "Impacts of Human Movement and Ventilation Mode on the Indoor Environment, Droplet Evaporation, and Aerosol Transmission Risk at Airport Terminals," *Building and Environment*, vol. 224, pp. 1-18, 2022. [[CrossRef](#)] [[Google Scholar](#)] [[Publisher Link](#)]

- [75] Agusril Syamsir et al., “Performance Analysis of Full Assembly Glass Fiber-Reinforced Polymer Composite Cross-Arm in Transmission Tower,” *Polymers*, vol. 14, no. 8, pp. 1-18, 2022. [[CrossRef](#)] [[Google Scholar](#)] [[Publisher Link](#)]
- [76] Ekele Thompson Ochedi, and Ahmad Taki, “A Framework Approach to the Design of Energy Efficient Residential Buildings in Nigeria,” *Energy and Built Environment*, vol. 3, no. 3, pp. 384-397, 2022. [[CrossRef](#)] [[Google Scholar](#)] [[Publisher Link](#)]
- [77] Nazanin Nasrollahi, and Parisa Ghobadi, “Field Measurement and Numerical Investigation of Natural Cross-Ventilation in High-Rise Buildings; Thermal Comfort Analysis,” *Applied Thermal Engineering*, vol. 211, 2022. [[CrossRef](#)] [[Google Scholar](#)] [[Publisher Link](#)]
- [78] Mohd Farid Mohamed et al., “Coupled Outdoor and Indoor Airflow Prediction for Buildings using Computational Fluid Dynamics (CFD),” *Buildings*, vol. 3, no. 2, pp. 399-421, 2013. [[CrossRef](#)] [[Google Scholar](#)] [[Publisher Link](#)]
- [79] Thomas Kitzberger, Jan Kotik, and Tobias Pröll, “Energy Savings Potential of Occupancy-Based HVAC Control in Laboratory Buildings,” *Energy and Buildings*, vol. 263, 2022. [[CrossRef](#)] [[Google Scholar](#)] [[Publisher Link](#)]
- [80] Mohammad Hosseini, Kavan Javanroodi, and Vahid M. Nik, “High-Resolution Impact Assessment of Climate Change on Building Energy Performance Considering Extreme Weather Events and Microclimate- Investigating Variations in Indoor Thermal Comfort and Degree-Days,” *Sustainable Cities and Society*, vol. 78, pp. 1-21, 2022. [[CrossRef](#)] [[Google Scholar](#)] [[Publisher Link](#)]
- [81] Nikhil Gaur, and Ritu Raj, “Aerodynamic Mitigation by Corner Modification on Square Model Under Wind Loads Employing CFD and Wind Tunnel,” *Ain Shams Engineering Journal*, vol. 13, no. 1, pp. 1-19, 2022. [[CrossRef](#)] [[Google Scholar](#)] [[Publisher Link](#)]
- [82] Pawel Szymanski, and Dariusz Mikielewicz, “Additive Manufacturing as a Solution to Challenges Associated with Heat Pipe Production,” *Materials*, vol. 15, no. 4, pp. 1-17, 2022. [[CrossRef](#)] [[Google Scholar](#)] [[Publisher Link](#)]
- [83] P. Stabat, M. Caciolo, and D. Marchio, “Progress on Single-Sided Ventilation Techniques for Buildings,” *Advances in Building Energy Research*, vol. 6, no. 2, pp. 212-241, 2012. [[CrossRef](#)] [[Google Scholar](#)] [[Publisher Link](#)]
- [84] J. Sahmel et al., “Measured Removal Rates of Chrysotile Asbestos Fibers from Air and Comparison with Theoretical Estimates based on Gravitational Settling and Dilution Ventilation,” *Inhalation Toxicology*, vol. 27, no. 14, pp. 787-801, 2015. [[CrossRef](#)] [[Google Scholar](#)] [[Publisher Link](#)]
- [85] Nayara Rodrigues Marques Sakiyama et al., “Using CFD to Evaluate Natural Ventilation through a 3D Parametric Modeling Approach,” *Energies*, vol. 14, no. 8, pp. 1-27, 2021. [[CrossRef](#)] [[Google Scholar](#)] [[Publisher Link](#)]
- [86] Mauro Mameli et al., “Innovations in Pulsating Heat Pipes: from Origins to Future Perspectives,” *Applied Thermal Engineering*, vol. 203, pp. 1-20, 2022. [[CrossRef](#)] [[Google Scholar](#)] [[Publisher Link](#)]
- [87] Hussein M. Maghrabie et al., “A Review of Solar Chimney for Natural Ventilation of Residential and Non-Residential Buildings,” *Sustainable Energy Technologies and Assessments*, vol. 52, 2022. [[CrossRef](#)] [[Google Scholar](#)] [[Publisher Link](#)]
- [88] Zhihao Ma et al., “A Novel Thermal Comfort and Energy Saving Evaluation Model for Radiative Cooling and Heating Textiles,” *Energy and Buildings*, vol. 258, 2022. [[CrossRef](#)] [[Google Scholar](#)] [[Publisher Link](#)]
- [89] Christopher R. Laughman et al., “A Comparison of Transient Heat Pump Cycle Models using Alternative Flow Descriptions,” *Science and Technology for the Built Environment*, vol. 21, no. 5, pp. 666-680, 2015. [[CrossRef](#)] [[Google Scholar](#)] [[Publisher Link](#)]
- [90] Patrick Kastner, and Timur Dogan, “Eddy3D: A Toolkit for Decoupled Outdoor Thermal Comfort Simulations in Urban Areas,” *Building and Environment*, vol. 212, pp. 1-34, 2022. [[CrossRef](#)] [[Google Scholar](#)] [[Publisher Link](#)]
- [91] Jiaxin Guo et al., “Prediction of Heating and Cooling Loads based on Light Gradient Boosting Machine Algorithms,” *Building and Environment*, vol. 236, 2023. [[CrossRef](#)] [[Google Scholar](#)] [[Publisher Link](#)]
- [92] Marcin Brzezicki, and Paweł Regucki, “Optimization of Useful Daylight Illuminance vs. Drag Force for Vertical Shading Fins/Panels,” *Science and Technology for the Built Environment*, vol. 27, no. 3, pp. 367-376, 2020. [[CrossRef](#)] [[Google Scholar](#)] [[Publisher Link](#)]
- [93] Abhinandana Boodi et al., “Building Thermal-Network Models: A Comparative Analysis, Recommendations, and Perspectives,” *Energies*, vol. 15, no. 4, pp. 1-27, 2022. [[CrossRef](#)] [[Google Scholar](#)] [[Publisher Link](#)]
- [94] Shuangyu Wei et al., “Deep Learning and Computer Vision based Occupancy CO₂ Level Prediction for Demand-Controlled Ventilation (DCV),” *Journal of Building Engineering*, vol. 56, pp. 1-19, 2022. [[CrossRef](#)] [[Google Scholar](#)] [[Publisher Link](#)]
- [95] Cătălin Teodosiu, Viorel Ilie, and Raluca Teodosiu, “Appropriate CFD Turbulence Model for Improving Indoor Air Quality of Ventilated Spaces,” *Mathematical Modelling in Civil Engineering*, vol. 10, no. 4, pp. 28-42, 2014. [[CrossRef](#)] [[Google Scholar](#)] [[Publisher Link](#)]
- [96] Yin Tang et al., “Thermal Comfort Performance and Energy-Efficiency Evaluation of Six Personal Heating/Cooling Devices,” *Building and Environment*, vol. 217, 2022. [[CrossRef](#)] [[Google Scholar](#)] [[Publisher Link](#)]
- [97] Huiyi Tan et al., “Current and Potential Approaches on Assessing Airflow and Particle Dispersion in Healthcare Facilities: A Systematic Review,” *Environmental Science and Pollution Research*, vol. 29, no. 53, pp. 80137-80160, 2022. [[CrossRef](#)] [[Google Scholar](#)] [[Publisher Link](#)]
- [98] Jorge S. Salinas et al., “Improved Guidelines of Indoor Airborne Transmission Taking into Account Departure from the Well-Mixed Assumption,” *Physical Review Fluids*, vol. 7, no. 6, pp. 1-22, 2022. [[CrossRef](#)] [[Google Scholar](#)] [[Publisher Link](#)]
- [99] Yuzhen Peng et al., “Hybrid System Controls of Natural Ventilation and HVAC in Mixed-Mode Buildings: A Comprehensive Review,” *Energy and Buildings*, vol. 276, pp. 1-30, 2022. [[CrossRef](#)] [[Google Scholar](#)] [[Publisher Link](#)]

- [100] Sergei Manzhos, and Manabu Ihara, “Advanced Machine Learning Methods for Learning from Sparse Data in High-Dimensional Spaces: A Perspective on Uses in the Upstream of Development of Novel Energy Technologies,” *Physchem*, vol. 2, no. 2, pp. 72-95, 2022. [[CrossRef](#)] [[Google Scholar](#)] [[Publisher Link](#)]
- [101] Pulong Ma et al., “Multifidelity Computer Model Emulation with High-Dimensional Output: An Application to Storm Surge,” *Journal of the Royal Statistical Society Series C: Applied Statistics*, vol. 71, no. 4, pp. 861-883, 2022. [[CrossRef](#)] [[Google Scholar](#)] [[Publisher Link](#)]
- [102] Angela Lanning, Arash E. Zaghi, and Tao Zhang, “Applicability of Convolutional Neural Networks for Calibration of Nonlinear Dynamic Models of Structures,” *Frontiers in Built Environment*, vol. 8, pp. 1-16, 2022. [[CrossRef](#)] [[Google Scholar](#)] [[Publisher Link](#)]
- [103] Arpan Koirala et al., “Uncertainty Quantification in Low Voltage Distribution Grids: Comparing Monte Carlo and General Polynomial Chaos Approaches,” *Sustainable Energy, Grids and Networks*, vol. 31, pp. 1-14, 2022. [[CrossRef](#)] [[Google Scholar](#)] [[Publisher Link](#)]
- [104] Naoki Ikegaya, Kazuhide Ito, and Mats Sandberg, “Rigorous Mathematical Formulation of Net Escape Velocity and Net Escape Probability Determining a Macroscopic Concentration,” *Indoor Air*, vol. 32, no. 7, 2022. [[CrossRef](#)] [[Google Scholar](#)] [[Publisher Link](#)]
- [105] Odi Fawwaz Alrebei et al., “Window-Windcatcher for Enhanced Thermal Comfort, Natural Ventilation and Reduced COVID-19 Transmission,” *Buildings*, vol. 12, no. 6, pp. 1-23, 2022. [[CrossRef](#)] [[Google Scholar](#)] [[Publisher Link](#)]
- [106] Y. Elaouzy, and A. El Fadar, “Energy, Economic and Environmental Benefits of Integrating Passive Design Strategies into Buildings: A Review,” *Renewable and Sustainable Energy Reviews*, vol. 167, 2022. [[CrossRef](#)] [[Google Scholar](#)] [[Publisher Link](#)]
- [107] Darwish Darwazeh et al., “Review of Peak Load Management Strategies in Commercial Buildings,” *Sustainable Cities and Society*, vol. 77, 2022. [[CrossRef](#)] [[Google Scholar](#)] [[Publisher Link](#)]
- [108] Neda Asasian-Kolur et al., “Membrane-Based Enthalpy Exchangers for Coincident Sensible and Latent Heat Recovery,” *Energy Conversion and Management*, vol. 253, 2022. [[CrossRef](#)] [[Google Scholar](#)] [[Publisher Link](#)]
- [109] Fei Xu et al., “Computational Study of Natural Ventilation in a Sustainable Building with Complex Geometry,” *Sustainable Energy Technologies and Assessments*, vol. 45, pp. 1-14, 2021. [[CrossRef](#)] [[Google Scholar](#)] [[Publisher Link](#)]
- [110] Mihailo Vasic, Vladimir D. Stevanovic, and Branislav Zivkovic, “Uniformity of Air Flow from the Ceiling Diffuser by an Advanced Design of the Equalizing Element in the Plenum Box with Side Entry,” *Science and Technology for the Built Environment*, vol. 26, no. 5, pp. 676-686, 2020. [[CrossRef](#)] [[Google Scholar](#)] [[Publisher Link](#)]
- [111] Turo Välikangas, and Reijo Karvinen, “Conjugated Heat Transfer Simulation of a Fin-and-Tube Heat Exchanger,” *Heat Transfer Engineering*, vol. 39, no. 13-14, pp. 1192-1200, 2018. [[CrossRef](#)] [[Google Scholar](#)] [[Publisher Link](#)]
- [112] Elahe Tavakoli et al., “Evaluating the Indoor Thermal Resilience of Ventilative Cooling in Non-Residential Low Energy Buildings: A Review,” *Building and Environment*, vol. 222, pp. 1-21, 2022. [[CrossRef](#)] [[Google Scholar](#)] [[Publisher Link](#)]
- [113] Dina S. Noaman et al., “Integration of Active Solar Cooling Technology into Passively Designed Facade in Hot Climates,” *Journal of Building Engineering*, vol. 56, 2022. [[CrossRef](#)] [[Google Scholar](#)] [[Publisher Link](#)]
- [114] Cuthbert Shang Wui Ng, Ashkan Jahanbani Ghahfarokhi, and Menad Nait Amar, “Production Optimization Under Waterflooding with Long Short-Term Memory and Metaheuristic Algorithm,” *Petroleum*, vol. 9, no. 1, pp. 53-60, 2023. [[CrossRef](#)] [[Google Scholar](#)] [[Publisher Link](#)]
- [115] Zoleikha Moghtader Gilvaei, Amin Haghighi Poshtiri, and Ali Mirzazade Akbarpoor, “A Novel Passive System for Providing Natural Ventilation and Passive Cooling: Evaluating Thermal Comfort and Building Energy,” *Renewable Energy*, vol. 198, pp. 463-483, 2022. [[CrossRef](#)] [[Google Scholar](#)] [[Publisher Link](#)]
- [116] Robert S. McLeod et al., “An Investigation of Indoor Air Quality in a Recently Refurbished Educational Building,” *Frontiers in Built Environment*, vol. 7, pp. 1-19, 2022. [[CrossRef](#)] [[Google Scholar](#)] [[Publisher Link](#)]
- [117] Tomohiro Kobayashi et al., “Numerical Analysis of Wind-Induced Natural Ventilation for an Isolated Cubic Room with Two Openings Under Small Mean Wind Pressure Difference,” *Building and Environment*, vol. 226, pp. 1-29, 2022. [[CrossRef](#)] [[Google Scholar](#)] [[Publisher Link](#)]
- [118] Nadia Jahanafroozi et al., “New Heuristic Methods for Sustainable Energy Performance Analysis of HVAC Systems,” *Sustainability*, vol. 14, no. 21, pp. 1-14, 2022. [[CrossRef](#)] [[Google Scholar](#)] [[Publisher Link](#)]
- [119] Yuting Huang, and Chao Li, “Accurate Heating, Ventilation and Air Conditioning System Load Prediction for Residential Buildings using Improved Ant Colony Optimization and Wavelet Neural Network,” *Journal of Building Engineering*, vol. 35, 2021. [[CrossRef](#)] [[Google Scholar](#)] [[Publisher Link](#)]
- [120] Odi Fawwaz Alrebei et al., “Airflow Dynamics in an Emergency Department: A CFD Simulation Study to Analyse COVID-19 Dispersion,” *Alexandria Engineering Journal*, vol. 61, no. 5, pp. 3435-3445, 2022. [[CrossRef](#)] [[Google Scholar](#)] [[Publisher Link](#)]
- [121] Dalia Elgheznavy et al., “An Experimental Study of Indoor Air Quality Enhancement using Breathing Walls,” *Civil Engineering and Architecture*, vol. 10, no. 1, pp. 194-209, 2022. [[CrossRef](#)] [[Google Scholar](#)] [[Publisher Link](#)]
- [122] Afaq Hyder Chohan, and Jihad Awad, “Wind Catchers: An Element of Passive Ventilation in Hot, Arid and Humid Regions, a Comparative Analysis of Their Design and Function,” *Sustainability*, vol. 14, no. 17, pp. 1-23, 2022. [[CrossRef](#)] [[Google Scholar](#)] [[Publisher Link](#)]

- [123] Sara Aghasizadeh, Behrouz Mohammad Kari, and Rima Fayaz, "Thermal Performance of Balcony Thermal Bridge Solutions in Reinforced Concrete and Steel Frame Structures," *Journal of Building Engineering*, vol. 48, 2022. [[CrossRef](#)] [[Google Scholar](#)] [[Publisher Link](#)]
- [124] Christina E. Mediastika et al., "Open Windows for Natural Airflow and Environmental Noise Reduction," *Architectural Science Review*, vol. 61, no. 5, pp. 338-348, 2018. [[CrossRef](#)] [[Google Scholar](#)] [[Publisher Link](#)]
- [125] Moon Keun Kim et al., "Prediction and Correlation Analysis of Ventilation Performance in a Residential Building using Artificial Neural Network Models based on Data-Driven Analysis," *Sustainable Cities and Society*, vol. 83, pp. 1-13, 2022. [[CrossRef](#)] [[Google Scholar](#)] [[Publisher Link](#)]
- [126] Amany Khalil, Osama Tolba, and Sherif Ezzeldin, "Optimization of an Office Building Form using a Lattice Incubate Boxes Method," *Advanced Engineering Informatics*, vol. 55, 2023. [[CrossRef](#)] [[Google Scholar](#)] [[Publisher Link](#)]
- [127] Luyang Kang, and Twan van Hooff, "Influence of Inlet Boundary Conditions on 3D Steady Rans Simulations of Non-Isothermal Mechanical Ventilation in a Generic Closure," *International Journal of Thermal Sciences*, vol. 182, pp. 1-20, 2022. [[CrossRef](#)] [[Google Scholar](#)] [[Publisher Link](#)]
- [128] Michael Jayjock, and Andrew Anthony Havics, "Residential Inter-Zonal Ventilation Rates for Exposure Modeling," *Journal of Occupational and Environmental Hygiene*, vol. 15, no. 5, pp. 376-388, 2018. [[CrossRef](#)] [[Google Scholar](#)] [[Publisher Link](#)]
- [129] Sajedeh Jafari, and Vali Kalantar, "Numerical Simulation of Natural Ventilation with Passive Cooling by Diagonal Solar Chimneys and Windcatcher and Water Spray System in a Hot and Dry Climate," *Energy and Buildings*, vol. 256, 2022. [[CrossRef](#)] [[Google Scholar](#)] [[Publisher Link](#)]
- [130] Hong Hu et al., "Comprehensive Validation of Experimental and Numerical Natural Ventilation Predictions based on Field Measurement with Experimental House," *Building and Environment*, vol. 207, pp. 1-27, 2022. [[CrossRef](#)] [[Google Scholar](#)] [[Publisher Link](#)]
- [131] Sahin Gungor, "Experimental Comparison on Energy Consumption and Heat Transfer Performance of Corrugated H-Type and L-Type Brazed Plate Heat Exchangers," *International Communications in Heat and Mass Transfer*, vol. 144, 2023. [[CrossRef](#)] [[Google Scholar](#)] [[Publisher Link](#)]
- [132] Jerzy M. Floryan et al., "Natural Convection and Pattern Interaction in a Two-Dimensional Vertical Slot," *Journal of Fluid Mechanics*, vol. 946, pp. 1-22, 2022. [[CrossRef](#)] [[Google Scholar](#)] [[Publisher Link](#)]
- [133] A. Dimoudi, "Solar Chimneys in Buildings-The State of the Art," *Advances in Building Energy Research*, vol. 3, no. 1, pp. 21-44, 2009. [[CrossRef](#)] [[Google Scholar](#)] [[Publisher Link](#)]
- [134] Yuwei Dai et al., "Scaled Outdoor Experimental Analysis of Ventilation and Interunit Dispersion with Wind and Buoyancy Effects in Street Canyons," *Energy and Buildings*, vol. 255, pp. 1-33, 2022. [[CrossRef](#)] [[Google Scholar](#)] [[Publisher Link](#)]
- [135] Lup Wai Chew, Chen Chen, and Catherine Gorré, "Improving Thermal Model Predictions for Naturally Ventilated Buildings using Large Eddy Simulations," *Building and Environment*, vol. 220, pp. 1-37, 2022. [[CrossRef](#)] [[Google Scholar](#)] [[Publisher Link](#)]
- [136] Fanghui Cheng et al., "Experimental Study of Thermal Comfort in a Field Environment Chamber with Stratum Ventilation System in Winter," *Building and Environment*, vol. 207, 2022. [[CrossRef](#)] [[Google Scholar](#)] [[Publisher Link](#)]
- [137] David Bienvenido-Huertas et al., "Holistic Overview of Natural Ventilation and Mixed Mode in Built Environment of Warm Climate Zones and Hot Seasons," *Building and Environment*, vol. 245, pp. 1-39, 2023. [[CrossRef](#)] [[Google Scholar](#)] [[Publisher Link](#)]
- [138] Fusuo Xu, and Zhi Gao, "Study on Indoor Air Quality and Fresh Air Energy Consumption Under Different Ventilation Modes in 24-Hour Occupied Bedrooms in Nanjing, using Modelica-Based Simulation," *Energy and Buildings*, vol. 257, pp. 1-16, 2022. [[CrossRef](#)] [[Google Scholar](#)] [[Publisher Link](#)]
- [139] Daniel Tschopp et al., "Measurement and Modeling of Diffuse Irradiance Masking on Tilted Planes for Solar Engineering Applications," *Solar Energy*, vol. 231, pp. 365-378, 2022. [[CrossRef](#)] [[Google Scholar](#)] [[Publisher Link](#)]
- [140] Agnieszka Ślosarczyk et al., "A Literature Review of the Latest Trends and Perspectives Regarding Alkali-Activated Materials in Terms of Sustainable Development," *Journal of Materials Research and Technology*, vol. 25, pp. 5394-5425, 2023. [[CrossRef](#)] [[Google Scholar](#)] [[Publisher Link](#)]
- [141] Anshuman Sinha et al., "Reduced Building Energy Consumption by Combined Indoor CO₂ and H₂O Composition Control," *Applied Energy*, vol. 322, pp. 1-23, 2022. [[CrossRef](#)] [[Google Scholar](#)] [[Publisher Link](#)]
- [142] Alireza Norouziasas et al., "Evaluation of Urban Form Influence on Pedestrians' Wind Comfort," *Building and Environment*, vol. 224, 2022. [[CrossRef](#)] [[Google Scholar](#)] [[Publisher Link](#)]
- [143] Nina Morozova et al., "A CFD-Based Surrogate Model for Predicting Flow Parameters in a Ventilated Room using Sensor Readings," *Energy and Buildings*, vol. 266, 2022. [[CrossRef](#)] [[Google Scholar](#)] [[Publisher Link](#)]
- [144] Nils Meyer et al., "A Probabilistic Virtual Process Chain to Quantify Process-Induced Uncertainties in Sheet Molding Compounds," *Composites Part B: Engineering*, vol. 249, 2023. [[CrossRef](#)] [[Google Scholar](#)] [[Publisher Link](#)]
- [145] Xiaoran Liu et al., "A Numerical Investigation on the Mixing Factor and Particle Deposition Velocity for Enclosed Spaces Under Natural Ventilation," *Building Simulation*, vol. 12, no. 3, pp. 465-473, 2019. [[CrossRef](#)] [[Google Scholar](#)] [[Publisher Link](#)]

- [146] Hao Hu et al., "Investigation of Inter-Zonal Heat Transfer in Large Space Buildings based on Similarity: Comparison of Two Stratified Air-Conditioning Systems," *Energy and Buildings*, vol. 254, 2022. [[CrossRef](#)] [[Google Scholar](#)] [[Publisher Link](#)]
- [147] Yi He et al., "Experimental and CFD Study of Ventilation Performance Enhanced by Roof Window and Mechanical Ventilation System with Different Design Strategies," *Building and Environment*, vol. 224, 2022. [[CrossRef](#)] [[Google Scholar](#)] [[Publisher Link](#)]
- [148] Robert Hart, Howdy Goudey, and D. Charlie Curcija, "Experimental Validation and Model Development for Thermal Transmittances of Porous Window Screens and Horizontal Louvred Blind Systems," *Journal of Building Performance Simulation*, vol. 11, no. 2, pp. 190-204, 2018. [[CrossRef](#)] [[Google Scholar](#)] [[Publisher Link](#)]
- [149] Christos H. Halios et al., "Determining the Ventilation and Aerosol Deposition Rates from Routine Indoor-Air Measurements," *Environmental Monitoring and Assessment*, vol. 186, no. 1, pp. 151-163, 2014. [[CrossRef](#)] [[Google Scholar](#)] [[Publisher Link](#)]
- [150] Xiaolei Fan et al., "Uniformity of Supply Air in the Plenum for Under-Floor Air Distribution Ventilation in a Circular Conference Room: A CFD Study," *Energies*, vol. 15, no. 17, pp. 1-18, 2022. [[CrossRef](#)] [[Google Scholar](#)] [[Publisher Link](#)]
- [151] Paul Danca et al., "Personalized Ventilation as a Possible Strategy for Reducing Airborne Infectious Disease Transmission on Commercial Aircraft," *Applied Sciences*, vol. 12, no. 4, pp. 1-24, 2022. [[CrossRef](#)] [[Google Scholar](#)] [[Publisher Link](#)]
- [152] J. Antonio Castillo et al., "Natural Ventilation of an Isolated Generic Building with a Windward Window and Different Wind Exchangers: CFD Validation, Sensitivity Study and Performance Analysis," *Building Simulation*, vol. 12, no. 3, pp. 475-488, 2019. [[CrossRef](#)] [[Google Scholar](#)] [[Publisher Link](#)]
- [153] Fan Bu et al., "Systematically Incorporating Spectrum-Selective Radiative Cooling into Building Performance Simulation: Numerical Integration Method and Experimental Validation," *Applied Energy*, vol. 312, 2022. [[CrossRef](#)] [[Google Scholar](#)] [[Publisher Link](#)]
- [154] Facundo Bre, and Juan M. Gimenez, "A Cloud-Based Platform to Predict Wind Pressure Coefficients on Buildings," *Building Simulation*, vol. 15, no. 8, pp. 1507-1525, 2022. [[CrossRef](#)] [[Google Scholar](#)] [[Publisher Link](#)]
- [155] Christos D. Argyropoulos et al., "Airborne Transmission of Biological Agents within the Indoor Built Environment: A Multidisciplinary Review," *Air Quality, Atmosphere & Health*, vol. 16, no. 3, pp. 477-533, 2023. [[CrossRef](#)] [[Google Scholar](#)] [[Publisher Link](#)]
- [156] Ardalan Aflaki, Masoud Esfandiari, and Saleh Mohammadi, "A Review of Numerical Simulation as a Precedence Method for Prediction and Evaluation of Building Ventilation Performance," *Sustainability*, vol. 13, no. 22, pp. 1-18, 2021. [[CrossRef](#)] [[Google Scholar](#)] [[Publisher Link](#)]
- [157] Sikai Zou et al., "Study on the Performance and Free Cooling Potential of a R32 Loop Thermosyphon System Used in Data Center," *Energy and Buildings*, vol. 256, 2022. [[CrossRef](#)] [[Google Scholar](#)] [[Publisher Link](#)]
- [158] Chaoqun Zhuang, Ruchi Choudhary, and Anna Mavrogianni, "Probabilistic Occupancy Forecasting for Risk-Aware Optimal Ventilation through Autoencoder Bayesian Deep Neural Networks," *Building and Environment*, vol. 219, pp. 1-17, 2022. [[CrossRef](#)] [[Google Scholar](#)] [[Publisher Link](#)]
- [159] Delika M. Weragoda et al., "A Comprehensive Review on Heat Pipe Based Battery Thermal Management Systems," *Applied Thermal Engineering*, vol. 224, pp. 1-25, 2023. [[CrossRef](#)] [[Google Scholar](#)] [[Publisher Link](#)]
- [160] Tsz Wun Tsang et al., "Influences of Home Kitchen Designs on Indoor Air Quality," *Indoor and Built Environment*, vol. 32, no. 7, pp. 1429-1438, 2023. [[CrossRef](#)] [[Google Scholar](#)] [[Publisher Link](#)]
- [161] Yoshihide Tominaga, and Mohammadreza Shirzadi, "Influence of Detailed Air Flow Distribution on Corrosion Damage Due to Airborne Sea Salt Adhesion in a Large Sports Stadium: A CFD Analysis," *Journal of Building Engineering*, vol. 64, pp. 1-17, 2023. [[CrossRef](#)] [[Google Scholar](#)] [[Publisher Link](#)]
- [162] Michal Szymański, Andrzej Górka, and Radosław Górzeński, "Large Buildings Airtightness Measurements using Ventilation Systems," *International Journal of Ventilation*, vol. 14, no. 4, pp. 395-408, 2016. [[CrossRef](#)] [[Google Scholar](#)] [[Publisher Link](#)]
- [163] Meng Su et al., "Predicting Moisture Condensation Risk on the Radiant Cooling Floor of an Office using Integration of a Genetic Algorithm-Back-Propagation Neural Network with Sensitivity Analysis," *Energy and Built Environment*, vol. 5, no. 1, pp. 110-129, 2024. [[CrossRef](#)] [[Google Scholar](#)] [[Publisher Link](#)]
- [164] Jaehoon Sim, Junseok Chang, and Jihad Badra, "CFD-Guided Optimization of the Injector and Injection Parameters for Light-Duty GCI Engine," *Fuel*, vol. 316, 2022. [[CrossRef](#)] [[Google Scholar](#)] [[Publisher Link](#)]
- [165] Alessio Ricci et al., "Impact of Surrounding Environments and Vegetation on Wind Comfort Assessment of a New Tower with Vertical Green Park," *Building and Environment*, vol. 207, pp. 1-26, 2022. [[CrossRef](#)] [[Google Scholar](#)] [[Publisher Link](#)]
- [166] Ute Poerschke et al., "The 'Air-Wall': Re-Evaluating a Mid-Twentieth Century Four-Sided Double-Skin Façade," *Technology|Architecture + Design*, vol. 3, no. 2, pp. 200-210, 2019. [[CrossRef](#)] [[Google Scholar](#)] [[Publisher Link](#)]
- [167] Chanawat Nitatwichit, Yottana Khunatorn, and Nakorn Tippayawong, "Investigation and Characterization of Cross Ventilating Flows Through Openings in a School Classroom," *Journal of the Chinese Institute of Engineers*, vol. 31, no. 4, pp. 587-603, 2008. [[CrossRef](#)] [[Google Scholar](#)] [[Publisher Link](#)]
- [168] Lokanath Mohanta et al., "Numerical Analysis of Fluid Flow and Heat Transfer in Wavy and Hybrid-Slit-Wavy Fin-and-Tube Heat Exchangers," *Science and Technology for the Built Environment*, vol. 25, no. 6, pp. 767-775, 2019. [[CrossRef](#)] [[Google Scholar](#)] [[Publisher Link](#)]

- [169] Elham Mohammadi et al., “Effect of Resilient Architecture in an Ancient Windmill in the Sistan Region on Natural Ventilation Enhancement,” *Scientific Reports*, vol. 12, no. 1, pp. 1-19, 2022. [[CrossRef](#)] [[Google Scholar](#)] [[Publisher Link](#)]
- [170] I. Meireles et al., “Domestic Hot Water Consumption Pattern: Relation with Total Water Consumption and Air Temperature,” *Renewable and Sustainable Energy Reviews*, vol. 157, 2022. [[CrossRef](#)] [[Google Scholar](#)] [[Publisher Link](#)]
- [171] Victoria Patricia López-Cabeza et al., “Effect of Thermal Inertia and Natural Ventilation on User Comfort in Courtyards Under Warm Summer Conditions,” *Building and Environment*, vol. 228, 2023. [[CrossRef](#)] [[Google Scholar](#)] [[Publisher Link](#)]
- [172] Han Li et al., “Study on the Impact of Parallel Jet Spacing on the Performance of Multi-Jet Stratum Ventilation,” *Applied Energy*, vol. 306, pp. 1-14, 2022. [[CrossRef](#)] [[Google Scholar](#)] [[Publisher Link](#)]
- [173] Jeehwan Lee, Haider Mohamed, and Jae D. Chang, “The Effect of Positions of Vertical Glass Fins inside a Double Skin Façade Air Cavity as Acoustical Barriers and Ventilation Potentials,” *Procedia Engineering*, vol. 145, pp. 892-899, 2016. [[CrossRef](#)] [[Google Scholar](#)] [[Publisher Link](#)]
- [174] Iliia Kravchenko et al., “Performance of Modern Passive Stack Ventilation in a Retrofitted Nordic Apartment Building,” *Buildings*, vol. 12, no. 2, pp. 1-27, 2022. [[CrossRef](#)] [[Google Scholar](#)] [[Publisher Link](#)]
- [175] Gaël F. Kemp et al., “Fluid Mechanics of Sash Windows,” *Flow*, vol. 2, pp. 1-15, 2022. [[CrossRef](#)] [[Google Scholar](#)] [[Publisher Link](#)]
- [176] K.K. Syrios, and G.R. Hunt, “Design Considerations for Roof-Mounted Ventilation Systems,” *International Journal of Ventilation*, vol. 3, no. 2, pp. 89-104, 2004. [[CrossRef](#)] [[Google Scholar](#)] [[Publisher Link](#)]
- [177] Sherzad Hawendi, Shian Gao, and Ahmed Qasim Ahmed, “Effect of Heat Loads and Furniture on the Thermal Comfort of an Isolated Family House Under a Naturally Ventilated Environment,” *International Journal of Ventilation*, vol. 19, no. 3, pp. 163-188, 2020. [[CrossRef](#)] [[Google Scholar](#)] [[Publisher Link](#)]
- [178] Md Farhad Hasan et al., “Natural Convection Flow Over a Vertical Permeable Circular Cone with Uniform Surface Heat Flux in Temperature-Dependent Viscosity with Three-Fold Solutions within the Boundary Layer,” *Computation*, vol. 10, no. 4, pp. 1-21, 2022. [[CrossRef](#)] [[Google Scholar](#)] [[Publisher Link](#)]
- [179] Hongwei Guo et al., “Physics-Informed Deep Learning for Three-Dimensional Transient Heat Transfer Analysis of Functionally Graded Materials,” *Computational Mechanics*, vol. 72, no. 3, pp. 513-524, 2023. [[CrossRef](#)] [[Google Scholar](#)] [[Publisher Link](#)]
- [180] Valentin Guichet et al., “Experimental and Theoretical Investigation of the Influence of Heat Transfer Rate on the Thermal Performance of a Multi-Channel Flat Heat Pipe,” *Energy*, vol. 250, pp. 1-19, 2022. [[CrossRef](#)] [[Google Scholar](#)] [[Publisher Link](#)]
- [181] Cary A. Faulkner et al., “Fast Prediction of Indoor Airflow Distribution Inspired by Synthetic Image Generation Artificial Intelligence,” *Building Simulation*, vol. 16, no. 7, pp. 1219-1238, 2023. [[CrossRef](#)] [[Google Scholar](#)] [[Publisher Link](#)]
- [182] Emad M.S. El-Said, Mohamed Abdulaziz, and Mohamed M. Awad, “A Numerical Investigation on Heat Transfer Enhancement and the Flow Characteristics in a New Type Plate Heat Exchanger Using Helical Flow Duct,” *Cogent Engineering*, vol. 4, no. 1, pp. 1-24, 2017. [[CrossRef](#)] [[Google Scholar](#)] [[Publisher Link](#)]
- [183] Sonny F. Díaz-Calderón, J.A. Castillo, and Guadalupe Huelsz, “Evaluation of Different Window Heights and Façade Porosities in Naturally Cross-Ventilated Buildings: CFD Validation,” *Journal of Wind Engineering and Industrial Aerodynamics*, vol. 232, 2023. [[CrossRef](#)] [[Google Scholar](#)] [[Publisher Link](#)]
- [184] Kai-Chung Cheng, Daisy Zheng, and Lynn M. Hildemann, “Impact of Fan Mixing on Air Pollutant Exposure Near Indoor Sources: An Analytical Model to Connect Proximity Effect with Energy,” *Building and Environment*, vol. 183, 2020. [[CrossRef](#)] [[Google Scholar](#)] [[Publisher Link](#)]
- [185] Anass Berouine et al., “A Predictive Control Approach for Thermal Energy Management in Buildings,” *Energy Reports*, vol. 8, pp. 9127-9141, 2022. [[CrossRef](#)] [[Google Scholar](#)] [[Publisher Link](#)]
- [186] Hongyu Bai et al., “A Review of Heat Recovery Technologies and their Frost Control for Residential Building Ventilation in Cold Climate Regions,” *Renewable and Sustainable Energy Reviews*, vol. 162, pp. 1-25, 2022. [[CrossRef](#)] [[Google Scholar](#)] [[Publisher Link](#)]
- [187] Jenan Abu Qadourah, “Energy and Economic Potential for Photovoltaic Systems Installed on the Rooftop of Apartment Buildings in Jordan,” *Results in Engineering*, vol. 16, pp. 1-12, 2022. [[CrossRef](#)] [[Google Scholar](#)] [[Publisher Link](#)]
- [188] Joan Lluís Zamora Mestre, and Andrea Niampira, “Lightweight Ventilated Façade: Acoustic Performance in Laboratory Conditions, Analysing the Impact of Controlled Ventilation Variations on Airborne Sound Insulation,” *Building Acoustics*, vol. 27, no. 4, pp. 367-379, 2020. [[CrossRef](#)] [[Google Scholar](#)] [[Publisher Link](#)]
- [189] Yao Tao et al., “A Theoretical Model of Natural Ventilation Enhanced by Solar Thermal Energy in Double-Skin Façade,” *Energy*, vol. 276, pp. 1-13, 2023. [[CrossRef](#)] [[Google Scholar](#)] [[Publisher Link](#)]
- [190] Helen Stopps, and Marianne F. Touchie, “Load Shifting and Energy Conservation Using Smart Thermostats in Contemporary High-Rise Residential Buildings: Estimation of Runtime Changes Using Field Data,” *Energy and Buildings*, vol. 255, 2022. [[CrossRef](#)] [[Google Scholar](#)] [[Publisher Link](#)]
- [191] Dragos Paul Schoplocher, Stefan Ettengruber, and Oliver Steffens, “Improvements for Building-Performance Simulations by a Comparative Finite-Element Method Analysis,” *Energy and Buildings*, vol. 278, pp. 1-12, 2023. [[CrossRef](#)] [[Google Scholar](#)] [[Publisher Link](#)]

- [192] Eduardo Roque et al., “The Impact of Thermal Inertia on the Indoor Thermal Environment of Light Steel Framing Constructions,” *Energies*, vol. 15, no. 9, pp. 1-17, 2022. [[CrossRef](#)] [[Google Scholar](#)] [[Publisher Link](#)]
- [193] Theodore Potsis, Yoshihide Tominaga, and Ted Stathopoulos, “Computational Wind Engineering: 30 Years of Research Progress in Building Structures and Environment,” *Journal of Wind Engineering and Industrial Aerodynamics*, vol. 234, 2023. [[CrossRef](#)] [[Google Scholar](#)] [[Publisher Link](#)]
- [194] Alexander F. Pashchenko, and Yuriy M. Rassadin, “Microclimate Monitoring System Design for the Smart Grid Analysis and Constructive Parameters Estimation,” *IFAC-PapersOnLine*, vol. 55, no. 9, pp. 479-484, 2022. [[CrossRef](#)] [[Google Scholar](#)] [[Publisher Link](#)]
- [195] Panayiotis M. Papadopoulos et al., “Distributed Diagnosis of Sensor and Actuator Faults in Air Handling Units in Multi-Zone Buildings: A Model-Based Approach,” *Energy and Buildings*, vol. 256, 2022. [[CrossRef](#)] [[Google Scholar](#)] [[Publisher Link](#)]
- [196] K.E. Anders Ohlsson, Gireesh Nair, and Thomas Olofsson, “Uncertainty in Model Prediction of Energy Savings in Building Retrofits: Case of Thermal Transmittance of Windows,” *Renewable and Sustainable Energy Reviews*, vol. 168, pp. 1-12, 2022. [[CrossRef](#)] [[Google Scholar](#)] [[Publisher Link](#)]
- [197] Acinia Nindartin et al., “Influencing of the Building Energy Policies upon the Efficiency of Energy Consumption: The Case of Courthouse Buildings in South Korea,” *Energies*, vol. 15, no. 18, pp. 1-17, 2022. [[CrossRef](#)] [[Google Scholar](#)] [[Publisher Link](#)]
- [198] P.H.V. Nimarshana, Rahu A. Attalage, and K. Kapila C.K. Perera, “Quantification of the Impact of RANS Turbulence Models on Airflow Distribution in Horizontal Planes of a Generic Building Under Cross-Ventilation for Prediction of Indoor Thermal Comfort,” *Journal of Building Engineering*, vol. 52, 2022. [[CrossRef](#)] [[Google Scholar](#)] [[Publisher Link](#)]
- [199] Mohammad Mortezaazadeh et al., “Cityffd - City Fast Fluid Dynamics for Urban Microclimate Simulations on Graphics Processing Units,” *Urban Climate*, vol. 41, 2022. [[CrossRef](#)] [[Google Scholar](#)] [[Publisher Link](#)]
- [200] Ahmed Megri et al., “A New Dynamic Zonal Model with Air-Diffuser (DOMA) - Application to Thermal Comfort Prediction,” *Indoor and Built Environment*, vol. 31, no. 7, pp. 1738-1757, 2022. [[CrossRef](#)] [[Google Scholar](#)] [[Publisher Link](#)]
- [201] Rafaela Mateus, José Manuel C. Pereira, and Armando Pinto, “Natural Ventilation of Large Air Masses: Experimental and Numerical Techniques Review,” *Energy and Buildings*, vol. 291, pp. 1-49, 2023. [[CrossRef](#)] [[Google Scholar](#)] [[Publisher Link](#)]
- [202] Victor Marty-Jourjon et al., “Identifiability Study of an RC Building Model based on the Standard ISO13790,” *Energy and Buildings*, vol. 276, pp. 1-19, 2022. [[CrossRef](#)] [[Google Scholar](#)] [[Publisher Link](#)]
- [203] Mara Magni, Fabian Ochs, and Wolfgang Streicher, “Comprehensive Analysis of the Influence of Different Building Modelling Approaches on the Results and Computational time Using a Cross-Compared Model as a Reference,” *Energy and Buildings*, vol. 259, pp. 1-34, 2022. [[CrossRef](#)] [[Google Scholar](#)] [[Publisher Link](#)]
- [204] Adnane M'Saouri El Bat et al., “Optimizing Urban Courtyard Form through the Coupling of Outdoor Zonal Approach and Building Energy Modeling,” *Energy*, vol. 264, 2023. [[CrossRef](#)] [[Google Scholar](#)] [[Publisher Link](#)]
- [205] Xiaoshu Lü et al., “Improving the Energy Efficiency of Buildings Based on Fluid Dynamics Models: A Critical Review,” *Energies*, vol. 14, no. 17, pp. 1-23, 2021. [[CrossRef](#)] [[Google Scholar](#)] [[Publisher Link](#)]
- [206] Fei Liu et al., “An Improved Wall-Mounted Displacement Ventilation System in a Large-Span Machining Workshop,” *Building Simulation*, vol. 15, no. 11, pp. 1943-1953, 2022. [[CrossRef](#)] [[Google Scholar](#)] [[Publisher Link](#)]
- [207] Simon Li, “Review of Engineering Controls for Indoor Air Quality: A Systems Design Perspective,” *Sustainability*, vol. 15, no. 19, pp. 1-46, 2023. [[CrossRef](#)] [[Google Scholar](#)] [[Publisher Link](#)]
- [208] Ali Akbar Heidari, and Hamid Eskandari, “Impact of Inlet and Outlet Opening Height Variation on the Air Quality and Ventilation Efficiency in the On-Top Wind Catcher Buildings: A CFD Simulation,” *Science and Technology for the Built Environment*, vol. 28, no. 10, pp. 1420-1438, 2022. [[CrossRef](#)] [[Google Scholar](#)] [[Publisher Link](#)]
- [209] Thea Hauge Broholt, Michael Dahl Knudsen, and Steffen Petersen Show, “The Robustness of Black and Grey-Box Models of Thermal Building Behaviour Against Weather Changes,” *Energy and Buildings*, vol. 275, pp. 1-19, 2022. [[CrossRef](#)] [[Google Scholar](#)] [[Publisher Link](#)]
- [210] Jian Hang et al., “Assessment of Exhaled Pathogenic Droplet Dispersion and Indoor-Outdoor Exposure Risk in Urban Street with Naturally-Ventilated Buildings,” *Building and Environment*, vol. 234, 2023. [[CrossRef](#)] [[Google Scholar](#)] [[Publisher Link](#)]
- [211] Mohammad Hadavi, and Hadi Pasdarsahri, “Impacts of Urban Buildings on Microclimate and Cooling Systems Efficiency: Coupled CFD and BES Simulations,” *Sustainable Cities and Society*, vol. 67, 2021. [[CrossRef](#)] [[Google Scholar](#)] [[Publisher Link](#)]
- [212] Anina Šarkić Glumac et al., “A Multi-Fidelity Wind Surface Pressure Assessment Via Machine Learning: A High-Rise Building Case,” *Building and Environment*, vol. 234, 2023. [[CrossRef](#)] [[Google Scholar](#)] [[Publisher Link](#)]
- [213] Gioia Fusaro et al., “Assessment of Acoustic Metawindow Unit through Psychoacoustic Analysis and Human Perception,” *Applied Acoustics*, vol. 196, pp. 1-24, 2022. [[CrossRef](#)] [[Google Scholar](#)] [[Publisher Link](#)]
- [214] Ashraf Farahat et al., “Solar Energy Potential on Surfaces with Various Inclination Modes in Saudi Arabia: Performance of an Isotropic and an Anisotropic Model,” *Applied Sciences*, vol. 12, no. 11, pp. 1-20, 2022. [[CrossRef](#)] [[Google Scholar](#)] [[Publisher Link](#)]

- [215] Abbas Ali Elmualim, "Utility of Wind Catchers for Nocturnal Ventilation," *International Journal of Ventilation*, vol. 8, no. 1, pp. 85-92, 2009. [[CrossRef](#)] [[Google Scholar](#)] [[Publisher Link](#)]
- [216] Mengfan Duan et al., "A Simplified Model for the Evaluation and Comparison of the Dynamic Performance of Different Heating Terminal Types," *Energy*, vol. 263, 2023. [[CrossRef](#)] [[Google Scholar](#)] [[Publisher Link](#)]
- [217] Andrea M. Dietrich, Wenchuo Yao, and Daniel L. Gallagher, "Exposure at the Indoor Water-Air Interface: Fill Water Constituents and the Consequent Air Emissions from Ultrasonic Humidifiers: A Systematic Review," *Indoor Air*, vol. 32, no. 11, pp. 1-11, 2022. [[CrossRef](#)] [[Google Scholar](#)] [[Publisher Link](#)]
- [218] Jose A. Candanedo et al., "Control-Oriented Archetypes: A Pathway for the Systematic Application of Advanced Controls in Buildings," *Journal of Building Performance Simulation*, vol. 15, no. 4, pp. 433-444, 2022. [[CrossRef](#)] [[Google Scholar](#)] [[Publisher Link](#)]
- [219] Seyedhadi Banihashemi et al., "Turbulent Flow Thermal Characteristics in a Pipe with Ring Insert: An Experimental and Numerical Study," *Chemical Engineering and Processing - Process Intensification*, vol. 172, 2022. [[CrossRef](#)] [[Google Scholar](#)] [[Publisher Link](#)]
- [220] Farzan Banihashemi, Manuel Weber, and Werner Lang, "Model Order Reduction of Building Energy Simulation Models Using a Convolutional Neural Network Autoencoder," *Building and Environment*, vol. 207, 2022. [[CrossRef](#)] [[Google Scholar](#)] [[Publisher Link](#)]
- [221] Yasaman Balali et al., "Energy Modelling and Control of Building Heating and Cooling Systems with Data-Driven and Hybrid Models- A Review," *Renewable and Sustainable Energy Reviews*, vol. 183, pp. 1-20, 2023. [[CrossRef](#)] [[Google Scholar](#)] [[Publisher Link](#)]
- [222] Ali Ahmed Alqahtani et al., "Performance of Flat-Plate, Flexible Polymeric Pulsating Heat Pipes at Different Bending Angles," *Applied Thermal Engineering*, vol. 216, pp. 1-11, 2022. [[CrossRef](#)] [[Google Scholar](#)] [[Publisher Link](#)]
- [223] Omer Abedrabboh, Muammer Koç, and Yusuf Biçer, "Sustainability Performance of Space-Cooling Technologies and Approaches," *Energy Sources, Part A: Recovery, Utilization, and Environmental Effects*, vol. 44, no. 4, pp. 9017-9042, 2022. [[CrossRef](#)] [[Google Scholar](#)] [[Publisher Link](#)]
- [224] Yulin Zheng, and Xiangguo Xu, "Predicting Indoor 3D Airflow Distribution using Artificial Neural Networks with Two Different Architectures," *Energy and Buildings*, vol. 303, 2024. [[CrossRef](#)] [[Google Scholar](#)] [[Publisher Link](#)]
- [225] Zhiqiang (John) Zhai, Jack Baum, and Danielle Griego, "Applying Natural Ventilation for Commercial Buildings with Atrium: Indoor Environment Prediction and Outdoor Pollutant Impact," *ASME Journal of Engineering for Sustainable Buildings and Cities*, vol. 4, no. 3, 2023. [[CrossRef](#)] [[Google Scholar](#)] [[Publisher Link](#)]
- [226] Yao Yu et al., "Calibrated Dynamic Zonal Model DOMA⁺ Using the SCE-UA Method - Application to Atrium Temperature Distribution Prediction," *Science and Technology for the Built Environment*, vol. 28, no. 10, pp. 1439-1455, 2022. [[CrossRef](#)] [[Google Scholar](#)] [[Publisher Link](#)]
- [227] T. Yazarlou, E. Barzkar, and M.D. Saghafi, "CFD Analysis of Cross-Ventilation in Buildings with External Louvers: Impact of Slat Angles," *Iranian Journal of Science and Technology, Transactions of Mechanical Engineering*, vol. 48, no. 1, pp. 81-101, 2023. [[CrossRef](#)] [[Google Scholar](#)] [[Publisher Link](#)]
- [228] Bin Yang et al., "Thermal Comfort and Energy Savings of Personal Comfort Systems in Low Temperature Office: A Field Study," *Energy and Buildings*, vol. 270, 2022. [[CrossRef](#)] [[Google Scholar](#)] [[Publisher Link](#)]
- [229] Haruna Yamasawa et al., "Influence of Inlet Turbulent Condition on the Formation Mechanism of Local Scalar Concentrations," *Japan Architectural Review*, vol. 5, no. 4, pp. 691-701, 2022. [[CrossRef](#)] [[Google Scholar](#)] [[Publisher Link](#)]
- [230] Yaowen Xia et al., "Penetration Height of Weak Axisymmetric Fountain in Homogeneous Fluid Under the Combined Temperature and Salinity Effect," *AIP Advances*, vol. 12, no. 3, pp. 1-15, 2022. [[CrossRef](#)] [[Google Scholar](#)] [[Publisher Link](#)]
- [231] Vincent J.L. Gan et al., "Physics-Based, Data-Driven Approach for Predicting Natural Ventilation of Residential High-Rise Buildings," *Building Simulation*, vol. 15, no. 1, pp. 129-148, 2022. [[CrossRef](#)] [[Google Scholar](#)] [[Publisher Link](#)]
- [232] Haidong Wang, Qianru Chen, and Yan Liu, "Investigation of the Quasi-Periodic Airflow Oscillation and Ventilation Performance of an Enclosed Environment with a Jet Air Supply," *Energy and Buildings*, vol. 265, 2022. [[CrossRef](#)] [[Google Scholar](#)] [[Publisher Link](#)]
- [233] Carolanne V.M. Vouriot et al., "Uniformly Distributed Floor Sources of Buoyancy can give Rise to Significant Spatial Inhomogeneities within Rooms," *Flow*, vol. 3, pp. 1-18, 2023. [[CrossRef](#)] [[Google Scholar](#)] [[Publisher Link](#)]
- [234] Robert C. Vella et al., "Prioritising Passive Measures over Air Conditioning to Achieve Thermal Comfort in Mediterranean Baroque Churches," *Sustainability*, vol. 14, no. 14, pp. 1-23, 2022. [[CrossRef](#)] [[Google Scholar](#)] [[Publisher Link](#)]
- [235] Anke Uytterhoeven et al., "Chance Constrained Stochastic MPC for Building Climate Control Under Combined Parametric and Additive Uncertainty," *Journal of Building Performance Simulation*, vol. 15, no. 3, pp. 410-430, 2022. [[CrossRef](#)] [[Google Scholar](#)] [[Publisher Link](#)]
- [236] Juan F. Torres et al., "Low-Energy Activation of Large Convective Heat Transfer Via Flow Resonance Triggered by Impinging Jet," *International Journal of Heat and Mass Transfer*, vol. 195, pp. 1-16, 2022. [[CrossRef](#)] [[Google Scholar](#)] [[Publisher Link](#)]
- [237] Fran Torbarina, Anica Trp, and Kristian Lenić, "Numerical Analysis of Geometry Influence on Heat Transfer in a Slotted Fin and Tube Heat Exchanger," *Heat Transfer Engineering*, vol. 44, no. 5, pp. 411-425, 2023. [[CrossRef](#)] [[Google Scholar](#)] [[Publisher Link](#)]
- [238] Xue Tian, and Zhang Lin, "Predicting Personalized Thermal Comfort in Stratified Micro-Environments using Turbulent Jet Theories and Data-Driven Models," *Building and Environment*, vol. 230, 2023. [[CrossRef](#)] [[Google Scholar](#)] [[Publisher Link](#)]

- [239] A.V. Busakhin, “Smoke Ventilation Differential Pressure System” *International Journal of Engineering Trends and Technology*, vol. 70, no. 7, pp. 449-454, 2022. [[CrossRef](#)] [[Publisher Link](#)]
- [240] Sinan Sousan et al., “Use of Prototype Side Stream Filtration System to Control Dust Levels in a Commercial Swine Farrowing Building,” *Journal of Occupational and Environmental Hygiene*, vol. 20, no. 12, pp. 633-645, 2023. [[CrossRef](#)] [[Google Scholar](#)] [[Publisher Link](#)]
- [241] Twan van Hooff, Peter V. Nielsen, and Yuguo Li, “Computational Fluid Dynamics Predictions of Non-Isothermal Ventilation Flow-How Can the User Factor Be Minimized?,” *Indoor Air*, vol. 28, no. 6, pp. 866-880, 2018. [[CrossRef](#)] [[Google Scholar](#)] [[Publisher Link](#)]
- [242] Reza Rahimi, and Rahim Hassanzadeh, “Impacts of Horizontal and Vertical Louvers on the Natural Cross-Ventilation Performance of a Generic Building,” *International Journal of Ventilation*, vol. 23, no. 1, pp. 51-74, 2024. [[CrossRef](#)] [[Google Scholar](#)] [[Publisher Link](#)]
- [243] Tran Van Quang et al., “Data-Driven Prediction of Indoor Airflow Distribution in Naturally Ventilated Residential Buildings Using Combined CFD Simulation and Machine Learning (ML) Approach,” *Journal of Building Physics*, vol. 47, no. 4, pp. 439-471, 2024. [[CrossRef](#)] [[Google Scholar](#)] [[Publisher Link](#)]
- [244] Abdultawab M. Qahtan, and Abdulkarem H.M. Almwagani, “Experimental Evaluation of Thermal and Lighting Performance Using Double Dynamic Insulated Glazing,” *Buildings*, vol. 12, no. 8, pp. 1-19, 2022. [[CrossRef](#)] [[Google Scholar](#)] [[Publisher Link](#)]
- [245] Carlos Prades-Gil et al., “An Agile Heating and Cooling Energy Demand Model for Residential Buildings. Case Study in a Mediterranean City Residential Sector,” *Renewable and Sustainable Energy Reviews*, vol. 175, pp. 1-13, 2023. [[CrossRef](#)] [[Google Scholar](#)] [[Publisher Link](#)]
- [246] Iván Polanco-Guzmán et al., “An Improved Ventilation System for Settling Stage of a Wastewater Treatment Plant: A Computational Simulation Analysis,” *International Journal of Construction Management*, vol. 23, no. 2, pp. 205-224, 2023. [[CrossRef](#)] [[Google Scholar](#)] [[Publisher Link](#)]
- [247] Murphy M. Peksen, “Artificial Intelligence-Based Machine Learning toward the Solution of Climate-Friendly Hydrogen Fuel Cell Electric Vehicles,” *Vehicles*, vol. 4, no. 3, pp. 663-680, 2022. [[CrossRef](#)] [[Google Scholar](#)] [[Publisher Link](#)]
- [248] Leslie K. Norvihoho et al., “Dispersion of Expectorated Cough Droplets with Seasonal Influenza in an Office,” *Physics of Fluids*, vol. 35, no. 8, 2023. [[CrossRef](#)] [[Google Scholar](#)] [[Publisher Link](#)]
- [249] Nima Najafi Ziarani, Malcolm Cook, and Paul D. O’Sullivan, “The Effect of Airflow Guiding Components on Effective Ventilation Rates in Single-Sided Ventilation Applications,” *International Journal of Ventilation*, vol. 22, no. 4, pp. 377-389, 2023. [[CrossRef](#)] [[Google Scholar](#)] [[Publisher Link](#)]
- [250] Maliki Moustapha, and Bruno Sudret, “Learning Non-Stationary and Discontinuous Functions Using Clustering, Classification and Gaussian Process Modelling,” *Computers & Structures*, vol. 281, pp. 1-15, 2023. [[CrossRef](#)] [[Google Scholar](#)] [[Publisher Link](#)]
- [251] Hossein Dehghani Mohamadabadi, Abdul Hamid Ghanbaran, and Ali Akbar Dehghan, “The Study of Air Distribution Quality in the Summer Section of Iranian Dry Climate Houses Equipped with Wind Tower,” *Sustainable Cities and Society*, vol. 86, 2022. [[CrossRef](#)] [[Google Scholar](#)] [[Publisher Link](#)]
- [252] Sen Miao, Marta Gangoells, and Blanca Tejedor Herran, “Data-Driven Model for Predicting Indoor Air Quality and Thermal Comfort Levels in Naturally Ventilated Educational Buildings Using Easily Accessible Data for Schools,” *Journal of Building Engineering*, vol. 80, pp. 1-22, 2023. [[CrossRef](#)] [[Google Scholar](#)] [[Publisher Link](#)]
- [253] Bart Merema, Dirk Saelens, and Hilde Breesch, “Demonstration of an MPC Framework for All-Air Systems in Non-Residential Buildings,” *Building and Environment*, vol. 217, 2022. [[CrossRef](#)] [[Google Scholar](#)] [[Publisher Link](#)]
- [254] Harry Mahon, Daniel Friedrich, and Ben Hughes, “Wind Tunnel Test and Numerical Study of a Multi-Sided Wind Tower with Horizontal Heat Pipes,” *Energy*, vol. 260, pp. 1-11, 2022. [[CrossRef](#)] [[Google Scholar](#)] [[Publisher Link](#)]
- [255] Emeka J. Mba et al., “Assessment of Floor-Level Impact on Natural Ventilation and Indoor Thermal Environment in Hot-Humid Climates: A Case Study of a Mid-Rise Educational Building,” *Buildings*, vol. 15, no. 5, pp. 1-31, 2025. [[CrossRef](#)] [[Google Scholar](#)] [[Publisher Link](#)]
- [256] Lim Eun-soo, Zheng Zhujuan, and Kazuhide Ito, “Formation Mechanism of Contaminant Concentration Distributions Under Re-Circulation of In Indoor Airflow and HVAC System,” *Journal of Environmental Engineering (Transactions of AIJ)*, vol. 87, no. 797, pp. 439-447, 2022. [[CrossRef](#)] [[Google Scholar](#)] [[Publisher Link](#)]
- [257] Scott W. Li, and Andrew W. Woods, “The Impact of Source Fluctuations in a Filling Box with Interior Diffusive Mixing,” *Journal of Fluid Mechanics*, vol. 944, pp. 1-22, 2022. [[CrossRef](#)] [[Google Scholar](#)] [[Publisher Link](#)]
- [258] Noemi Schelar Leitão, and Eloísa Castilho, “Heat Transfer Analysis of Infrastructures Subjected to Environmental Actions: A Finite Element Solver PAT,” *Thermal Science and Engineering Progress*, vol. 34, 2022. [[CrossRef](#)] [[Google Scholar](#)] [[Publisher Link](#)]
- [259] Nelson James et al., “Investigation of Ventilation-Coupled High Energy Density Sensible Thermal Energy Storage,” *Applied Energy*, vol. 387, pp. 1-37, 2025. [[CrossRef](#)] [[Google Scholar](#)] [[Publisher Link](#)]
- [260] Brian Landsberger, Liangcai Tan, and Xin Hu, “Energy and Acoustic Performance Effects Due to VAV Duct Design and Installation Practice Variations,” *HVAC&R Research*, vol. 14, no. 4, pp. 597-613, 2008. [[CrossRef](#)] [[Google Scholar](#)] [[Publisher Link](#)]

- [261] Hamza Laloui, Noor Hanita Abdul Majid, and Aliyah Nur Zafirah Sanusi, “The Impacts of Introducing Voids Combinations on Indoor Ventilation Performance in High-Rise Residential Buildings,” *Engineering, Construction and Architectural Management*, vol. 29, no. 7, pp. 2736-2759, 2021. [[CrossRef](#)] [[Google Scholar](#)] [[Publisher Link](#)]
- [262] Betty Lala, and Aya Hagishima, “A Review of Thermal Comfort in Primary Schools and Future Challenges in Machine Learning Based Prediction for Children,” *Buildings*, vol. 12, no. 11, pp. 1-27, 2022. [[CrossRef](#)] [[Google Scholar](#)] [[Publisher Link](#)]
- [263] Kusnandar et al., “Energy Consumption Analysis for Coupling Air Conditioners and Cold Storage Showcase Equipment in a Convenience Store,” *Energies*, vol. 15, no. 13, pp. 1-13, 2022. [[CrossRef](#)] [[Google Scholar](#)] [[Publisher Link](#)]
- [264] K.A. Krishnaprasad et al., “Fluid Mechanics of Air Recycling and Filtration for Indoor Airborne Transmission,” *Physics of Fluids*, vol. 35, no. 1, pp. 1-32, 2023. [[CrossRef](#)] [[Google Scholar](#)] [[Publisher Link](#)]
- [265] Hong Yee Kek et al., “Particle Dispersion for Indoor Air Quality Control Considering Air Change Approach: A Novel Accelerated CFD-DNN Prediction,” *Energy and Buildings*, vol. 306, pp. 1-33, 2024. [[CrossRef](#)] [[Google Scholar](#)] [[Publisher Link](#)]
- [266] Bill Kayser et al., “Wind Turbine Noise Uncertainty Quantification for Downwind Conditions Using Metamodeling,” *The Journal of the Acoustical Society of America*, vol. 151, no. 1, pp. 390-401, 2022. [[CrossRef](#)] [[Google Scholar](#)] [[Publisher Link](#)]
- [267] James D. Johnston, Ashlin E. Cowger, and K. Scott Weber, “Bioaerosol and Microbial Exposures from Residential Evaporative Coolers and Their Potential Health Outcomes: A Review,” *Indoor Air*, vol. 32, no. 9, pp. 1-17, 2022. [[CrossRef](#)] [[Google Scholar](#)] [[Publisher Link](#)]
- [268] Bongchan Jeong et al., “Developing a Window Behaviour Model Incorporating A/C Operation States,” *Building and Environment*, vol. 214, 2022. [[CrossRef](#)] [[Google Scholar](#)] [[Publisher Link](#)]
- [269] A.K.R. Jayakumari et al., “Scaling Effects on Experimentally Obtained Pressures on an Idealized Building: Possible Implications Towards Asbestos Containment,” *Journal of Wind Engineering and Industrial Aerodynamics*, vol. 239, pp. 1-12, 2023. [[CrossRef](#)] [[Google Scholar](#)] [[Publisher Link](#)]
- [270] Samy Iousef et al., “Wall-Resolved Versus Wall-Modeled LES of the Flow Field and Surface Forced Convective Heat Transfer for a Low-Rise Building,” *Building and Environment*, vol. 244, pp. 1-21, 2023. [[CrossRef](#)] [[Google Scholar](#)] [[Publisher Link](#)]
- [271] Yunjae Hwang, and Catherine Gorré, “Large-Eddy Simulations to Define Building-Specific Similarity Relationships for Natural Ventilation Flow Rates,” *Flow*, vol. 3, pp. 1-19, 2023. [[CrossRef](#)] [[Google Scholar](#)] [[Publisher Link](#)]
- [272] G.R. Hunt, and K. Syrios, “Roof-Mounted Ventilation Towers - Design Criteria for Enhanced Buoyancy-Driven Ventilation,” *International Journal of Ventilation*, vol. 3, no. 3, pp. 193-208, 2004. [[CrossRef](#)] [[Google Scholar](#)] [[Publisher Link](#)]
- [273] Ihab Hasan Hatif et al., “Comparative Evaluation of Air Distribution Systems for Controlling the Airborne Infection Risk in Indoor Environments,” *Journal of Building Engineering*, vol. 79, 2023. [[CrossRef](#)] [[Google Scholar](#)] [[Publisher Link](#)]
- [274] H. Hareesh Krishnan et al., “Experimental and Numerical Study of Wind Tower Integrated with Solar Heating Unit to Meet Thermal Comfort in Buildings During Cold and Sunny Climate Conditions,” *Journal of Building Engineering*, vol. 68, 2023. [[CrossRef](#)] [[Google Scholar](#)] [[Publisher Link](#)]
- [275] Abdalla Gomaa, Gamal B. Abd El Aziz, and Momen I. Radwan, “Performance Characteristics of Wet Air-Conditioning Cooling Coils with Different Fin Patterns,” *Science and Technology for the Built Environment*, vol. 21, no. 2, pp. 126-136, 2015. [[CrossRef](#)] [[Google Scholar](#)] [[Publisher Link](#)]
- [276] Li Ge et al., “Improvement and Validation of the System Analysis Model and Code for Heat-Pipe-Cooled Microreactor,” *Energies*, vol. 15, no. 7, pp. 1-22, 2022. [[CrossRef](#)] [[Google Scholar](#)] [[Publisher Link](#)]
- [277] Hu Gao et al., “Rapid Prediction of Indoor Airflow Field Using Operator Neural Network with Small Dataset,” *Building and Environment*, vol. 251, 2024. [[CrossRef](#)] [[Google Scholar](#)] [[Publisher Link](#)]
- [278] Kaito Furuhashi, Takashi Nakaya, and Yoshihiro Maeda, “Prediction of Occupant Behavior toward Natural Ventilation in Japanese Dwellings: Machine Learning Models and Feature Selection,” *Energies*, vol. 15, no. 16, pp. 1-26, 2022. [[CrossRef](#)] [[Google Scholar](#)] [[Publisher Link](#)]
- [279] Daria Frank et al., “Air Curtains: Validation of Results from Small-Scale Laboratory Waterbath Experiments by Real-Scale Measurements in Climate Chambers and Numerical Simulations,” *Energy and Buildings*, vol. 277, pp. 1-12, 2022. [[CrossRef](#)] [[Google Scholar](#)] [[Publisher Link](#)]
- [280] Sepehr Foroushani, John Wright, and David Naylor, “Convection at the Indoor Side of Complex Fenestration Systems: The ASHWAT Model Revisited,” *Journal of Building Performance Simulation*, vol. 12, no. 2, pp. 133-144, 2019. [[CrossRef](#)] [[Google Scholar](#)] [[Publisher Link](#)]
- [281] Simone Ferrari, “Ventilation in a Group of Courtyard Buildings,” *EPJ Web of Conferences: EFM21-15th International Conference “Experimental Fluid Mechanics 2021”*, vol. 264, pp. 1-6, 2022. [[CrossRef](#)] [[Google Scholar](#)] [[Publisher Link](#)]
- [282] Revanth Eluru, and Dillip Kumar Mohanty, “Significance of Magnetic Nano Fluids in Pulsating Heat Pipes - A Review,” *Energy Sources, Part A: Recovery, Utilization, and Environmental Effects*, vol. 47, no. 1, pp. 10677-10706, 2025. [[CrossRef](#)] [[Google Scholar](#)] [[Publisher Link](#)]

- [283] Tao Du et al., "Propagation and Entrainment of Buoyancy-Driven Flows in a Narrow Horizontal Space and Implications for Buoyant Contaminant Transport Under Natural Ventilation," *Building and Environment*, vol. 132, pp. 214-224, 2018. [[CrossRef](#)] [[Google Scholar](#)] [[Publisher Link](#)]
- [284] Alaa R. Al-Badri et al., "Improving Thermal Performance in Building Heating, Ventilation, and Air Conditioning Systems: A Study of Natural Convection and Entropy in Plus-Shaped Cavity," *Heat Transfer*, vol. 54, no. 3, pp. 2235-2250, 2025. [[CrossRef](#)] [[Google Scholar](#)] [[Publisher Link](#)]
- [285] Yi Ding et al., "Self-Adaptive Physics-Driven Deep Learning for Seismic Wave Modeling in Complex Topography," *Engineering Applications of Artificial Intelligence*, vol. 123, 2023. [[CrossRef](#)] [[Google Scholar](#)] [[Publisher Link](#)]
- [286] Ho Kam Dai, Yifu Shi, and Chun Chen, "Developing A Deep Neural Network Model for Predicting Ventilation Rates in Public Housing Buildings in Hong Kong," *Energy and Buildings*, vol. 307, 2024. [[CrossRef](#)] [[Google Scholar](#)] [[Publisher Link](#)]
- [287] Andrea Carlo D'Alicandro, and Alessandro Mauro, "Experimental and Numerical Analysis of CO₂ Transport Inside a University Classroom: Effects of Turbulent Models," *Journal of Building Performance Simulation*, vol. 16, no. 4, pp. 434-459, 2023. [[CrossRef](#)] [[Google Scholar](#)] [[Publisher Link](#)]
- [288] Shuqing Cui et al., "A Global Modelling Approach of Natural Ventilation with Acoustic and Daylighting Constraints," *International Journal of Ventilation*, vol. 15, no. 3-4, pp. 233-252, 2016. [[Google Scholar](#)] [[Publisher Link](#)]
- [289] Chia-Ren Chu, and Kai-Jie Yang, "Transport Process of Outdoor Particulate Matter into Naturally Ventilated Buildings," *Building and Environment*, vol. 207, 2022. [[CrossRef](#)] [[Google Scholar](#)] [[Publisher Link](#)]
- [290] Kai-Chung Cheng et al., "PM_{2.5} Exposure Close to Marijuana Smoking and Vaping: A Case Study in Residential Indoor and Outdoor Settings," *Science of The Total Environment*, vol. 802, pp. 1-39, 2022. [[CrossRef](#)] [[Google Scholar](#)] [[Publisher Link](#)]
- [291] Dounia Chaatouf et al., "Parametric Analysis of a Sensible Heat Storage Unit in an Indirect Solar Dryer Using Computational Fluid Dynamics," *Journal of Energy Storage*, vol. 49, 2022. [[CrossRef](#)] [[Google Scholar](#)] [[Publisher Link](#)]
- [292] Giovanni Calzolari, and Wei Liu, "Deep Learning to Develop Zero-Equation Based Turbulence Model for CFD Simulations of the Built Environment," *Building Simulation*, vol. 17, no. 3, pp. 399-414, 2024. [[CrossRef](#)] [[Google Scholar](#)] [[Publisher Link](#)]
- [293] Layla Iskandar et al., "Climate Change Impact on Natural Ventilation Cooling Effectiveness Using CFD Simulations in Low Thermal Mass Historic Buildings," *International Journal of Architectural Heritage*, vol. 19, no. 11, pp. 2919-2943, 2025. [[CrossRef](#)] [[Google Scholar](#)] [[Publisher Link](#)]
- [294] Christian Blad, Simon Bøgh, and Carsten Skovmose Kallesøe, "Data-Driven Offline Reinforcement Learning for HVAC-Systems," *Energy*, vol. 261, pp. 1-11, 2022. [[CrossRef](#)] [[Google Scholar](#)] [[Publisher Link](#)]
- [295] AbdMonem H. Beitelmal, Jorge E. Gonzalez-Cruz, and John Zhai, "Special Issue on the Advances on Indoor Air Quality Systems for Healthy and Sustainable Buildings," *Journal of Engineering for Sustainable Buildings and Cities*, vol. 4, no. 3, pp. 1-2, 2023. [[CrossRef](#)] [[Google Scholar](#)] [[Publisher Link](#)]
- [296] Germilly Barreto et al., "An Innovative Window Heat Recovery (WHR) System with Heat Pipe Technology: Analytical, CFD, Experimental Analysis and Building Retrofit Performance," *Energy Reports*, vol. 8, pp. 3289-3305, 2022. [[CrossRef](#)] [[Google Scholar](#)] [[Publisher Link](#)]
- [297] Seyedhadi Banihashemi et al., "Thermal Performance Investigation in Circular Tube with Stationary and Rotating Conical-Obstacle Inserts," *Journal of Thermophysics and Heat Transfer*, vol. 36, no. 2, pp. 242-255, 2022. [[CrossRef](#)] [[Google Scholar](#)] [[Publisher Link](#)]
- [298] Azraf Azman et al., "Numerical Investigation of Flow Characteristics and Heat Transfer Efficiency in Sawtooth Corrugated Pipes with Al₂O₃-Cu/Water Hybrid Nanofluid," *Results in Physics*, vol. 53, pp. 1-13, 2023. [[CrossRef](#)] [[Google Scholar](#)] [[Publisher Link](#)]
- [299] Adam Arabian, and Ellen Brehob, "Optimization of Aerosol Sensor Placement in Common Ventilation Ductwork," *International Journal of Ventilation*, vol. 9, no. 3, pp. 249-260, 2010. [[CrossRef](#)] [[Google Scholar](#)] [[Publisher Link](#)]
- [300] Calcabrini Andres et al., "Time-Varying, Ray Tracing Irradiance Simulation Approach for Photovoltaic Systems in Complex Scenarios with Decoupled Geometry, Optical Properties and Illumination Conditions," *Progress in Photovoltaics*, vol. 31, no. 2, pp. 134-148, 2023. [[CrossRef](#)] [[Google Scholar](#)] [[Publisher Link](#)]
- [301] C. Allison, and B. Dally, "Assessment of Compact Heat Exchanger Consisting Entirely of Tubes Arranged in a Turbulence Generating Mesh," *Australian Journal of Mechanical Engineering*, vol. 4, no. 1, pp. 51-57, 2007. [[CrossRef](#)] [[Google Scholar](#)] [[Publisher Link](#)]
- [302] Ammar Alkhalidi, Bassam Darwish Ahmad, and Mohamad K. Khawaja, "Novel INVELOX Design with Unique Intake to Improve Wind Capturing Mechanism," *Results in Engineering*, vol. 16, pp. 1-11, 2022. [[CrossRef](#)] [[Google Scholar](#)] [[Publisher Link](#)]
- [303] Yousef Al Horr et al., "Thermal Comfort in Buildings: Scientometric Analysis and Systematic Review," *Journal of Architectural Engineering*, vol. 29, no. 2, pp. 1-61, 2023. [[CrossRef](#)] [[Google Scholar](#)] [[Publisher Link](#)]

Appendix 1. List of Tables

Table 1(a). Notations defined for the study

α_i	Absorptivity of glass material i
$\Delta\theta$	Angle difference
A_r	Archimedes number
A^*	Area coefficient
χ	Bernoulli continuity coefficient for Gregory's series
f	Bessel corrected variance
B	Buoyancy flux (m^2s^2)
x_i, y_i	Cartesian coordinates
C_d	Coefficient of discharge
h_i	Convective heat transfer coefficient at i
\bar{G}	Dirichlet integral of discharge
τ	Dirichlet integral of temperature
\bar{U}	Dirichlet integral of transmissivity
v_ϕ	Eigenfunction for the Fourier transform of absorptivity
ρ_ϕ	Eigenfunction for the Fourier transform of reflectivity
E	Energy term (J)
\mathcal{P}	Flajolet-Odlyzko constant
ρ	Fluid density ($kg\ m^{-3}$)
σ_ϕ	Fourier integral of feedback components
F_r	Froude number
Γ	General diffusion coefficient
G_r	Grashof number
H	Height (m)
Ω_θ	Hyper-harmonic median of Dirichlet series
ξ	Khinchin-Lévy constant
K	Kullback-Leibler divergent coefficient
\mathcal{K}	Lagrange polynomial multiplier
ϕ	Laplace limit of flow variable
θ	Lemniscate constant representing the integral covariance of stochastic data
θ_l	Louver angle
C_{jv}	Louver resistance coefficient
\bar{R}	Maclaurin series expansion derivative
Y	Mean squared deviation
η	Oscillatory integral operator for inflow
μ	Oscillatory integral operator for turbulence
β	Peak frequency density of model (louver shading calibration) data
α	Peak frequency density of observation data
λ_β	Peak wavelength density of model data
λ_α	Peak wavelength density of observation data
P	Pressure (Pa)
$h_{r,i}$	Radiative heat transfer coefficient at i
B_τ	Recursive Bayesian Estimation of Relative Conjugate Error
ρ_i	Reflectivity of glass material i
ζ	Riemann zeta function represents the Dirichlet series
δ	Single blind width (m)
θ_s	Solar incident angle
I	Solar intensity (Wm^{-2})
S_ϕ	Source term (J)
C_p	Specific heat ($Jkg^{-1}\ K^{-1}$)
A	Surface area (m^2)

\mathcal{C}_n	Sylvester sequence of Eigen solutions
V	Taylor series expansion derivative
T	Temperature (K)
t	Time (s)
ϕ	Time series of model data
ψ	Time series of observation data
τ_i	Transmissivity of glass material i
ε	Turbulent dissipation rate ($m^2 s^{-3}$)
k	Turbulent kinetic energy ($m^{-2}s^{-2}$)
\ddot{H}	Vandermonde polynomial multiplier
U	Velocity magnitude (ms^{-1})
\vec{u}_i	Velocity vector (ms^{-1})
V	Volume flow rate (m^3s^{-1})
y^+	y_i -positive axial value

Table 1(b). Comparative thermal and environmental efficacy of natural ventilation strategies

Metric	Ventilation Type	Modified Value	Unit	Specific Mechanism/Basis of Improvement
Performance Gains	Internal Air Quality Index Elevation	15.01	units	Minimisation of the short-circuiting effect observed in SSV, leading to efficient pollutant removal.
	Auxiliary Cooling Load Decrease	21.05%	%	Achieved through the judicious balance of energy efficiency targets and critical air exchange requirements
	Thermal Comfort Provision (Brisbane)	71.40%	% of time	Utilisation of wind-induced pressure differentials across opposing facade elements for comprehensive air turnover
	Thermal Comfort Provision (Brisbane)	1.05%	% of time	Limited airflow and internal mixing capacity characteristic of single facade aperture placement
Extreme Weather Improvements	Temperature Reduction (Athens)	1.53	°C	Demonstrates superior cooling capacity during hot summer circumstances due to high ventilation rates
	Ventilation Rate Enhancement (Athens)	13.7	times	Superior volumetric airflow is achieved by leveraging multiple openings on different walls and wind-driven flow.
Reynolds Number (Re)	$\rho uL/\mu$	-	$Re_b > 20,200$ (Building scale)	Ratio of inertial forces (ρuL) to viscous forces (μ); governs the onset of fully turbulent flow around bluff bodies.
Reynolds Number at Opening (Re_o)	Calculated using opening size and velocity	-	$Re_o > 102,000$ (Opening scale)	Threshold value above which the discharge coefficient for sharp openings becomes independent of the Reynolds number
Archimedes Number (A_r)	$g\beta L\Delta T/u^2$	-	ΔT adjusted to maintain A_r constancy.	Ratio of buoyancy forces to inertial forces; essential for maintaining flow similarity in non-isothermal reduced-scale models

Table 1(c). Measurement data used for modelling twin house N2 and information about the sensors (IEA EBC Annex 71 [231-258])

Measurement	Unit	Location	Sensor	Accuracy
Ambient air temperature	°C	Weather station	Meteomedia GmbH	0.21
Atmospheric pressure	hPa	Weather station	Meteomedia GmbH	-
Global horizontal radiation	W/m^2	Weather station	CMP11 Kipp & Zonen	< 3%
Diffuse radiation	W/m^2	Weather station	CMP11 Kipp & Zonen	< 3%
Relative humidity	%	Weather station	Meteomedia GmbH	$\pm 2\%$
Snow height	mm	Weather station	Meteomedia GmbH	-
Soil temperature	°C	Weather station	Heraeus Holding GmbH	0.16

Wind speed	m/s	Weather station	Adolf Thies GmbH & Co.KG	< 0.5 m/s: 0.1 greater than 0.5 m/s: ±2%
Wind direction	°	Weather station	Adolf Thies GmbH & Co.KG	±1°
Downward longwave radiation	W/m ²	Weather station	Kipp & Zonen CGR4	±7 W/m ² & ± 1%
Indoor air temperature	°C	All rooms	Radiation-shielded PT100; 4-wire	±0.016 K(±1.5 K sol. irradiation)
Radiator electrical power	W	All rooms	EL3403-0010 WSK 40 10/1A	1.7 + 0.5%
Window position	-	Child 1	Thermokon SRW01	-
Door position	-	Kitchen	Thermokon SRW01	-
Exhaust air volume flow rate	m ³ /h	Dining, bath, child 1 & child 2	SS 20.501 Schmidt Technology	±3.7 m ³ /h
Supply air volume flow rate	m ³ /h	Living, child 1 & child 2	SS 20.501 Schmidt Technology	±3.7 m ³ /h
Supply air temperature	°C	Living, child 1 & child 2	PT100; 4-wire	±0.016 K(±1.5 K sol. irradiation)
Power of air fans	W	Living, dining, bath, child 1 & child 2	Beckhoff EL3403-0010	1.8%
Power of supply air heaters	W	Living, child 1 & child 2	Beckhoff EL3403-0010	1.3%

Table 2. Experimental configuration of the simulated phases of the main experiment in Twin House N2 (Twin house experiment, IEA EBC Annex 71 [231-258])

	Coheating (12 days)	User Phase 1 (35 days)	User Phase 2 (30 days)
Set temperature	Constant (21°C)	Identical for all rooms (21°C) with a night setback (17°C)	Room-wise profile including stochastic deviations
Thermal user profile	-	With stochastic deviations	With stochastic deviations
Kitchen door	Open	Open	Operated
Sleeping door	Open	Open	Closed
Roller blinds	All open	Living west closed	Kitchen and living west closed
Child 1 window	Closed	Closed	Operated
Trap door to attic	Open	Closed	Open
Mechanical ventilation	OFF	ON	ON

Table 3. Total thickness and overall heat transfer coefficient (U-value) of each construction in Twin House (Twin house experiment, IEA EBC Annex 71 [231-258])

Construction	Thickness (m)	U(W/m ² · K)
West exterior wall	0.568	0.318
East exterior wall	0.518	0.322
North exterior wall	0.568	0.315
North knee wall	0.578	0.391
South exterior wall	0.568	0.307
Railing south wall	0.463	0.354
South Knee wall	0.578	0.376
Roof (without tiles)	0.380	0.316
Floor	0.472	0.394
Ceiling	0.430	0.517
Interior wall (slim)	0.235	2.603
Interior wall (broad)	0.360	2.013
Interior wall (attic)	0.197	1.628

Table 4. Infiltrations in the N2 house: air changes per hour (ACH), air flow rates at 50 Pa and flow coefficients at 1 Pa(C_e)

	ACH	ṁ[kg/s at 50 Pa]	Cs[kg/s at 1 Pa]	Crack
Ground floor	2.19	0.1845	0.0567	1
Attic	1.42	0.1214	0.0317	2

Table 5. RMSE, CV(RMSE), and NMBE values calculated for measured and simulated heating during the coheating phase per thermal zone and for the entire house

Coheating	Door	Kitchen	Living	Bath	Sleeping	Dining	Child 1	Child 2	House
RMSE [Wh]	3.78	7.41	15.21	5.01	4.34	4.72	8.46	8.47	41.25
CV(RMSE) [%]	21.72	19.11	27.63	27.11	13.51	13.77	12.04	12.39	13.72
NMBE [%]	2.54	-5.63	-16.09	1.22	-3.68	1.37	1.73	-6.89	-9.35

Table 6. RMSE, CV(RMSE), NMBE, and MAE values calculated for the measured and simulated average indoor temperatures during user phase 1 (19/12/18–01/02/19) per thermal zone

User Phase 1	Door	Kitchen	Living	Bath	Sleeping	Hall	Dining	Child 1	Child 2
RMSE [°C]	0.56	0.85	0.94	0.43	0.43	0.62	0.73	0.75	0.97
CV(RMSE) [%]	2.37	3.67	4.48	1.97	1.69	2.58	2.96	3.72	4.39
NMBE [%]	0.67	1.30	3.92	1.18	0.54	1.93	1.74	-0.78	2.37
MAE [°C]	0.41	0.66	0.92	0.34	0.27	0.45	0.59	0.64	0.86

Table 7. RMSE, CV(RMSE), NMBE, and MAE values calculated between the measured and simulated average indoor temperatures during user phase 2 (01/02/19–01/03/19) per thermal zone

User Phase 2	Door	Kitchen	Living	Bath	Sleeping	Hall	Dining	Child 1	Child 2
RMSE [°C]	0.95	0.95	0.57	0.75	0.69	0.73	0.72	0.83	0.56
CV(RMSE) [%]	4.77	4.56	2.68	3.62	2.97	2.89	3.35	3.84	2.64
NMBE [%]	-4.36	-2.98	-0.74	-3.07	-2.51	-2.32	-1.44	0.43	0.77
MAE [°C]	0.87	0.89	0.44	0.66	0.61	0.68	0.57	0.59	0.45

Table 8. Thermal bridges of the ground floor: total length and equivalent Ψ -value (W/m/K) per orientation for introduction in TRNBUILD (Twin house experiment, IEA EBC Annex 71 [231-258])

Thermal zone	Type	Orientation	Length (m)	Ψ -value (W/m · K)	% Length
Kitchen	Wall-ceiling	North	4.36	0.475	36%
	Wall-ceiling	West	4.22	0.389	28%
	Wall-wall	North-West	3.96	-0.126	32%
	Window	West	6.54	0.039	47%
	Wall-floor	North	4.36	-0.037	36%
	Wall-floor	West	4.22	-0.036	28%
	All	West	12.98	0.108	100%
	All	North	10.68	0.086	100%
Living	Wall-ceiling	South wall	6.79	0.386	28%
	Wall-ceiling	West wall	8.06	0.359	32%
	Wall-Wall	West-South	3.96	-0.135	14%
	Window	South	10.76	0.032	47%
	Window	West	6.54	0.039	25%
	Wall-floor	South wall	6.79	-0.042	28%
	Wall-floor	West wall	8.06	-0.045	32%
	All	South	22.34	0.109	100%
All	West	23.62	0.106	100%	
Dining	Wall-ceiling	South wall	5.42	0.391	26%
	Wall-ceiling	East wall	4.4	0.384	52%
	Wall-Wall	South-East	3.96	-0.096	18%
	Window	South	6.54	0.038	33%
	Wall-floor	South wall	5.42	-0.039	26%
	Wall-floor	East wall	4.4	-0.037	52%
	All	South	18.34	0.081	100%
	All	East	7.8	0.175	100%
Bath	Wall-ceiling	East	4.66	0.384	29%
	Window	East	6.54	0.028	44%
	Wall-floor	East	4.66	-0.037	26%
	All	East	13.86	0.113	100%

Sleeping	Wall-ceiling	North wall	5.42	0.378	23%
	Wall-ceiling	East wall	4.22	0.384	58%
	Wall-Wall	East-North	3.96	-0.096	19%
	Window	North	6.54	0.039	33%
	Wall-floor	North wall	5.42	-0.033	26%
	Wall-floor	East wall	4.22	-0.037	52%
	All	North	18.34	0.082	100%
	All	East	7.44	0.175	100%
Doorway	Wall-floor	North	3.43	-0.039	50%
	Wall-ceiling	North	3.43	0.376	56%
	All	North	5.86	0.167	100%

Table 9. Thermal bridges of the attic: total length and equivalent Ψ -value ($W/m \cdot K$) per orientation for introduction in TRNBUILD (Twin house experiment, IEA EBC Annex 71 [231-258])

Thermal	Type	Orientation	Length (m)	Ψ -value value ($W/m \cdot K$)	% Length
Children 1	Rake Junction-MW	West	12	0.046	69%
	Eaves Junction	North	2.771	0.072	47%
	Eaves Junction	South	5.917	0.073	35%
	Window	Roof (S)	4.897	0.039	29%
	Window	West	5.576	0.033	36%
	Wall-Wall	North-West	0.484	-0.113	9%
	Wall-Wall	West-South	0.495	-0.114	4%
	Ceiling-knee wall	South	5.864	0.023	35%
	Ceiling-knee wall	North	2.675	0.029	47%
	All	North	5.798	0.035	100%
	All	West	17.741	0.047	100%
	All	South	16.931	0.043	100%
Children 2	Rake Junction-PU	East wall	12	0.052	63%
	Eaves Junction	South	4.424	0.071	49%
	Eaves Junction	North	4.723	0.075	45%
	Window	East	7.343	0.039	37%
	Wall-Wall	South-East	0.454	-0.096	6%
	Wall-Wall	East-North	0.451	-0.097	5%
	Ceiling-knee wall	South	4.425	0.023	47%
	Ceiling-knee wall	North	4.427	0.024	44%
	All	East	19.386	0.046	100%
	All	South	9.292	0.049	100%
	All	North	9.298	0.079	100%
Staircase	Eaves Junction	North	3.123	0.073	50%
	Ceiling-knee wall	North	3.121	0.025	50%
	All	North	6.249	0.046	100%

Table 10. Values of internal thermal bridges (Twin house experiment, IEA EBC Annex 71 [231-258])

Type	Ψ -value value ($W/m \cdot K$)	X-value (W/K)
Column-Floor	-	0.652
Column-Ceiling	-	0.647
Internal wall, thin-ceiling	0.046	-
Internal wall, thin-floor	0.249	-
Internal wall, thick-ceiling	0.055	-
Internal wall, thick-floor	0.341	-

Table 11(a). Compilation of all airflow links needed to define the airflow network in Twin House N2 (Note: Zones in overpressure or zones with no exterior doors or windows were assumed to have a factor equal to 0)

No.	Type of link	From node	To node	Factor
1	Crack 1	Ext. node N	Kitchen	0.32
2	Crack 1	Ext. node W	Kitchen	0.21
3	Crack 1	Ext. node N	Doorway	0.13
4	Crack 1	Ext. node N	Sleeping	0
5	Crack 1	Ext. node E	Sleeping	0
6	Crack 1	Ext. node S	Living	0
7	Crack 1	Ext. node W	Living	0
8	Crack 1	Ext. node E	Bathroom	0.23
9	Crack 1	Ext. node S	Dining	0.16
10	Crack 1	Ext. node E	Dining	0.06
11	Crack 2	Ext. node W	Children 1	0.89
12	Crack 2	Ext. node S	Children 1	0.13
13	Crack 2	Ext. node E	Children 2	0

Table 11(b). Compilation of all airflow links needed to define the airflow network in Twin House N2. Factor 0 indicates closed doors and windows, whereas Factor 1 is used for open elements (Note: During the simulation, fans with a factor of zero were not working)

No.	Type of link	From node	To node	Factor
14	Internal door	Doorway	Living	1
15	Internal door	Living	Kitchen	Operated [0/1]
16	Internal door	Living	Hall	1
17	Internal door	Hall	Sleeping	Operated [0/1]
18	Internal door	Hall	Bathroom	1
19	Internal door	Hall	Dining	1
20	Internal door	Staircase	Children 1	1
21	Internal door	Staircase	Children 2	1
22	Trap door	Living	Staircase	Operated [0/1]
23	Fan 100 m ³ /h	Ext. node E	Aux. node 1	Operated
24	Exit straight duct	Aux. node 1	Living	-
25	Fan 50 m ³ /h	Ext. node W	Aux. node 2	Operated
26	Exit straight duct	Aux. node 2	Children 1	-
27	Fan 50 m ³ /h	Ext. node E	Aux. node 3	Operated
28	Exit straight duct	Aux. node 3	Children 2	-
29	Entry straight duct	Children 2	Aux. node 4	-
30	Fan 50 m ³ /h	Aux. node 4	Ext. node E	Operated
31	Entry straight duct	Dining	Aux. node 5	-
32	Fan 50 m ³ /h	Aux. node 5	Ext. node E	Operated
33	Entry straight duct	Bathroom	Aux. node 6	-
34	Fan 50 m ³ /h	Aux. node 6	Ext. node E	Operated
35	Entry straight duct	Children 1	Aux. node 7	-
36	Fan 50 m ³ /h	Aux. node 7	Ext. node W	Operated
37	Window	Ext. node W	Children 1	Operated [0/0.09]

Table 12. Properties of glass

Properties	Value	Unit
glass thickness	0.007	m
thermal conductivity	1.2	W/m · K
Density	2670[34]	kg/m ³
specific heat capacity	785[34]	J/kg · K
Emissivity	0.87[34]	
absorption coefficient	see Sections 2 and 3	1/m
refractive index	see Sections 2 and 3	

Table 13. Numerical scenarios

Scenarios		Symbol	values	unit
Environment	-	solar incident angle	θ	0 – 80 [°]
	-	radiation intensity	I	50 – 1100 [W/m ²]
NVDSF	low-e	absorptance	α_i (const. ρ_i)	see Table 5
	material	reflectance	ρ_i (const. α)	-
	-	absorptance + reflectance	$\alpha_i + \rho_i$ (const. τ_i)	-
	façade dimension	cavity depths	D	0.1 – 0.4 [m]
	-	vent heights	H	0.1 – 0.5 [m]

Table 14. Numerical scenarios and selected design ranges

Category	Design factor	Value	Interval	Unit
Room configuration	Window area	1.0 – 1.8	0.3	m ²
Attic configuration	Ceiling vent area	1.0 – 1.8	0.3	m ²
	Ceiling vent position	2.0 – 3.0	0.3	m
Chimney configuration	Cavity gap	0.3 – 1.7	0.1 – 0.3	m
	Cavity height	1.0 – 4.0	0.6	m
Environment	Solar radiation	220 – 1160	210	W/m ²

Table 15. The hazard index H was calculated from an ensemble-based simulation of oil releases at sea for one year of realistic currents

Coastline segment	H index values
French North Atlantic	0.83
Madeira Island	0.34
Bahia region (Brazil)	0.15
Mexico	0.19
U.S. North Atlantic	0.22

Table 16. Boundary conditions and material properties used in the validation model

Boundary Conditions			Box Material Properties			
Type	Feature	Values	Parameters	Glass ID	Wall ID	Units
[Box]			thickness [63–86]	6	12	mm
glass	transparent	Table 4	density	2680[31 – 56]	1300	kg/m ³
back wall	heat exchanger	in [72–92]	conductivity	1	0.01	W/m · K
wall	opaque		specific heat	796 [44–61]	1380	J/kg · K
[Ambient]			absorption coefficient			
bottom, sides	pressure-in	0 Pa	VIS: CG6/FG6/RG6	5/121/126	60	1/m
front, back, top	pressure-out	0 Pa	IR: CG6/FG6/RG6	49/91/94		1/m

Table 17. Optical properties and comparison between CFD and experimental data [41–74]

Glass type	τ		A		T _{glass} Exp. [°C]	T _{glass} CFD			
	VIS	Solar	VIS	Solar		Steady		Transient	
						[°C]	error	[°C]	error
CG-6	0.93	0.88	0.13	0.22	69.78	58.44	–3.2%	61.60	5.2%
FG-6	0.53	0.52	0.62	0.57	80.22	69.89	–2.3%	72.99	3.3%
RG-6	0.19	0.28	0.63	0.58	78.11	75.98	4.3%	74.05	–2.7%

Table 18. Comparison of NVDSF I and II with typical optical properties of clear glazing and low-e glazing

NVDSF	Inner Glass type	Optical properties						CFD results			
		$\bar{\rho}_i$			α_i			Flow Rate		T _{glass}	
		VIS	IR	Solar	VIS	IR	Solar	[m ³ /s]	Diff.	Outer [°C]	Inner [°C]
I	clear	0.078	0.075	0.072	0.049	0.105	0.103	0.039	14%	45.3	33.7
II	low-e	0.054	0.418	0.245	0.158	0.184	0.198	0.048	22%	46.5	39.8

Table 19. Low-e glazing optical properties for the sensitivity study

Case	α_1	α_2	α_3	α_4	α_5	ρ_1	ρ_2	ρ_3	ρ_4	ρ_5	τ_1	τ_2	τ_3	τ_4
τ_{vis}	0.44	0.65	0.73	0.79	0.75	0.55	0.64	0.72	0.75	0.79	0.34	0.36	0.32	0.33
τ_{IR}	0.39	0.49	0.53	0.47	0.49	0.59	0.65	0.68	0.73	0.75	0.82	0.84	0.82	0.82
α_{vis}	0.53	0.49	0.42	0.27	0.23	0.18	0.17	0.17	0.17	0.17	0.51	0.56	0.68	0.64
α_{IR}	0.26	0.25	0.26	0.14	0.14	0.15	0.19	0.19	0.19	0.19	0.23	0.24	0.39	0.34
ρ_{vis}	0.08	0.06	0.15	0.07	0.06	0.36	0.23	0.16	0.14	0.08	0.24	0.19	0.19	0.08
ρ_{IR}	0.45	0.47	0.51	0.53	0.47	0.32	0.24	0.17	0.18	0.08	0.27	0.18	0.27	0.08

Appendix 2. List of Figures

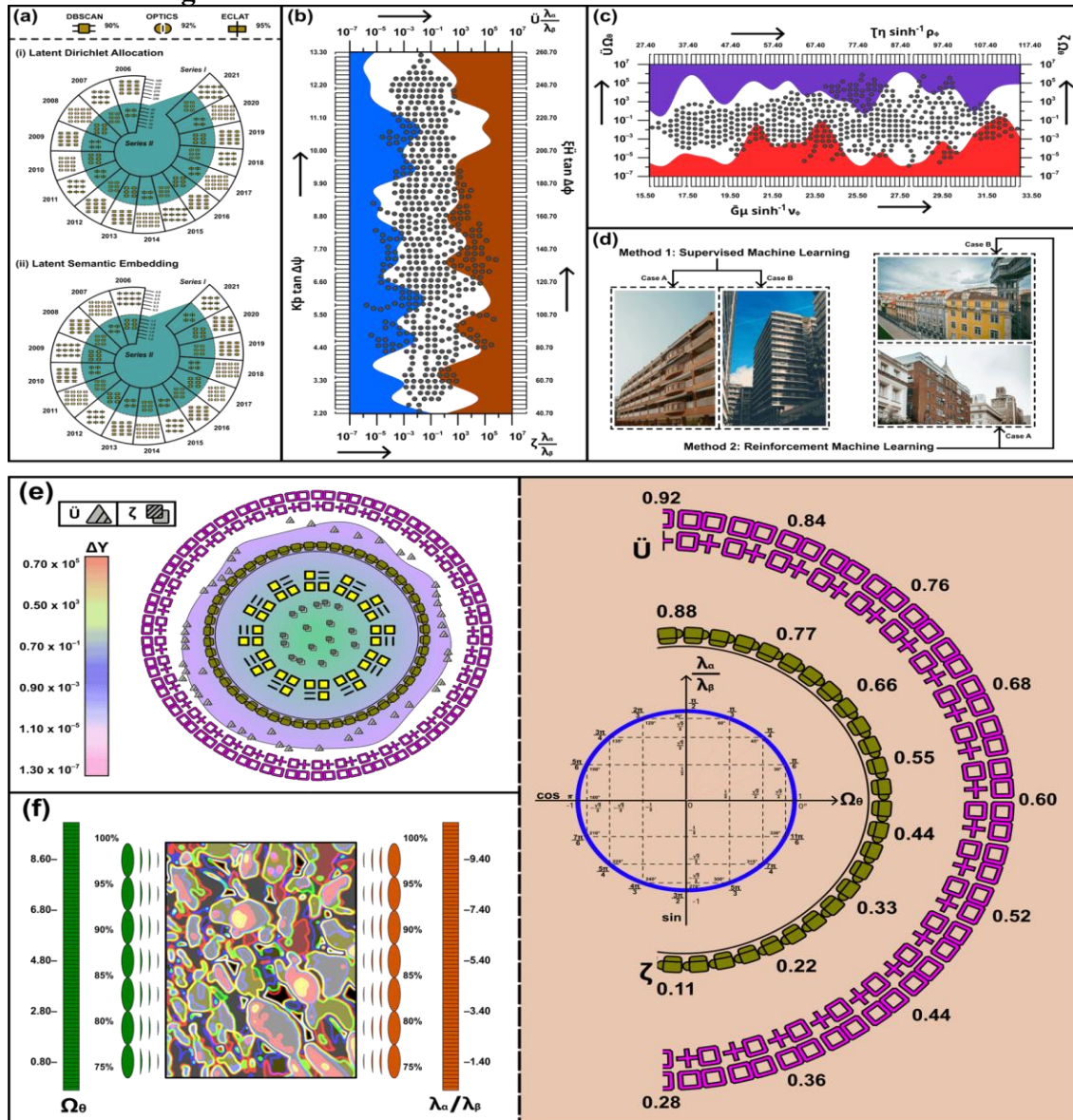


Fig. 1 (a) Differential allocation of apriori machine learning algorithms across two scenarios over a 15-year period, as determined by a principal component analysis of the data described in Section 2, (b) Fibonacci sequences of LES results, wherein the total pressure remains constant in the stream tube when the ventilation rate is moderate, (c) Projected cytometry of total pressure at the opening position of a sealed room model (i.e., similar to the tangential dynamic pressure at the opening), with significant Marks–Kendall metric, whereby scatter plots of Trellis–density correlations express the impact of varying wind direction on the coefficient of variation (CV), (d) Clockwise schematics of case studies conducted for the machine learning analysis, (e) Polar Akima Interpolation (rectified using Python t–SNE Dimensionality Reduction) of prevailing wind angles varying between four fluctuating periods in wind tunnel, and (f) Normalized Laplace transform of the relationship between discharge coefficient inflow directions in a wind tunnel using a revolving turntable and wind direction fluctuations, determined and modified by on-site measurements using an ultrasonic anemometer.

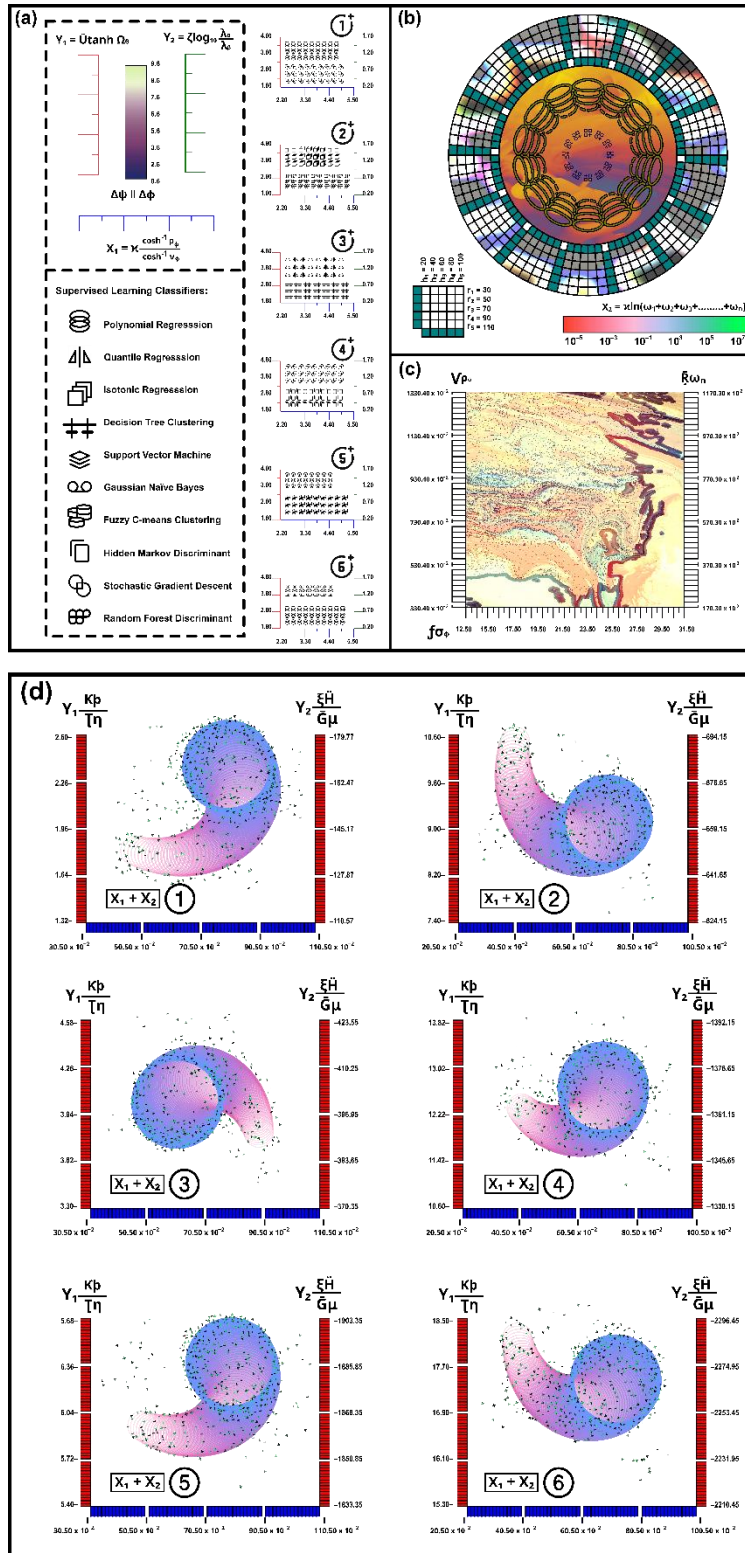


Fig. 2 (a) Simulated stacked hierarchical band structure of supervised learning classifiers within Trellis–density correlations, clustered by double Y–axes' offsets in standard XY scale, using 6–set nominal range sensitivity analysis, (b) Sankey–visualization of stacked histogram plots illustrating a normal distribution of the relationship between discharge coefficient and windward side opening, thereby experimentally validating the Local dynamic similarity model, (c) Schoeller–Contour profile of two–equation turbulence model (i.e., the RNG framework involving indoor airflow, double skin façade and solar chimney), depicted alongside a spectroscopic packing of Bland–Altman density data, and (d) Stochastic cylindrical resonances illustrate the covariance of façade temperature changes with absorptivity ranging from, presented using offset dual Y–axes on a standard XY scale.

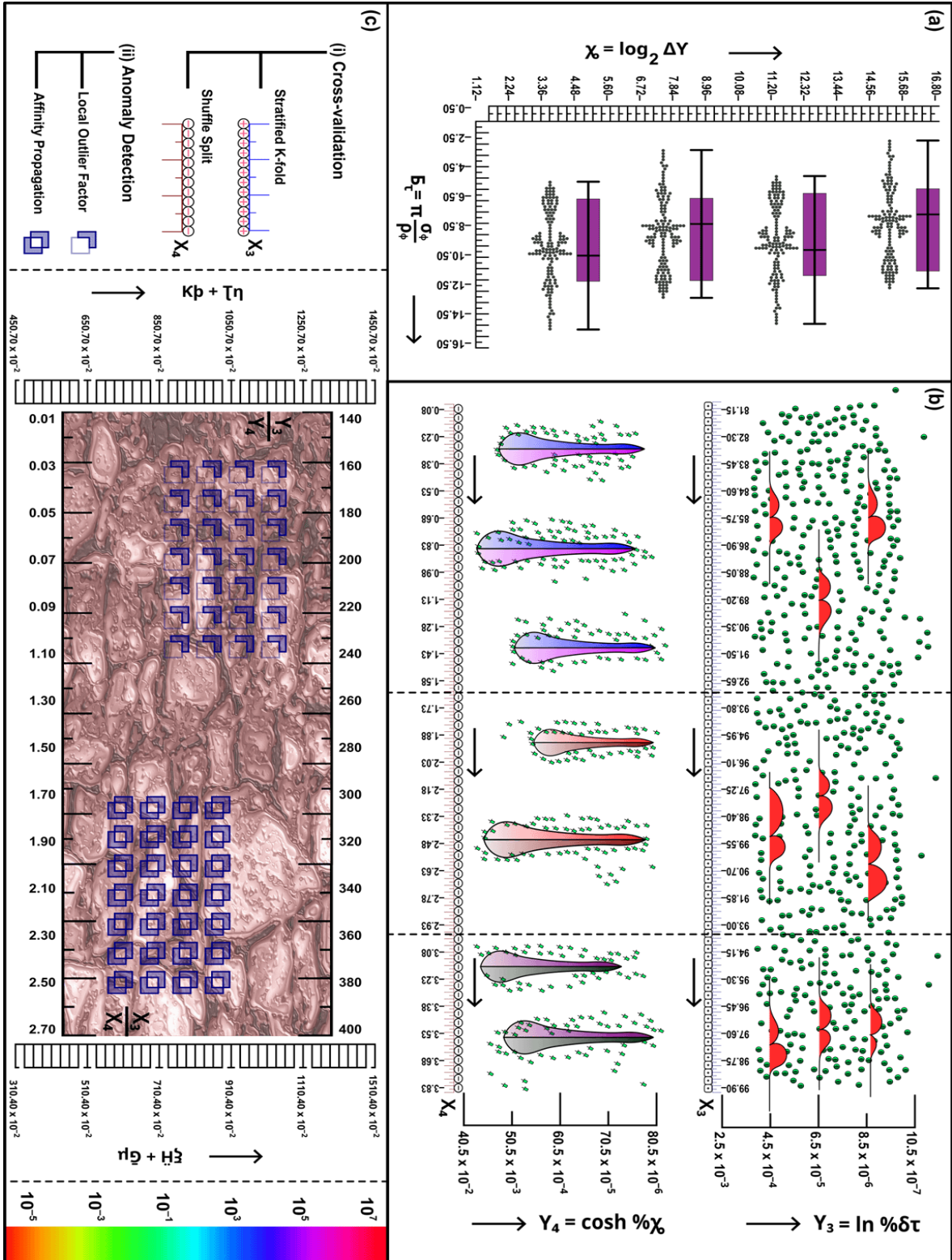


Fig. 3 (a) RNG framework simulation outcomes, employing an enhanced wall function for initial layers, while showing strong concordance between the preliminary hypothesis and experimental findings, represented through a notched box-chart including outliers, (b) Verification of experimental results through direct absorption (which determines the influence of the low-e coating's reflectivity on the outer façade via secondary reflection) illustrated as raincloud and grouped-violin plots, and (c) Posthoc verification of ventilation rate data plots, showing a power function correlation for both NVDSF I with NVDSF II (based on volumetric flow rate and the solar incidence angle), utilized for cross-validation and anomaly detection.

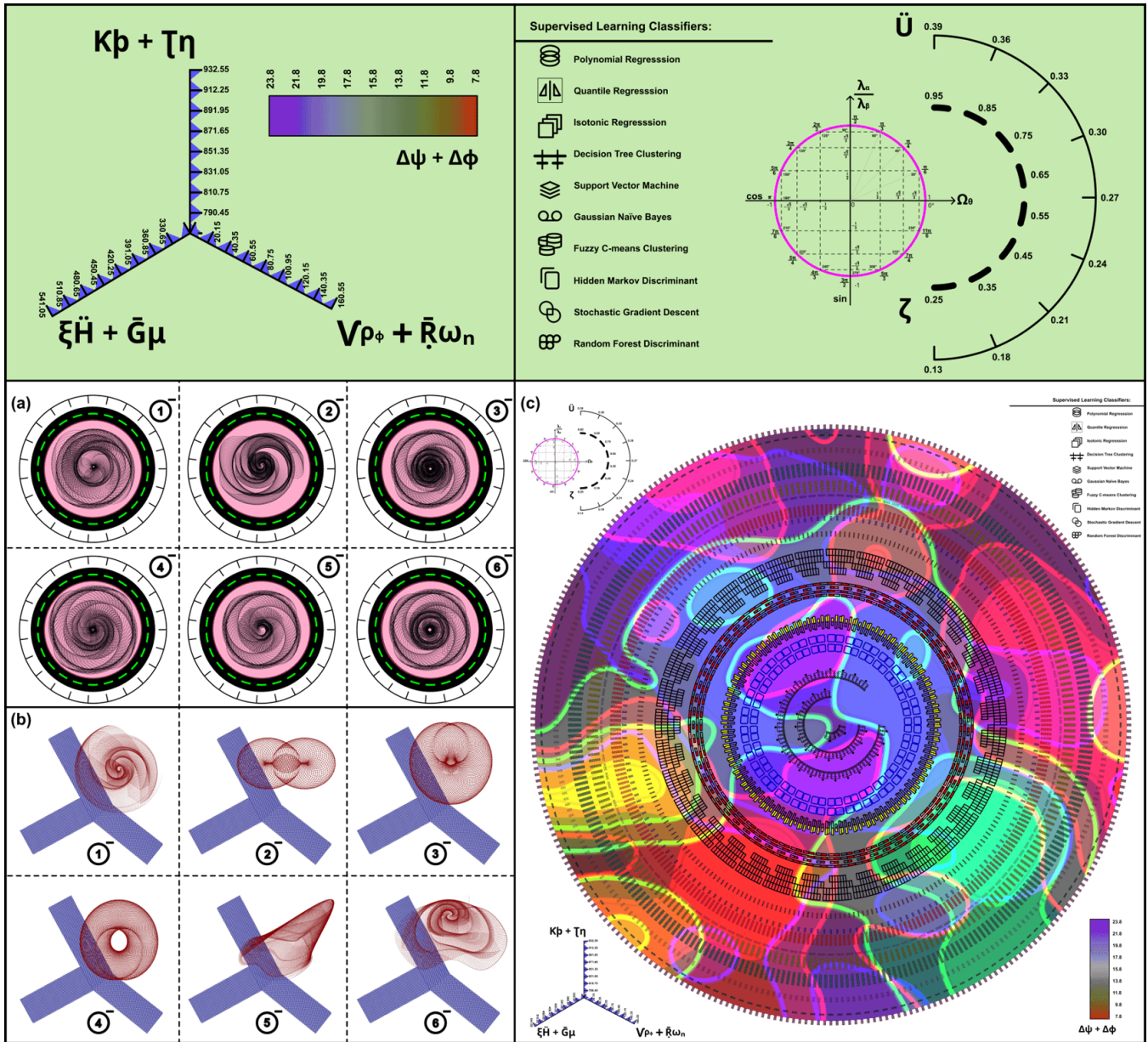


Fig. 4 (a) Angular response–surface plots of natural convection showing that absorptivity increase improves performance, though less significantly compared to fixed reflectivity (which declines with higher absorptivity) estimated using the 6-set hierarchical bands of machine-learning classifiers (Note: (i) Highest reflectivity results in an exterior glass temperature of 52.0°C and an interior glass temperature of 52.7°C, and (ii) as the fraction of absorptivity increases, façades attain a higher interior temperature of 54.5°C but a lower exterior temperature), (b) Stochastic response spectra correlating flow rates and solar intensities for NVDSF I and NVDSF II indicating (i) a minimal decrease in breathing for intensities above 300 W/m² (averaging 0.7% reduction per 100 W/m²), while; (ii) the decrease in breathing intensifies, for intensities below 300 W/m², averaging a 3.5% reduction per 100 W/m², and (c) Mass flow rates across the eight solar angles in both NVDSF I and II fluctuating with solar radiation intensity (while the ventilation rates consistently remain higher) represented as a dendrogram of stacked hierarchical machine-learning classifier bands.